Calorimeter event selection for small-angle Bhabha scattering at LEP1

N. P. Merenkov[a)]

Kharkov Institute of Physics and Technology National Science Center, 310108 Kharkov, Ukraine

(Submitted 29 November 1996; resubmitted 13 January 1997)
Pis'ma Zh. Éksp. Teor. Fiz. **65**, No. 3, 225–230 (10 February 1997)

An analytical method is applied for description of calorimeter event selection in small-angle electron-positron scattering at LEP1. The selections CALO1 and CALO2 are investigated specifically. The first-order correction to the Born cross section is given in the case of wide-narrow angular acceptance. © *1997 American Institute of Physics.* [S0021-3640(97)00103-5]

PACS numbers: 13.65.+i, 29.40.Vj, 12.15.−y

The small-angle Bhabha scattering (SABS) process is used to measure the luminosity of electron–positron colliders. Accurate theoretical determination of the SABS cross section therefore has a direct bearing on the physical values measured in LEP1 experiments.[1] In recent years considerable attention has been devoted to the Bhabha scattering process (see Refs. 2–5 and references therein).

There are two methods of theoretical investigation of the SABS cross section at LEP1: an approach based on Monte Carlo calculations and an analytical approach. The latter is used to check different Monte Carlo programs for *ideal* experimental conditions. In this letter I give for the first time an analytical result for the two calorimeter event selections (CES) labeled in Ref. 3 as CALO1 and CALO2 in the case of wide–narrow angular acceptance. Discussion is restricted to the first-order correction. The second- and third-order leading corrections can be written with the help of the electron structure function, but the second-order next-to-leading correction requires considerable additional effort.

Before studying CES it is helpful to clarify the inclusive event selection (IES), when only the final electron and positron energies are recorded by means of wide–narrow circular detectors. The result will be widely applicable for the description of CES.

1. We introduce the dimensionless quantity

$$\Sigma = \frac{1}{4\pi\alpha^2}\, Q_1^2 \sigma_{\exp}, \tag{1}$$

where $Q_1^2 = \varepsilon^2 \theta_1^2$ (ε is the beam energy and θ_1 is the minimum angle of the wide detector). The ''experimentally'' measurable cross section $\sigma_{\exp}$ is defined as

$$\sigma_{\exp} = \int dx_1 dx_2 \Theta d^2 q_1^{\perp} d^2 q_2^{\perp} \Theta_1^c \Theta_2^c \, \frac{d\sigma(e^+ + e^- \to e^+ + e^- + X)}{dx_1 dx_2 d^2 q_1^{\perp} d^2 q_2^{\perp}}, \tag{2}$$

where X represents undetected final particles, and $x_1(x_2)$ and $\mathbf{q}_1^\perp(\mathbf{q}_2^\perp)$ are the energy fraction and the transverse component of the momentum of the electron (positron) in the final state. The functions Θ_i^c take into account the angular cuts, while the function Θ takes into account the cutoff on the invariant mass of detected electron and positron:

$$\Theta_1^c=\theta(\theta_3-\theta_-)\,\theta(\theta_--\theta_1),\quad \Theta_2^c=\theta(\theta_4-\theta_+)\,\theta(\theta_+-\theta_2),\quad \Theta=\theta(x_1x_2-x_c),$$

$$\theta_-=\frac{|\mathbf{q}_1^\perp|}{x_1\varepsilon},\quad \theta_+=\frac{|\mathbf{q}_2^\perp|}{x_2\varepsilon}. \tag{3}$$

For the wide–narrow case

$$\theta_3>\theta_4>\theta_2>\theta_1,\quad \rho_i=\theta_i/\theta_1>1.$$

The first-order correction Σ_1, which includes the contributions of virtual and real soft and hard photon emission processes, is given by

$$\Sigma_1=\frac{\alpha}{2\pi}\left\{\int_1^{\rho_3^2}\frac{dz}{z^2}\left[-\Delta_{42}\delta(1-x)+\int_{x_c}^1\left((L-1)P_1(x)(\Delta_{42}+\Delta_{42}^{(x)})+\frac{1+x^2}{1-x}\,\overline{K}\right)dx\right]\right.$$
$$\left.+\int_{\rho_2^2}^{\rho_4^2}\frac{dz}{z^2}\left[-\delta(1-x)+\int_{x_c}^1\left((L-1)P_1(x)(1+\theta_3^{(x)})+\frac{1+x^2}{1-x}\,K\right)dx\right]\right\}, \tag{4}$$

where

$$P_1(x)=\frac{1+x^2}{1-x}\theta(1-x-\Delta)+\left(2\,\ln\,\Delta+\frac{3}{2}\right)\delta(1-x),\quad \Delta\to 0,$$

$$\overline{K}(x,z;\rho_4,\rho_2)=\frac{(1-x)^2}{1+x^2}(\Delta_{42}+\Delta_{42}^{(x)})+\Delta_{42}\overline{L_1}+\Delta_{42}^{(x)}\overline{L_2}$$
$$+(\overline{\theta_4^{(x)}}-\theta_2^{(x)})\overline{L_3}+(\overline{\theta_4}-\theta_2)\overline{L_4},$$

$$K(x,z;\rho_3,1)=\frac{(1-x)^2}{1+x^2}(1+\theta_3^{(x)})+L_1+\theta_3^{(x)}L_2+\overline{\theta_3^{(x)}}L_3,$$

$$\overline{L_1}=\ln\left|\frac{(z-\rho_2^2)(\rho_4^2-z)x^2}{(x\rho_4^2-z)(x\rho_2^2-z)}\right|,\quad \overline{L_2}=\ln\left|\frac{(z-x^2\rho_2^2)(x^2\rho_4^2-z)}{x^2(x\rho_4^2-z)(x\rho_2^2-z)}\right|,$$

$$\overline{L_3}=\ln\left|\frac{(z-x^2\rho_2^2)(x\rho_4^2-z)}{(x^2\rho_4^2-z)(x\rho_2^2-z)}\right|,\quad \overline{L_4}=\ln\left|\frac{(z-\rho_2^2)(x\rho_4^2-z)}{(\rho_4^2-z)(x\rho_2^2-z)}\right|, \tag{5}$$

$$\Delta_{42}^{(x)}=\theta_4^{(x)}-\theta_2^{(x)},\quad \Delta_{42}+\theta_4-\theta_2,\quad \theta_i^{(x)}=\theta(x^2\rho_i^2-z),$$

$$\theta_i=\theta(\rho_i^2-z),\quad \overline{\theta_i^{(x)}}=1-\theta_i^{(x)},\quad \overline{\theta_i}=1-\theta_i,$$

$$\theta_3^{(x)}=\theta(x^2\rho_3^2-z),\quad \overline{\theta_3^{(x)}}=1-\theta_3^{(x)}=\theta(z-x^2\rho_3^2),$$

and L_i can be obtained from $\overline{L_i}$ by the substitution $\rho_4\to\rho_3$, $\rho_2\to 1$. See Ref. 4 for a definition of the variables used.

The term in the first (second) set of square brackets in Eq. (4) is the contribution due to real virtual photon emission by the positron (electron). The terms containing x-dependent θ functions under the integral sign correspond to initial-state corrections, while the rest correspond to final-state corrections.

2. The CALO1 cluster is a cone with angular radius $\delta=0.01$ around the final electron (or positron) momentum direction. If a photon belongs to a cluster, then the whole cluster energy is measured by the detector, and the electron can have any energy. Therefore the limits of integration of $\sigma_{\exp}$ over x are expanded to the interval 0 to 1 in this case. If the photon escapes from the cluster, the event looks the same as in the IES. The above restrictions on the limits of integration over x can be written symbolically as follows:

$$\int_{x_c}^{1} dx + \int_{0}^{x_c} (if\,|\mathbf{r}|<\theta_0)\,dx \equiv \int_{0}^{1} dx - \int_{0}^{x_c} (if\,|\mathbf{r}|>\theta_0)\,dx, \tag{6}$$

where $\mathbf{r}=\mathbf{k}/\omega-\mathbf{q}_1/\varepsilon_1$, and $\omega(\mathbf{k})$ is the energy (transverse momentum) of the hard photon. It is convenient to separate the contributions due to electron and positron emission:

$$\Sigma_1=\Sigma^{\gamma}+\Sigma_{\gamma}, \quad \Sigma^{\gamma}=\Sigma_i+\Sigma_f+\Sigma_i^c+\Sigma_f^c, \quad \Sigma_{\gamma}=\widetilde{\Sigma}_i+\widetilde{\Sigma}_f+\widetilde{\Sigma}_i^c+\widetilde{\Sigma}_f^c. \tag{7}$$

The contributions in Eq. (7) labeled with a superscript c depend on both the shape and size of the cluster, while the rest are universal and are suitable for any cluster.

For calculation of the initial-state corrections, labeled by a subscript i, we use the left-hand side of relation (6), while for the final-state corrections, labeled with a subscript f, we use the right-hand side of this relation.

The quantity Σ_i coincides exactly with the case of IES (see Eq. (4) and the comments following it), while Σ_f looks like the contribution due to final-state electron emission in IES except for expanded limits of integration over x.

It may be written in the following simple form:

$$\Sigma_f=\frac{\alpha}{2\pi}\int_{\rho_2^2}^{\rho_4^2}\frac{dz}{z^2}\left\{-\frac{1}{2}+\int_0^1\left[1-x+\frac{1+x^2}{1-x}\,L_1\right]dx\right\}. \tag{8}$$

To find the additional (cluster-shape-dependent) contributions it is sufficient to use the simplified form of the differential cross section for single photon emission suitable for semi-collinear kinematics. The additional contribution for the initial-state electron emission reads

$$\Sigma_i^c=\frac{\alpha}{2\pi}\int_0^{x_c}\frac{1+x^2}{1-x}\,dx\int\frac{dz}{z^2}\int dz_1\Psi\Phi(z_1,z;\lambda,x), \quad \lambda=\delta/\theta_1. \tag{9}$$

The quantity Φ specifies the limits of integration, and

$$\Psi=[a^2,a_0^2](x^2z_+,x^2)+[b^2,a^2](x^2z_+,x^2z_-)+[b_0^2,b^2](x^2\rho_3^2,x^2z_-),$$

$$z_{\pm}=(\sqrt{z}\pm\lambda(1-x))^2,$$

where the pairs in the square brackets and parentheses give the upper and lower limits of integration over z and z_1, respectively. For wide–narrow angular acceptance

$$a_0=\rho_2, \quad b_0=\rho_4, \quad a=\max(\rho_2,1+\lambda(1-x)), \quad b=\min(\rho_4,\rho_3-\lambda(1-x)).$$

The function Φ under the integral sign in the right-hand side of Eq. (9) is given by

$$\Phi=\frac{2}{\pi}\left(\frac{1}{z_1-xz}+\frac{1}{z-z_1}\right)\arctan\left\{\frac{z-z_1}{(\sqrt{z}-\sqrt{z_1})^2}\,R\right\},$$
$$R=\sqrt{\frac{\lambda^2x^2(1-x)^2-(\sqrt{z_1}-x\sqrt{z})^2}{(\sqrt{z_1}+x\sqrt{z})^2-\lambda^2x^2(1-x)^2}}. \tag{10}$$

The additional contribution due to final-state electron emission may be written as

$$\Sigma_f^c=\frac{\alpha}{2\pi}\int_0^{x_c}\frac{1+x^2}{1-x}\,dx\left[\int_{a_0^2}^{b^2}\frac{dz}{z^2}\left(\ln\left|\frac{x\rho_3^2-z}{\rho_3^2-z}\right|+l_+\right)+\int_{a^2}^{b_0^2}\frac{dz}{z^2}\left(\ln\left|\frac{x-z}{1-z}\right|+l_-\right)\right.$$
$$\left.+\int\frac{dz}{z^2}\int dz_1\Psi F(z_1,z;\lambda,x)\right], \quad l_\pm=\ln\frac{\lambda[2\sqrt{z}\pm\lambda(1-x)]}{z\mp2x\lambda\sqrt{z}-\lambda^2x(1-x)},$$
$$F=\frac{2}{\pi}\left(\frac{1}{z_1-xz}-\frac{1}{z_1-x^2z}\right)\arctan\left\{\frac{(\sqrt{z_1}-x\sqrt{z})^2}{z_1-x^2z}\,R^{-1}\right\}. \tag{11}$$

As to the contribution due to the positron emission, the quantity $\tilde{\Sigma}_i$ is equal to the part in the first square brackets in Eq. (4) which is multiplied by the x-dependent θ functions. To obtain $\tilde{\Sigma}_f$ it is sufficient to expand the limits of integration over x to the interval 0 to 1 for the rest of this part of Eq. (4). The result is

$$\tilde{\Sigma}_f=\frac{\alpha}{2\pi}\int_1^{\rho_3^2}\frac{dz}{z^2}\left[-\frac{1}{2}\,\Delta_{42}+\int_0^1\left((1-x+\frac{1+x^2}{1-x}\,\tilde{L}_1)\Delta_{42}+\frac{1+x^2}{1-x}\right.\right.$$
$$\left.\left.\times(\overline{\theta_4}-\theta_2)\tilde{L}_4\right)dx\right]. \tag{12}$$

The cluster-shape-dependent contribution due to initial positron emission coincides with the right-hand side of Eq. (9) except for the limits of integration over z and z_1 and can be derived by using $\tilde{\Psi}$ instead of Ψ:

$$\tilde{\Psi}=[\tilde{b}^{\,2},\tilde{a}^{\,2}](x^2z_+,x^2\rho_2^2)+[\tilde{c}^{\,2},\tilde{b}^{\,2}](x^2z_+,x^2z_-)+[\tilde{d}^{\,2},\tilde{c}^{\,2}](x^2\rho_4^2,x^2z_-), \tag{13}$$

where

$$\tilde{a}=\max(1,\rho_2-\lambda(1-x)), \quad \tilde{b}=\rho_2+\lambda(1-x),$$
$$\tilde{c}=\rho_4-\lambda(1-x), \quad \tilde{d}=\min(\rho_4+\lambda(1-x),\rho_3).$$

Finally, the quantity $\tilde{\Sigma}_f^c$ may be written as

$$\tilde{\Sigma}_f^c=\frac{\alpha}{2\pi}\int_0^{x_c}\frac{1+x^2}{1-x}\,dx\left[\int_{\tilde{a}^2}^{\tilde{c}^2}\frac{dz}{z^2}\left(\ln\left|\frac{x\rho_4^2-z}{\rho_4^2-z}\right|+l_+\right)+\int_{\tilde{b}^2}^{\tilde{d}^2}\frac{dz}{z^2}\left(\ln\left|\frac{x\rho_2^2-z}{\rho_2^2-z}\right|+l_-\right)\right.$$
$$\left.+\int_1^{\rho_3^2}\frac{dz}{z^2}\,[\,\theta(\tilde{a}^{\,2}-z)-\theta(z-\tilde{d}^{\,2})]\tilde{L}_4+\int\frac{dz}{z^2}\int dz_1\tilde{\Psi}F(z_1,z;\lambda,x)\right]. \qquad (14)$$

For symmetrical angular acceptance one must suppose that $\rho_2=1$, $\rho_4=\rho_3=\rho$. In this case, of course, $\Sigma^\gamma=\Sigma_\gamma$.

3. The CALO2 event selection differs from CALO1 in the shape of the cluster (see Ref. 3). Only the cluster-dependent contributions to Σ_1 will change in this case. The analytical formulas are very cumbersome, and we give the result only for the symmetrical wide–wide case ($\Sigma^\gamma=\Sigma_\gamma$):

$$\Sigma_i^c=\frac{\alpha}{2\pi}\int_0^{x_c}\frac{1+x^2}{1-x}\,dx\int\frac{dz}{z^2}\int dz_1\,\frac{2}{\pi}\left(\frac{1}{z_1-xz}+\frac{1}{z-z_1}\right)$$
$$\times[\Psi_1\Phi_1+\Psi_2\Phi_2+\Psi_3\Phi_3], \qquad (15)$$

$$\Phi_1=\arctan\,Q_i^{(-)}-\arctan\,\eta,\quad \Phi_2=\arctan\,\eta^{-1},\quad \Phi_3=\arctan\frac{1}{Q_i^{(+)}},$$

$$\eta=r_i\cot\frac{\Phi-\delta}{2},\quad r_i=\frac{(\sqrt{z}-\sqrt{z_1})^2}{z-z_1},$$

$$Q_i^{\pm}=r_i\sqrt{\frac{x^2(\sqrt{z}+\sqrt{z_1})^2-(1-x)^2(\sqrt{z_1}\pm x\overline{\lambda})^2}{(1-x)^2(\sqrt{z_1}\pm x\overline{\lambda})^2-x^2(\sqrt{z}-\sqrt{z_1})^2}},$$

$$\Psi_1=[z_3^{(-)},1](x^2J_+^2,x^2z_+)+[(\rho_3-(1-x)\overline{\lambda})^2,z_3^{(-)}](x^2\rho_3^2,x^2z_+),$$

$$\Psi_2=[z_1^{(+)},1](x^2z_+,x^2)+[(\rho_3-(1-x)\overline{\lambda})^2,z_1^{(+)}](x^2z_+,x^2J_-^2)$$
$$+[\rho_3^2,(\rho_3-(1-x)\overline{\lambda})^2](x^2\rho_3^2,x^2J_-^2),$$

$$\Psi_3=[z_1^{(+)},(1+(1-x)\overline{\lambda})^2](x^2J_+^2,x^2)+[\rho_3^2,(1+(1-x)\overline{\lambda})^2](x^2J_-^2,x^2z_-). \qquad (16)$$

The corresponding formula for the contribution due to the final-electron emission reads

$$\Sigma_f^c=\frac{\alpha}{2\pi}\int_0^{x_c}\frac{1+x^2}{1-x}\,dx\left[\int\frac{dz}{z^2}\int dz_1\,\frac{2}{\pi}\left(\frac{1}{z_1-xz}-\frac{1}{z_1-x^2z}\right)[\Psi_1F_1+\overline{\Psi}_2F_2\right.$$
$$+\Psi_3F_3]+\int_1^{z_3^{(-)}}\frac{dz}{z^2}\ln\left|\frac{(x\rho_3^2-z)(J_+^2-z)}{(\rho_3^2-z)(xJ_+^2-z)}\right|+\int_{(1+(1-x)\overline{\lambda})^2}^{\rho_3^2}\frac{dz}{z^2}$$
$$\left.\times\left(\ln\left|\frac{x-z}{1-z}\right|+\overline{l_-}\right)\right]; \qquad (17)$$

TABLE I. The SABS cross section at LEP1 with the first-order QED correction.

x_c	BHLUMI ww	ww	nn	wn
		CALO1		
0.1	166.329	166.285	131.032	134.270
0.3	166.049	166.006	130.833	134.036
0.5	165.287	165.244	130.416	133.466
0.7	161.794	161.749	128.044	130.542
0.9	149.925	149.866	118.822	120.038
		CALO2		
0.1	131.032	130.997	94.666	98.354
0.3	130.739	130.705	94.491	98.127
0.5	130.176	130.141	94.177	97.720
0.7	127.528	127.491	92.981	95.874
0.9	117.541	117.491	86.303	87.696

$$F_1=\arctan\frac{1}{Q_f^{(-)}},\quad F_2=\arctan\,\zeta,\quad F_3=\arctan\,Q_f^{(+)},\quad \zeta=r_f\cot\frac{\Phi-\delta}{2},$$

$$r_f=\frac{(\sqrt{z_1}-x\sqrt{z})^2}{z_1-x^2z},\quad \overline{l_-}=l_-(\lambda\to\overline{\lambda}),\quad Q_f^{(\pm)}=\frac{r_f}{r_i}Q_i^{(\pm)},\quad \sin\,\delta=\sqrt{\frac{z_1}{z}}\sin\,\Phi,$$

$$\overline{\Psi}_2=[z_1^{(+)},1](x^2J_+x^2)+[z_3^{(-)},z_1^{(+)}](x^2J_+^2,x^2J_-^2)+[\rho_3^2,z_3^{(-)}](x^2\rho_3^2,x^2J_-^2). \qquad (18)$$

The quantities Φ and $\overline{\lambda}$ in Eqs. (15)–(18) specify the shape and size of the CALO2 cluster, namely

$$\Phi=\frac{3\pi}{32},\quad \overline{\lambda}=\frac{\theta_0}{\theta_1},\quad \theta_0=\frac{0.051}{16}.$$

Finally, the functions $J_\pm$ and $z_i^{(\pm)}$ are defined as follows:

$$J_{(\pm)}=\frac{1}{\beta}\left[\sqrt{z\beta-x^2(1-x)^2\overline{\lambda}^2\,\sin^2\,\Phi}\pm(1-x)\overline{\lambda}\left(1-2x\,\sin^2\frac{\Phi}{2}\right)\right],$$

$$\beta=1-4x(1-x)\sin^2\frac{\Phi}{2},\quad z_i^{(\pm)}=(\rho_i\pm(1-x)\overline{\lambda})^2-4x(1-x)\rho_i(\rho_i\pm\overline{\lambda})\sin^2\frac{\Phi}{2}.$$

The results of calculations of the QED correction with the vacuum polarization switched off are shown in Table I for three different angular acceptances: symmetrical wide–wide and narrow–narrow and asymmetrical wide–narrow. For comparison we give also the corresponding numbers obtained using the Monte Carlo (MC) program BHLUMI[3] for the symmetrical wide–wide case.

As one can see from Table I, there is an approximately constant difference, at a level of 0.3 per thousand, between our analytical results and the MC results within the first-order correction. A possible cause of this effect is as follows. In our calculation we

systematically ignore terms containing $\theta^2 \simeq |t|/s$ as compared with unity. But it is well known that terms of this kind have double-logarithmic asymptotic behavior and are parametrically equal to $(\alpha|t|/\pi s)\ln^2(|t|/s)$, which is 0.1 per thousand for the conditions at LEP1. We note that the MC program BHLUMI takes into account all the first-order contributions.[5]

The author thanks E. Kuraev and A. Arbuzov for discussions and for critical remarks and V. Yu. Gontchar for help in the numerical calculation. This study was supported by INTAS Grant 93-1867.

[a)]e-mail: kfti@rocket.kharkov.ua

---

[1] *Neutrino Counting in Z Physics at LEP*, G. Barbiellini *et al.*, L. Trentadue (conv.); G. Altarelli, R. Kleiss, and C. Verzegnassi eds., CERN Report 89-08.
[2] S. Jadach, M. Skrzypek, and B. F. L. Ward, Phys. Rev. D **47**, 3733 (1993); S. Jadach *et al.*, Phys. Lett. B **353**, 349, 362 (1995); A. B. Arbuzov *et al.*, Zh. Eksp. Teor. Fiz. **108**, 1164 (1995) [JETP **81**, 638 (1995)]; G. Montanga *et al.*, Nucl. Phys. B **401**, 3 (1993).
[3] *Events Generator for Bhabha Scattering*, H. Anlauf *et al.*, Conveners: S. Jadach and O. Nicrosini, Yell. Rep. CERN 96-01, Vol. 2, p. 229.
[4] A. B. Arbuzov *et al.*, Preprint CERN-TH/95-313, UPRF-95-438.
[5] S. Jadach and B. F. L. Ward, Phys. Rev. D **40**, 3582 (1989).

Published in English in the original Russian journal. Edited by Steve Torstveit.

Effect of time reversal in the magnetization of an atom by a resonant light pulse

A. I. Alekseev
Moscow State Engineering-Physics Institute, 115409 Moscow, Russia

(Submitted 2 December 1996)
Pis'ma Zh. Éksp. Teor. Fiz. **65**, No. 3, 231–236 (10 February 1997)

It is shown that the even dependence of the light-induced magnetic moment on the detuning $\omega-\omega_{ba}$ from resonance in the case of a circularly polarized pulse and an isotropic initial state of the atom and the odd dependence on $\omega-\omega_{ba}$ in the case of a linearly polarized pulse and an anisotropic initial state in the form of alignment of the atom are consequences of the symmetry under time reversal $t\rightarrow -t$ and of the initial conditions at time $t=0$. In a number of cases, this fundamental law makes it possible to determine the vector properties of a light-induced magnetic moment and its dependence on the time t and $\omega-\omega_{ba}$ without solving the equation for the density matrix in detail and without calculating the sum over the projections of the angular momenta in the formula for the magnetization of an atom by light.
 [S0021-3640(97)00203-X]

PACS numbers: 32.10.Dk, 32.90.+a

1. For an atom in an electromagnetic field described by the vector potential $\mathbf{A}(\mathbf{r}, t)$ with a zero scalar potential, symmetry under time reversal holds if when

$$t\rightarrow -t, \quad \mathbf{A}(\mathbf{r},-t)\rightarrow -\mathbf{A}(\mathbf{r},t), \tag{1}$$

which leaves the electric field $\mathbf{E}(\mathbf{r}, t)$ unchanged and changes the sign of the magnetic field $\mathbf{H}(\mathbf{r},t)$. This symmetry is expressed in the fact that after the transformation (1) is carried out and the wave function Ψ is replaced by its complex conjugate Ψ^*, the Schrödinger equation remains unchanged in the absence of a static magnetic field.[1] The electric current density in the atom, taking account of electron spin, changes sign. Therefore the magnetic moment of the atom also changes sign but remains constant in magnitude.

2. Let the atom interact over the time interval $0\leqslant t\leqslant \tau$ with the electric field of a resonant circularly polarized pulse

$$\mathbf{E}(\mathbf{r},t)=\mathbf{l}_{\mathbf{k}\lambda}a(t')\exp[i(\mathbf{k}\cdot\mathbf{r}-\omega t)]+\text{c.c.}, \tag{2}$$

where

$$\mathbf{l}_{\mathbf{k}\lambda}\cdot\mathbf{l}^*_{\mathbf{k}\lambda'}=\delta_{\lambda\lambda'}, \quad \mathbf{l}_{-\mathbf{k}\lambda}=\mathbf{l}^*_{\mathbf{k}\lambda}, \quad t'=t-\mathbf{k}\cdot\mathbf{r}/\omega,$$

$\mathbf{l}_{\mathbf{k}\lambda}$ is a right-hand circular polarization vector if $\lambda=1$ and a left-hand circular polarization vector if $\lambda=-1$, $a(t')$ is a real amplitude, which is a slowly varying function compared with $\exp[i(\mathbf{k}\cdot\mathbf{r}-\omega t)]$, and $t=0$ is the moment at which the leading edge of the

pulse (2) arrives at the location $\mathbf{r}=0$ of the center of mass of the atom (nucleus). The frequency ω is close to the dipole transition frequency $\omega_{ba}=(E_b-E_a)\hbar^{-1}$, where E_a and E_b are the energies of the ground and excited states of the atom, respectively. Besides the energies, the ground state of an atom with zero nuclear spin is characterized by the quantum numbers J_a and J_b of the angular momentum $\mathbf{J}$ and its projections M_a and M_b on the quantization axis. The duration τ of the pulse (2) is short compared with the radiative lifetime of the excited state, so that relaxation can be neglected. In the center-of-mass frame the evolution of the atom is described by the density matrix $\rho=\Psi^*(q',t)\Psi(q,t)$, where q is a set of variables describing the state of the atom. In the dipole approximation the density matrix $\rho=\rho(q',q,t)$ satisfies the equation

$$\frac{\partial\rho}{\partial t}=\frac{i}{\hbar}[H_0'-\mathbf{d}'\cdot\mathbf{E}(0,t)-H_0+\mathbf{d}\cdot\mathbf{E}(0,t)]\rho, \tag{3}$$

where H_0 is the Hamiltonian and $\mathbf{d}$ is the dipole moment operator of the free atom. Initially, at $t=0$, prior to the arrival of the pulse (2), the atom is in an isotropic state, which in the JM representation is described by the density matrix $\rho=\rho(t)$ at $t=0$ with the components

$$\rho_{M_bM_a}(0)=\rho_{M_bM_b'}(0)=0, \quad \rho_{M_aM_a'}(0)=(2J_a+1)^{-1}\delta_{M_aM_a'}. \tag{4}$$

The magnetic moment of the atom in the JM representation is calculated according to the formula

$$\vec{\mu}(t)=-\mu_B\mathrm{Tr}(g\rho\mathbf{J}), \tag{5}$$

where μ_B the Bohr magneton and g is the gyromagnetic factor.

If the amplitude $a(t)$ is an even function of time, $a(-t)=a(t)$, then giving it in the region $0\leqslant t\leqslant\infty$ in the form $a(t)$ for $0\leqslant t\leqslant\tau$ and $a(t)=0$ for $\tau<t\leqslant\infty$ is equivalent to giving this amplitude on the entire time axis $-\infty\leqslant t\leqslant\infty$. Then the field $\mathbf{E}(0,t)$ in Eq. (3) is also defined in the region $-\infty\leqslant t\leqslant\infty$ and remains unchanged under the simultaneous operations

$$t\rightarrow -t, \quad \mathbf{k}\rightarrow -\mathbf{k}. \tag{6}$$

If $a(t)$ in the given interval $0\leqslant t\leqslant\tau$ depends on t arbitrarily and if $a(t)=0$ for $\tau<t\leqslant\infty$, then formally we define the amplitude $a(t)$ on the negative time axis $-\infty\leqslant t\leqslant 0$ as $a(t)=a(-t)$ for $-\tau\leqslant t\leqslant 0$ and $a(t)=0$ for $-\infty\leqslant t\leqslant-\tau$. For an atom in the field Eq. (2) with $\mathbf{r}=0$, symmetry with respect to time reversal holds, just as in the case of Eq. (1). Then the Schrödinger equation with the Hamiltonian $H_0-\mathbf{d}\cdot\mathbf{E}(0,t)$ remains unchanged after the operations (6) and $\Psi\rightarrow\Psi^*$. Equation (3) is also unaffected by the operations (6) and $\rho\rightarrow\rho^*$. However, the magnetic moment of the atom (5) changes sign: $\vec{\mu}(-t)=-\vec{\mu}(t)$. This property of the magnetic moment was obtained without using the initial conditions (4). At the same time, in the present problem the time $t=0$ is the initial moment at which the atom first interacts with the field (2) in the interval $0\leqslant t\leqslant\tau$. Therefore, here, in the presence of symmetry under time reversal the reference point $t=0$ on the time axis in Eq. (6) is a physically distinguished moment in time. If the magnetic moment (5) is calculated in the nonstationary regime with the aid of Eqs.

(3)–(5), then besides the property $\vec{\mu}(-t)=-\vec{\mu}(t)$ mentioned above, other characteristics of $\vec{\mu}(t)$, which are due to symmetry under time reversal (6) and the initial conditions at $t=0$, can be found.

From the symmetry of the atom in the field of a circularly polarized pulse (2) it follows, with allowance for Eq. (4), that the light-induced magnetic moment (5) is proportional to the only axial vector in this case,

$$i\mathbf{l}_{\mathbf{k}\lambda}\times\mathbf{l}^{*}_{\mathbf{k}\lambda}=(\mathbf{k}/k)\lambda\beta, \tag{7}$$

where β is a unit pseudoscalar, equal to $\beta=1$ in a right-handed and -1 in a left-handed coordinate system. Furthermore, solving the operator equation (3), taking account of Eq. (4) according to second-order perturbation theory in $\mathbf{E}(0,t)$, we show that for $0\leqslant t\leqslant\tau$ the density matrices in the ground and excited states exhibit the same dependence on the time t and the detuning $\Delta=\omega-\omega_{ba}$, as described by the integral $I(t)$ in the form

$$\rho_{M_aM'_a}(t)=R_{M_aM'_a}I(t)+\text{h.c.},\quad \rho_{M_bM'_b}(t)=R_{M_bM'_b}I(t)+\text{h.c.}, \tag{8}$$

where

$$I(t)=\int_0^t d\tau_2\int_0^{\tau_2}d\tau_1 a^{*}(\tau_2)a(\tau_1)\exp[i\Delta(\tau_2-\tau_1)],$$

$R_{M_aM'_a}$ and $R_{M_bM'_b}$ are matrices. If the matrices (8) are substituted into Eq. (5), then the magnetic moment $\vec{\mu}(t)$ separates into a sum of terms which are proportional to $I(t)$ or $I^{*}(t)$. These terms must contain $I(t)$ and $I^{*}(t)$ in a combination so that the equality $\vec{\mu}(-t)=-\vec{\mu}(t)$ holds after the operations (6). Hence it follows that, on account of Eq. (7), the desired vector $\vec{\mu}(t)$ is proportional to the sum $I(t)+I^{*}(t)$. Therefore, taking account of Eqs. (7) and (8), the magnetic moment (5) can be represented in the form

$$\vec{\mu}(t)=-(\mathbf{k}/k)\lambda\beta M_0X_0(t,\Delta), \tag{9}$$

where

$$X_0(t,\Delta)=(\tau a_0)^{-2}[I(t)+I^{*}(t)], \tag{10}$$

a_0 is the maximum value of $|a(t)|$ in the prescribed interval $0\leqslant t\leqslant\tau$, M_0 is a constant with dimensions of magnetic moment and depends on the characteristics of the resonance transition, and $X_0(t,\Delta)$ is a universal function of the time t and the detuning $\Delta=\omega-\omega_{ba}$ and does not depend on the atomic characteristics.

The vector properties of $\vec{\mu}(t)$ in Eq. (9) are determined by the symmetry of the atom in the field of the circularly polarized pulse (2) with the initial conditions (4); this leads to the axial vector (7). At the same time, $\vec{\mu}(t)$ is an even function of Δ because of the symmetry under time reversal (6) in the presence of the axial vector (7). The constant M_0 is determined by a detailed calculation of the density matrices (8) in solving Eq. (3) together with Eq. (4) and the subsequent summation in Eq. (5) over the projections of the angular momenta of the atom in the ground and excited states. The characteristics of $\vec{\mu}(t)$ obtained with a more complicated dependence on t and Δ remain valid outside of perturbation theory for an ultrashort, square, circularly polarized pulse; this follows from an exact solution of the problem in the absence of relaxation.[2]

3. We shall now consider the magnetization of an atom by a resonant linearly polarized pulse:

$$\mathbf{E}(\mathbf{r},t)=\mathbf{l}_{\mathbf{k}}a(t')\exp[i(\mathbf{k}\cdot\mathbf{r}-\omega t)]+\text{c.c.}, \tag{11}$$

where $\mathbf{l}_{\mathbf{k}}$ is a unit polarization vector, which is not affected by reversal of the wave vector $\mathbf{k}\rightarrow-\mathbf{k}$. The other physical quantities in Eq. (11) are the same as in Eq. (2). Since the pulse (11) does not magnetize an atom in the isotropic initial state (4), let us assume that prior to the interaction with the pulse (11) the atom was optically polarized by a strong, linearly polarized, resonant pulse with vector $\mathbf{k}_0$, which is collinear to $\mathbf{k}$, and unit polarization vector $\mathbf{l}_0$, which is not affected by the operation $\mathbf{k}_0\rightarrow-\mathbf{k}_0$. Then the initial conditions for Eq. (3) in the JM representation have the form

$$\rho_{M_bM_a}(0)=\rho_{M_bM_b'}(0)=0, \quad \rho_{M_aM_a'}(0)=\rho^{al}_{M_aM_a'}, \tag{12}$$

where the density matrix $\rho^{al}_{M_aM_a'}$ describes the initial optical polarization of the atom, called alignment (see, for example, Ref. 3). Here the alignment of the atom is characterized by two orthogonal symmetry axes, the first of which is directed along $\mathbf{l}_0$ and the second is collinear to $\mathbf{k}_0$. In this case, when the atom interacts with the pulse (11), there exists a unique axial vector which corresponds to the given symmetry and determines the direction of the magnetic moment (5). This vector has the form

$$\mathbf{l}_0\times\mathbf{l}_{\mathbf{k}}=(\mathbf{k}/k)\sin\,\varphi_{\mathbf{k}}, \tag{13}$$

where the positive direction of the angle $\varphi_{\mathbf{k}}$ is from the unit vector $\mathbf{l}_0$ to the unit vector $\mathbf{l}_{\mathbf{k}}$ (clockwise when viewed along $\mathbf{k}$). Therefore, under the operation $\mathbf{k}\rightarrow-\mathbf{k}$, we have $\varphi_{-\mathbf{k}}=-\varphi_{\mathbf{k}}$, so that the angle $\varphi_{\mathbf{k}}$ is a pseudoscalar. Furthermore, only one of the two orthogonal symmetry axes possesses the prescribed direction $\mathbf{l}_0$; the direction of the second axis is not fixed (all orientations are equally good). The direction of the third axis, which is orthogonal to the two axes indicated above, is also not fixed and all directions are equally good. Hence it follows that for a prealigned atom the magnetic moment (5) should not change when $\mathbf{l}_{\mathbf{k}}$ is chosen to be parallel or antiparallel to the third axis. The rotation angles $\varphi_{\mathbf{k}}=\pi/2$ and $\varphi_{\mathbf{k}}=-\pi/2$ correspond to these two directions of $\mathbf{l}_{\mathbf{k}}$. Invariance of the magnetic moment (5) under such rotations under the conditions of the present symmetry is attained after the axial vector (13) is multiplied by $\cos\varphi_{\mathbf{k}}$. Therefore the desired magnetic moment (5) in the case at hand is proportional to the following axial vector:

$$(\mathbf{k}/k)\sin(2\varphi_{\mathbf{k}}). \tag{14}$$

For the initial conditions (12), the dependence of the density matrices (8) on t and Δ remains in force for other values of $R_{M_aM_a'}$ and $R_{M_bM_b'}$ than those in Eq. (4). We also take account of the fact that for a prealigned atom in the field of a linearly polarized pulse (11) symmetry under time reversal (6) holds and leads to the equality $\vec{\mu}(-t)=-\vec{\mu}(t)$. This equality is possible only if, after the density matrices (8) are substituted into Eq. (5), the quantities $I(t)$ and $I^*(t)$ appear in $\vec{\mu}(t)$ in the form of the real combination $i[I^*(t)-I(t)]$. Finally, the magnetic moment (5) for a prealigned atom has the form

$$\vec{\mu}(t)=-(\mathbf{k}/k)\sin(2\varphi_{\mathbf{k}})M_2X_2(t,\Delta), \tag{15}$$

where

$$X_2(t,\Delta)=i(\tau a_0)^{-2}[I^*(t)-I(t)].$$

Here the constant M_2, which has dimensions of a magnetic moment, is calculated by summing in Eq. (5) over the projections of the angular momenta. The subscript 2 on the constant M_2 and on the universal function $X_2(t,\Delta)$ was chosen so as to coincide with the rank of the polarization multipole moment characterizing the alignment of the atom in Eq. (12). The vector properties of the magnetic moment in Eq. (15) are determined by the symmetry of the interaction of a prealigned atom with the linearly polarized pulse (11). At the same time, the odd dependence on Δ in Eq. (15) is due to the symmetry under time reversal (6) in the presence of the initial conditions (12), which lead to the axial vector (14).

4. The following general law follows from what has been said above. If the magnetic moment $\vec{\mu}(t)$ induced by the resonant light pulse is proportional to the axial vector (7), then it is an even function of the detuning Δ with a maximum at $\Delta=0$. If $\vec{\mu}(t)$ is proportional to an axial vector, which is invariant under the operation $\mathbf{k}\rightarrow-\mathbf{k}$, then $\vec{\mu}(t)$ is an odd function of Δ with a maximum at $0<|\Delta|$. This law is fundamental, since it is a consequence of the symmetry of the atom in the field of a resonant light pulse (2) or (11) as well as the symmetry under time reversal (6) with allowance for the initial conditions at $t=0$. In many cases this law makes it possible to determine the vector properties of the magnetic moment (5) and its dependence on t and Δ to within a common factor with dimensions of magnetic moment, without performing detailed perturbation-theory calculations.

If the amplitude $a(t)$ is an odd function of time $a(-t)=-a(t)$, then specifying it in the region $0\leqslant t\leqslant\infty$ is equivalent to specifying its amplitude on the entire time axis $-\infty\leqslant t\leqslant\infty$. However, it must enter in Eqs. (2) and (11) in the form $a(t)\exp(i\pi/2)$ or $a(t)\exp(-i\pi/2)$ in order that the operations (6) not change the electric fields (2) and (11). In this case the foregoing arguments and Eqs. (9) and (15) with the integral $I(t)$ remain in force after the operations $a(t)\rightarrow a(t)\exp(\pm i\pi/2)$.

5. Let the center of mass of the atom in the laboratory coordinate system be located at time t at the point $\mathbf{r}$ in some volume. The leading edge of the circularly polarized pulse (2) crosses the boundary point $\mathbf{r}_0$ of this volume at time t_0 and reaches the location $\mathbf{r}$ of the atom at time t. The propagation of a circularly polarized pulse (2) in this volume is described by the formula

$$\mathbf{E}(\mathbf{r},t)=\mathbf{l}_{\mathbf{k}\lambda}a(t')\exp(-i\omega t')+\text{c.c.},\tag{16}$$

where

$$t'=t-t_0-\mathbf{k}\cdot(\mathbf{r}-\mathbf{r}_0).\tag{17}$$

Here the amplitude $a(t')$ is given for $0\leqslant t'\leqslant\tau$ and $a(t')=0$ for $\tau<t'\leqslant\infty$ and it is defined on the entire time axis $-\infty\leqslant t'\leqslant\infty$ in analogy with the discussion in Sec. 2. The leading edge of the pulse (16) crosses the center of mass of the atom with zero argument of the ampltude $a(t')$ and zero phase $-i\omega t'=0$, just as in the case (2). If the atom at the point $\mathbf{r}$ possesses a velocity $\mathbf{v}$ at time t, then its state is described by the equation

$$\left(\frac{\partial}{\partial t}+\mathbf{v}\cdot\nabla\right)\rho=\frac{i}{\hbar}[H_0'-\mathbf{d}'\cdot\mathbf{E}(\mathbf{r},t)-H_0+\mathbf{d}\cdot\mathbf{E}(\mathbf{r},t)]\rho, \tag{18}$$

which remains unchanged under the simultaneous operations

$$t\to -t,\quad t_0\to -t_0,\quad \mathbf{k}\to -\mathbf{k},\quad \rho\to\rho^*,\quad \mathbf{v}\to -\mathbf{v}. \tag{19}$$

Therefore, for an atom moving with velocity $\mathbf{v}$, there exists a symmetry with respect to time reversal (19) accompanied by the operation $t'\to -t'$. In accordance with Eqs. (16) and (17), the density matrix ρ is a function of t', and the leading edge of the pulse (16) crosses the center of mass of the atom at time $t=t_0+\mathbf{k}\cdot(\mathbf{r}-\mathbf{r}_0)$ or $t'=0$. In addition, the initial value $\rho=\rho(t')$ at $t'=0$ has the form (4). Repeating the arguments leading up to Eqs. (7)–(10), we find, taking account of the Doppler shift $\mathbf{k}\cdot\mathbf{v}$ of the frequency ω, that the magnetic moment (5) of a moving atom is given by expression (9) with the operations

$$t\to t',\quad \Delta\to\Delta-\mathbf{k}\cdot\mathbf{v}. \tag{20}$$

The linearly polarized pulse (11) in the given volume has the form (16) after the operation $\mathbf{l}_{\mathbf{k}\lambda}\to\mathbf{l}_{\mathbf{k}}$. It induces in the moving atom a magnetic moment given by Eq. (15) with the operations (20).

Let us now apply the above results to a gas of identical atoms located in the indicated volume. Then we find that the magnetization $\vec{\mu}_q(t')$ induced in the gas by circularly or linearly polarized pulses is given by

$$\vec{\mu}_q(t')=-\mathbf{L}_q N M_q\int f(v)X_q(t',\Delta-\mathbf{k}\cdot\mathbf{v})d\mathbf{v}, \tag{21}$$

where

$$q=0,2,\quad \mathbf{L}_0=(\mathbf{k}/k)\lambda\beta,\quad \mathbf{L}_2=(\mathbf{k}/k)\sin(2\varphi_{\mathbf{k}}),$$

N is the density of atoms, $f(v)$ is Maxwell's distribution, and t' is the time with allowance for the delay of the wave, as defined in Eq. (17). Under the time reversal (19) the equality $\vec{\mu}_q(-t')=-\vec{\mu}_q(t')$ holds, and the quantity $\vec{\mu}_q(t')$ is an even (for $q=0$) or odd (for $q=2$) function of the detuning Δ, just as in the case (9) and (15).

In the experiments with a gas[4] and a solid[5] the light-induced magnetization was measured in relative units. If the experimental method of those studies[4,5] is used, then the constants M_0 and M_2, which were not calculated, do not affect the investigation of the vector properties of the light-induced magnetization (21) and its dependence on t' and Δ in the time interval $0\leqslant t'\leqslant\tau$.

[1] L. D. Landau and E. M. Lifshitz, *Quantum Mechanics: Non-Relativistic Theory*, 3rd edition, Pergamon Press, New York, 1977 [Russian original, Nauka, Moscow, 1974].
[2] A. I. Alekseev, Opt. Spektrosk. **75**, 842 (1993) [Opt. Spectrosc. **75**, 499 (1993)].
[3] A. I. Alekseev, Zh. Eksp. Teor. Fiz. **106**, 1319 (1994) [JETP **79**, 714 (1994)].
[4] A. A. Dabagyan, M. E. Movsesyan, and R. E. Movsesyan,JETP Lett. **29**, 534 (1979).
[5] R. G. Usmanov and E. P. Khaĭmovich, Opt. Spektrosk. **79**, 378 (1995) [Opt. Spectrosc. **79**, 348 (1995)].

Translated by M. E. Alferieff

Nonlinear effects in a two-dimensional electron gas with a periodic lattice of scatterers

G. M. Gusev, Z. D. Kvon, A. G. Pogosov, and M. M. Voronin
Institute of Semiconductor Physics, 630090 Novosibirsk, Russia

(Submitted 3 December 1996)
Pis'ma Zh. Éksp. Teor. Fiz. **65**, No. 3, 237–241 (10 February 1997)

The magnetoresistance of two-dimensional (2D) electrons in a periodic lattice of antidots is found to be substantially influenced by an applied electric field. The non-Ohmic behavior of the resistance in the region of commensurability oscillations originates from the electric-field-induced breakdown of the trajectories skipping along the lattice arrays. In the region of magnetic fields where the cyclotron diameter is less than the distance between antidots the breakdown of the orbits skipping around antidots is responsible for the nonlinear behavior of the magnetoresistance. © *1997 American Institute of Physics.*
[S0021-3640(97)00303-4]

PACS numbers: 73.61.Ey, 72.20.My

The transport of a 2D electron gas in a periodic lattice of antidots has been actively investigated in the last few years. One of the most interesting features of this system is the commensurability oscillations of the magnetoresistance, which have been observed and studied in a number of works.[1–4] In Ref. 2 a ''pinball'' model was proposed, which explained these oscillations as being due to the existence of electron cyclotron orbits which do not collide with antidots at certain magnetic fields. It was later shown[4,5] that this model cannot explain all of the features of the magnetoresistance. In Ref. 3 the diffusion coefficient in a magnetic field was calculated by means of numerical simulations of chaotic dynamics of electron in the lattice of antidots. These calculations were able to account for all the features of the commensurability oscillations of the magnetoresistance. Moreover, it was shown in Ref. 3 that the cause of these oscillations is the appearance of electron trajectories which skip along the lattice arrays. In addition, the model of dynamical chaos predicts some other interesting effects—for example, non-Ohmic behavior of magnetoresistance. In the present work the influence of high electric fields on the electron transport in a periodic lattice of antidots is investigated.

The test samples were Hall bars based on the 2D electron gas in a GaAs/AlGaAs heterojunction ($\mu = 2 \cdot 10^5$ cm^2/V·s, $n_s = 4.5 \cdot 10^{11}$ cm^{-2}). The distance between potential probes was 500 μm, and the width of the device was 200 μm. The part of the sample between the potential probes was covered by a lattice of antidots created by electron beam lithography and reactive ion etching. Samples with different lattice periods, $d = 0.6$, 0.7, 0.8, 0.9 and 1.3 μm, were investigated. The antidot diameter was about $2a = 0.15–0.2$ μm. The magnetoresistance was measured by the four-terminal method using an ac bridge operating at 70–700 Hz in magnetic fields up to 0.8 T at temperatures 1.3–4.2 K. In order to measure nonlinear effects a dc electric field E up to 7 V/cm was

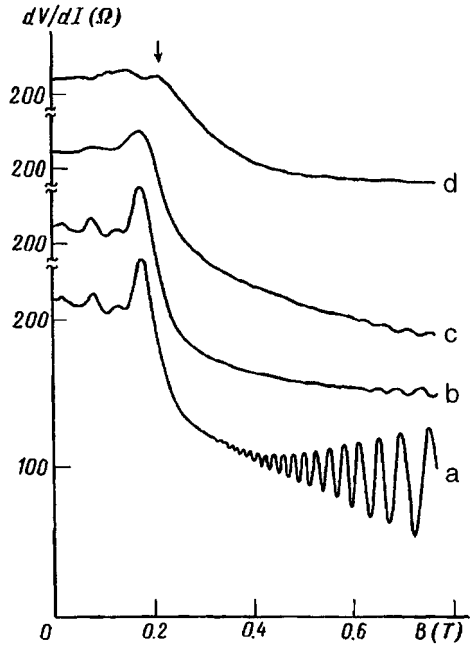

FIG. 1. The magnetoresistance of the sample with $d=1.3$ μm as a function of magnetic field for different values of applied dc electric field E and lattice temperature T_L: a—$T_L=1.3$ K, $E=0$ V/cm; b—$T_L=4.2$ K, $E=0$ V/cm; c—$T_L=1.3$ K, $E=0.76$ V/cm; d—$T_L=1.3$ K, $E=2.4$ V/cm.

applied. The amplitude of the ac electric field on which the signal was measured was less than 0.03 V/cm. Thus, the differential magnetoresistance of the samples was measured experimentally as a function of applied electric field E.

The magnetoresistance traces for the sample with the lattice period $d=1.3$ μm at different lattice temperatures and applied electric fields are shown in Fig. 1. Comparison of curves *a* and *b* in Fig. 1 shows that at low values of E the amplitude of the Shubnikov–de Haas (SdH) oscillations decreases with temperature, while the amplitude of the commensurability oscillations remains unchanged. This result is consistent with Ref. 2, where it was shown that the commensurability oscillations do not depend on temperature up to 50 K. As the applied electric field is increased to 0.8 V/cm, the amplitude of the SdH oscillations falls to a value corresponding to a temperature of 4.2 K, and the amplitude of the commensurability oscillations falls by a factor of two (curve c). In a stronger applied electric field the commensurability oscillations disappear, and in the region of magnetic fields where $2R_c<d$ the resistance increases (curve d in Fig. 1), and an additional small maximum (marked by an arrow on the curve) appears, which was not present at lower electric fields.

It should be noted that an applied electric field increases the electron temperature T_e above the lattice temperature T_L (the overheating of the lattice is negligible). The electron temperature can be determined from the SdH oscillations, and for the curve (c) in Fig. 1 it is about $T_e=4.2$ K, as is seen from a comparison of the SdH oscillations.

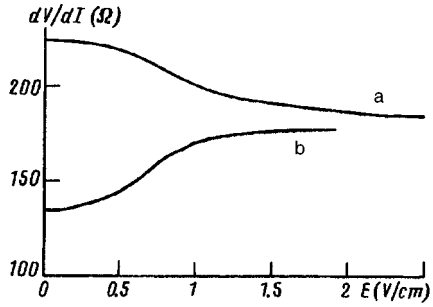

FIG. 2. The resistance of the sample with $d=1.3$ μm as a function of applied electric field E for two different values of the magnetic field B: a—$B=0.17$ T ($2R_c=d$)—commensurability maximum; b—$B=0.27$ T ($2R_c<d-2a$)—corresponds to rosette-like orbits.

However the commensurability oscillations on curve c in Fig. 1 are strongly suppressed in comparison with curve b. This leads to the conclusion that the suppression of commensurability oscillations is not due to heating effects.

The sample resistance as a function of E is presented in Fig. 2 for two different values of the magnetic field. One can see that for magnetic fields satisfying the commensurability condition $2R_c=d$ (curve a) the resistance decreases with E, whereas for stronger magnetic fields it increases with E (curve b). It is also seen that at low and high electric field both curves reach saturation. The same behavior was observed for all of the samples tested. From the dependence of the magnetoresistance on E we determine the electric field $E_{1/2}$ at which the commensurability oscillations are suppressed to half their magnitude. The values of $E_{1/2}$ for the magnetoresistance maximum at $2R_c=d$ are shown in Fig. 3a for the samples with different lattice periods. One can see that $E_{1/2}$ falls off with increasing d roughly according to $E_{1/2}\propto d^{-2}$.

As was mentioned above, there are two models explaining the magnetoresistance maxima in Fig. 1. One of them is based on the presence of ''running trajectories'' that skip along the lattice arrays and which are responsible for the maximum in the diffusion coefficient and, consequently, in the resistance (for the magnetic fields under consideration we have $\sigma_{xy}>\sigma_{xx}$, and the maximum in σ_{xx} therefore corresponds to a maximum in ρ_{xx}). The other explanation involves pinned orbits which do not collide with antidots. It is important that the running trajectories are substantially more sensitive to the initial conditions and to possible distortion of the electron orbit. An applied electric field leads to drift of the cyclotron orbit. For the running trajectories a relatively small drift is sufficient to shift them off the region of stability and therefore break the stable running motion. The critical drift distance l_d during the time between two successive collisions with antidots is in any case considerably smaller than the antidot radius a. Precise estimation of the drift distance l_d necessary for breaking the running trajectories and of the dependence of l_d on the lattice period d requires more-detailed theoretical study of the region of stability of the running trajectories. On the other hand, in order to break the pinned orbit with $2R_c=d$ (corresponding to the main commensurability maximum) the

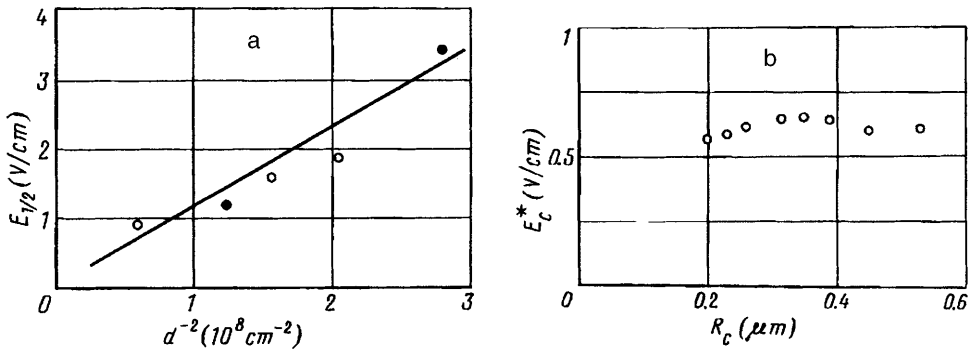

FIG. 3. a: The electric field $E_{1/2}$ resulting in the suppression of the main commensurability oscillation (in a magnetic field satisfying the condition $2R_c=d$) to half its value, measured for the samples with different d as a function of d^{-2}. The solid line is drawn as a guide to the eye. b: The experimental dependence of the critical field E_c^* corresponding to breakdown of the trajectories skipping around antidots on the cyclotron radius R_c for the sample with lattice period $d=1.3$ μm.

average drift over the time $\tau\sim 2\pi/\omega_c$ ($\omega_c=eH/mc$) should be of the order $l_d\sim d/2-a$.

One can estimate l_d from the experimentally measured value of the critical field $E_{1/2}$: $l_d=\pi v_d/\omega_c$ ($v_d=cE_{1/2}/H$ is the drift velocity). At a lattice period $d=1.3$ μm, l_d is 0.003 μm. This value is significantly smaller than the radius of an antidot. Therefore, taking into account the above discussion, one can conclude that the model based on the running trajectories more likely explains the main commensurability maximum at $2R_c\approx d$, and the breaking of these trajectories by an applied electric field leads to the experimentally observed suppression of the commensurability oscillations.

At higher magnetic field when $2R_c<d-2a$ the magnetoresistance also exhibits nonlinear dependence on the electric field. This dependence has the opposite sign from that in the region of commensurability oscillations described above. This behavior of the magnetoresistance can be explained on the assumption that in this region of magnetic fields the electrons move on rosette-like orbits skipping around antidots. These electrons are localized and do not contribute to the conductivity. But a high electric field (above a certain critical value E_c^*) results in breakdown of the localized motion due to the drift of the cyclotron orbit by analogy with the trajectories that skip along the arrays. It leads to an increase in the conductivity and resistance of the samples and thus affects the experimental dependence of the magnetoresistance on the electric field (Fig. 1).

The experimental dependence of E_c^* on R_c is shown in Fig. 3b. One can see that the critical field E_c^* does not depend on the cyclotron radius. Theoretical support for this fact as well as the numerical estimation of E_c^* requires further theoretical consideration.

It should be noted that the electron orbits corresponding to the condition $2R_c=d-2a$ show a threshold behavior for the applied electric field. For higher B a delocalization of the electrons by the electric field is observed, but for lower B the electron trajectories become diffusive. Thus a new maximum in the resistance at high electric fields is observed, as indicated above (Fig. 1). The corresponding value of the antidot

radius a is consistent with the measurement of a by other methods.[5]

Thus in the present work the magnetoresistance of 2D periodic lattices of antidots with a wide variety of periods has been found to exhibit nonlinear behavior in the applied electric field. Analysis of the results within the framework of dynamical chaos theory shows that the model of runaway electron trajectories can explain the suppression of the main commensurability maximum by the applied electric field for all of the samples tested. In higher magnetic fields the nonlinear effects are connected with breaking of the localized rosette motion. More-detailed comparison of some of our findings (such as the values of the critical electric fields for breaking of the regular motion and their dependence on the lattice period) with the theory requires further theoretical study of the region of stability of the runaway and rosette-like orbits.

We thank E. M. Baskin and M. V. Entin for helpful discussions. This study was supported by the Russian Fund for Fundamental Research (Grants 95-02-04583a, 96-02-19377a).

[1] K. Ensslin and P. M. Petroff, Phys. Rev. B **41**, 12307 (1990).
[2] D. Weiss, M. L. Roukes, A. Menschig *et al.*, Phys. Rev. Lett. **66**, 2790 (1991).
[3] E. M. Baskin, G. M. Gusev, Z. D. Kvon *et al.*, JETP Lett. **55**, 678 (1992).
[4] G. M. Gusev, V. T. Dolgopolov, Z. D. Kvon *et al.*, JETP Lett. **54**, 364 (1991).
[5] G. M. Gusev, Z. D. Kvon, L. V. Litvin *et al.*, J. Phys., Condens. Matter. **4**, L269 (1992).

Published in English in the original Russian journal. Edited by Steve Torstveit.

Interplay between fermion condensation and density-wave instability

V. A. Khodel[a)]
Kurchatov Institute Russian Research Center, 123182 Moscow, Russia

V. R. Shaginyan[b)]
St. Petersburg Nuclear Physics Institute, Russian Academy of Sciences, 188350 Gatchina, Russia

M. V. Zverev[c)]
Moscow Engineering Physics Institute, 115409 Moscow, Russia

(Submitted 15 December 1996; resubmitted 9 January 1997)
Pis'ma Zh. Éksp. Teor. Fiz. **65**, No. 3, 242–247 (10 February 1997)

It is shown that the phase transition of density-wave origin in homogeneous liquids is preceded by fermion condensation. Thus fermion condensation may be observed in low-density electron liquids, neutron stars, and liquid He^3. Three-dimensional (3D) and two-dimensional (2D) liquids are considered. © *1997 American Institute of Physics.* [S0021-3640(97)00403-9]

PACS numbers: 71.45.Gm, 73.20.Dx, 73.40.Lq

Several years ago an extremely powerful method was developed[1] for measuring the electronic structure close to the Fermi level: angle-resolved photoemission spectroscopy (ARPES). ARPES measurements of electronic spectra in the vicinity of the Fermi level exhibit a dispersionless sharp peak, i.e., an extended Van Hove singularity (VHS). Recently measured ARPES data from single-crystal Sr_2RuO_4 reveal a VHS with extension in both directions, in contrast to the usual case, where the saddle point extends in only one direction.[2,3] Thus, it turns out that there is a broad plateau in the spectrum $\varepsilon(p_x,p_y)$, which lies at or within 17 meV of the Fermi level. It is noteworthy that the observed Fermi surface differs from the LDA calculations.[1,2] We submit that the above-described behavior of the electronic spectra $\varepsilon(\mathbf{p})$ can be understood within the framework of the theory of fermion condensation, based on the Landau theory of the Fermi liquid.[4] Landau postulated that the entropy S, which, like the other thermodynamic functions, is a functional of the quasiparticle distribution $n(p)$, has the form

$$S=-\int\left[n(p,T)\ln(n(p,T))+(1-n(p,T))\ln(1-n(p,T))\right]\frac{d^3p}{(2\pi)^3}.$$

Then, the variational condition for the free energy $F=E_0-TS$ yields the relation

$$\frac{\delta(F-\mu N)}{\delta n(p)}=\varepsilon(p,T)-\mu(T)-T\ln\frac{1-n(p,T)}{n(p,T)}=0, \tag{1}$$

where T is the temperature and μ is the chemical potential. Equation (1) is usually rewritten in the Gibbs form,

$$n(p)=\frac{1}{1+e^{(\varepsilon(p,T)-\mu)/T}}, \tag{2}$$

with $\varepsilon(p)$ given by[4]

$$\frac{\delta E_0}{\delta n(p,T)}=\varepsilon(p,T), \tag{3}$$

where E_0 is the ground state energy functional. Equation (2) is a compact form of Eq. (1) rather then its solution, since the quasiparticle energy $\varepsilon(p)$ appearing in Eq. (2) is a nontrivial functional of $n(p)$.

Landau's suggestion that the derivative $d\varepsilon(p)/dp$ is positive and finite at the Fermi level immediately implies that the function $n(p,T=0)$ coincides with the Fermi step function. But this solution of Eq. (1) is not the only one. There exist ''anomalous'' solutions[5–10] of Eq. (1) involving the so-called fermion condensation.[5] Being continuous within a region Ω in p, such a solution $n(p)$ admits a finite limit for the logarithm in Eq. (1) at $T\to 0$, yielding[8]

$$\varepsilon(p)=\frac{\delta E_0}{\delta n(p)}=\mu, p_i\leqslant p\leqslant p_f. \tag{4}$$

Thus, within the region p_i, $p_f\in\Omega$ the solution $n(p)$ deviates from the Fermi step function $n_F(p)$ in such a way that the energy $\varepsilon(p)$ stays constant, while, outside this region, $n(p)$ coincides with $n_F(p)$. Therefore, the occupation numbers $n(p)$ serve as variational parameters, since the energy E_0 can be reduced by varying them. Since the single-particle energy $\varepsilon(p)$ remains constant at exactly the chemical potential (Eq. (4)), one can conclude that $p_i<p_F<p_f$, where p_F is the Fermi momentum. When the condensation is just starting, the momenta obey $p_i=p_f=p_F$. This fact means that the effective mass M^*, given by the formula

$$\frac{1}{M^*}=\frac{1}{p_F}\frac{d}{dp}\,\varepsilon(p)|_{p=p_F}, \tag{5}$$

has a value $M^*\to\infty$. So we can conclude that the beginning of the fermion-condensation phase transition manifests itself in the absolute growth of the effective mass.

In this letter we show that the onset of the density-wave instability in a homogeneous Fermi liquid must be preceded by unlimited growth of the effective mass. Thus fermion condensation can be thought of as a widespread effect rather than as an uncommon and ''anomalous'' solution of Eq. (2).

Let us briefly outline the main points of calculations of the effective mass.[9,11] The energy E_0 is given by the equation

$$E_0=T-\int\left[\mathrm{Im}\left(\frac{\chi_0(q,\omega)}{1-R(q,\omega,g)\chi_0(q,\omega)}\right)+2\pi\rho\delta(\omega)\right]v(q)\,\frac{d^3q\;d\omega\;dg}{(2\pi)^4}, \tag{6}$$

where T is the kinetic energy of noninteracting particles and $\chi_0(q,\omega)$ is the linear response function of noninteracting particles as a function of the momentum q and frequency ω. The effective interaction R tends to the bare interparticle interaction $gv(q)$ as the coupling constant $g\to 0$. The integration over frequency ω goes along the

real axis from 0 to $+\infty$, while the integration over g goes from 0 to a real value g_0. Substituting Eq. (6) into Eq. (3), using Eq. (5), and doing some tedious algebra, we get

$$\frac{1}{M^*}=\frac{1}{M}-\frac{d}{2p_F\,dp}\int\left[\frac{\frac{\delta\chi_0(q,\omega)}{\delta n(p)}}{(1-R(q,\omega,g)\chi_0(q,\omega))^2}\right]v(q)\,\frac{d^3q\;d\omega\;dg}{(2\pi)^4 i}$$

$$-\frac{d}{2p_F\,dp}\int\left[\frac{\frac{\delta R(q,\omega,g)}{\delta n(p)}\,\chi_0^2(q,\omega)}{(1-R(q,\omega,g)\chi_0(q,\omega))^2}\right]v(q)\,\frac{d^3q\;d\omega\;dg}{(2\pi)^4 i}. \tag{7}$$

Here M is the bare mass of a particle of the system under consideration, and the integration over ω goes along the imaginary axis. We recall that the derivative d/dp is taken at $p=p_F$. One can calculate the function

$$I_0(p_F,q,\omega)=\frac{d}{dp}\,\frac{\delta}{\delta n_p}\,\chi_0(q,\omega)|_{p=p_F},$$

taking into account the explicit form of χ_0 (Ref. 12),

$$\chi_0(q,\omega)=-\sum_k\, n_k(1-n_{k+q})\,\frac{2\omega_{kq}}{\omega^2+\omega_{kq}^2}. \tag{8}$$

Here $\omega_{kq}=(\mathbf{k}+\mathbf{q})^2/(2M)-\mathbf{k}^2/(2M)$. Now the calculation of the derivatives is performed directly,

$$\frac{d}{dp}\,\frac{\delta}{\delta n_p}\,\chi_0(q,\omega)|_{p\to p_F}\simeq I_0(p_F,q,\omega)=-\frac{4\pi}{p_F^2}\,\delta(p_F-|\mathbf{p}+\mathbf{q}|)\,\delta(\omega)\mathbf{p}(\mathbf{p}+\mathbf{q})|_{p=p_F}. \tag{9}$$

It is seen from Eq. (9) that I_0 is a singular function. But this singular function will make a major contribution to the effective mass M^* only if it meets another singular function. Otherwise, the four-dimensional integration removes the two-dimensional singularity, and the first term on the right-hand side of Eq. (7) will be finite and quite comparable to the second one. Let us consider a homogeneous Fermi system located in the vicinity of the density-wave instability, i.e., close to the phase transition, when the system in question possesses a density wave characterized by the momentum q_c. The instability threshold is reached when the linear response function

$$\chi(q,\omega)=\frac{\chi_0(q,\omega)}{1-R(q,\omega,g)\chi_0(q,\omega)} \tag{10}$$

of the system possesses a pole at

$$q=q_c;\quad p_F=p_{Fc}=(3\pi^2\rho_c)^{1/3},$$

and at frequency $\omega=0$, or the denominator of the terms on the right-hand side of Eq. (7) vanishes.[12] Here ρ_c is the critical density at which the density-wave instability sets in, while p_{Fc} is the corresponding Fermi momentum.

Thus the desired singular function can be conveyed by the denominator of the first term in the integrand, provided that the system is close to instability. In that case the

integrand of the second term on the right-hand side of Eq. (7) has only a two-dimensional singularity, and so its contribution to the effective mass can be omitted. Now we can simplify Eq. (7), keeping the main contribution, which comes from the function I_0 given by Eq. (9),

$$\frac{1}{M^*}=\frac{1}{M}+\frac{p_F}{4\pi^2}\int_{-1}^{1}\int_{0}^{g_0}\frac{v(p_F\sqrt{2(1-x)})x\ dx\ dg}{[1-R(p_F\sqrt{2(1-x)},\omega=0,g)\chi_0(p_F\sqrt{2(1-x)},\omega=0)]^2}. \tag{11}$$

It should be noted that $p_F\sqrt{2(1-x)}$ is the momentum transfer q. Below we adopt the shorthand notation $p_F\sqrt{2(1-x)}=q(x)$. It is seen from Eq. (11) that the integral, which is negative, is logarithmically divergent in the limit $p\to p_{Fc}$. Of course, we suppose that $q_c\simeq 2p_{Fc}$, since there is no other vector but $\mathbf{p}_F$. On the other hand, in the case of an electron gas, direct calculations of the effective interaction R (Ref. 9), including ones based on Monte Carlo calculations,[13–15] have shown that R becomes negative at $q\simeq 2p_F$. Since $\chi_0(q,\omega=0)$ is negative, $R(q,\omega=0)$ must be negative in order to produce a pole in the linear response function (10). Fermion condensation occurs when the effective mass becomes infinite, i.e., the condensation starts as soon as the integral on the right-hand side of Eq. (11) cancels the term $1/M$. It is clear that it must take place long before the density-wave instability manifests itself.

Now let us consider a 2D liquid. The path from a 3D to a 2D liquid is clear, since the form of the singular function I_0 is preserved because the dimension is not taken into account in the calculation of this function. We arrive at the final result, bearing in mind that instead of dx we have to write $dx/\sqrt{1-x^2}$:

$$\frac{1}{M^*}=\frac{1}{M}+\frac{1}{4\pi^2}\int_{-1}^{1}\int_{0}^{g_0}\frac{v(q(x))}{[1-R(q(x),\omega=0,g)\chi_0(q(x),\omega=0)]^2}\frac{x\ dx\ dg}{\sqrt{1-x^2}}. \tag{12}$$

The fermion condensation occurs more ''easily'' in a 2D liquid than in the 3D case. To see this, we note that the integrand of Eq. (12) is multiplied by a factor $1/\sqrt{1-x^2}\geqslant 1$. On the other hand, the density-wave instability is also expected to take place more easily in the 2D case than in the 3D case (see below).

Consider a particular kind of liquid which is a 2D and 3D electron gas. In the case of the 3D electron gas the bare interaction $gv(q)$ is of the form

$$gv(q)=\frac{4\pi^2e^2}{q^2}, \tag{13}$$

and the effective mass M^*, when the system under consideration is not far from the instability point, can be obtained directly by putting Eq. (13) into Eq. (11):

$$\frac{1}{M^*}=\frac{1}{M}+\frac{e^2}{p_F\pi}\int_{-1}^{1}\int_{0}^{1}\frac{x\ dx\ dg}{(1-x)[1-R(q(x),\omega=0,g)\chi_0(q(x),\omega=0)]^2}. \tag{14}$$

One can get the well-known Gell-Mann result for the effective mass of a dense electron gas[16] by putting $R=4\pi e^2/q^2$, as should be the case in the weak-coupling limit. It has

been shown that the charge-density-wave instability takes place in a 3D gas at $r_s \simeq 30$, and $q_c \simeq 2p_F$ (Ref. 17, 14, 18). At the same time, Wigner crystallization is predicted by the Monte Carlo calculations at $r_s \sim 100$ (Ref. 19).

In the case of a 2D electron gas one gets

$$\frac{1}{M^*} = \frac{1}{M} + \frac{e^2}{p_F \pi} \int_{-1}^{1} \int_{0}^{1} \frac{x\, dx\, dg}{(1-x)\sqrt{2(1+x)}[1 - R(q(x), \omega = 0, g)\chi_0(q(x), \omega = 0)]^2}. \tag{15}$$

Here we put $g\upsilon(q) = 2\pi e^2/q$. We stress that the effective interaction R of both 2D and 3D electron systems tends to the Coulomb interaction as $q \to 0$, and the integrands of Eqs. (14) and (15) have no singularities at $x = 1$. Monte Carlo calculations of the ground state properties of an electron gas predict Wigner crystallization at a density $r_s \simeq 37$ in the 2D electron gas.[20] However, density waves should arise before crystallization takes place, as is indeed found to be the case: the charge-density-wave instability has been shown to occur at $r_s = 5$–10) and $q_c \simeq 2p_F$ in parallel electron layers separated by potential barriers.[13,15] Thus, as we have shown above, fermion condensation will inevitably arise as a result of the possibility of the charge-density-wave instability. Our calculations predict fermion condensation in a 3D electron gas at $r_s \simeq 21$ (Ref. 11), while calculations in the 2D case give the value $r_s \simeq 8$ (these will be published elsewhere). Wigner crystallization has also been predicted to occur for dense neutron matter.[21] Different calculations yield varying values for the solidification density of neutron matter in the interior of neutron stars.[22] One can imagine that before forming crystal structures a liquid becomes unstable against small-amplitude density fluctuations, i.e., that the linear response function has a pole at q_c (Ref. 12 and 17). We suppose that the same is true for the solidification of liquid ^{3}He. Therefore, we can conclude that such liquids should exhibit fermion condensation.

In summary, we have shown that fermion condensation could take place in any Fermi liquid (electron gas, nuclear matter, neutron matter, or liquid ^{3}He) which undergoes a density-wave instability under some conditions.

We thank E. K. U. Gross, R. Kúmmel, O. E. Kvyatkovskii, P. Nozières, P. Schuck, and G. E. Volovik for helpful discussions. This research was supported in part by the Russian Fund for Fundamental Research under Grant 95-02-04481 and Grant 96-02-19292.

[a)]e-mail: khodel@cerber.net.kiae.su
[b)]e-mail: vrshag@thd.pnpi.spb.ru
[c)]e-mail: zverev@ct.infn.it

[1] Z.-X. Shen and D. S. Dessau, Phys. Rep. **253**, 1 (1995).
[2] T. Yokoya, A. Chainani, T. Takahashi, H. Katayama-Yoshida, M. Kasai, and Y. Tokura, Phys. Rev. Lett. **76**, 3009 (1996).
[3] D. H. Lu, M. Schmidt, T. R. Cummins, S. Schuppler, F. Lichtenberg, and J. G. Bendorz, Phys. Rev. Lett. **76**, 4845 (1996).
[4] L. D. Landau, Zh. Éksp. Teor. Fiz. **30**, 1058 (1956) [Sov. Phys. JETP **3**, 920 (1956)].
[5] V. A. Khodel and V. R. Shaginyan, JETP Lett. **51**, 553 (1990).
[6] P. Nozières, J. Phys. (France) I **2**, 443 (1992).

[7] G. E. Volovik, JETP Lett. **59**, 830 (1994).
[8] V. A. Khodel, J. W. Clark, and V. R. Shaginyan, Solid State Commun. **96**, 353 (1995).
[9] V. A. Khodel, V. R. Shaginyan, and V. V. Khodel, Phys. Rep. **249**, 1 (1994).
[10] G. E. Volovik, JETP Lett. **63**, 763 (1996).
[11] M. V. Zverev, V. A. Khodel, V. R. Shaginyan, Zh. Éksp. Teor. Fiz. **109**, 1054 (1996) [JETP **82**, 567 (1996)].
[12] D. Pines and P. Nozières, *The Theory of Quantum Liquids*, Benjamin, New York (1966).
[13] L. Świerkowski, D. Neilson, and J. Szymański, Phys. Rev. Lett. **67**, 240 (1991).
[14] B. Farid, V. Heine, G. E. Engel, and I. J. Robertson, Phys. Rev. B **48**, 11602 (1993).
[15] A. Gold and L. Calmels, Phys. Rev. B **48**, 11622 (1993).
[16] M. Gell-Mann, Phys. Rev. **106**, 369 (1957).
[17] H. B. Shore, E. Zaremba, J. H. Rose, and L. Sander, Phys. Rev. B **18**, 6506 (1978).
[18] M. Levy and J. P. Perdew, Phys. Rev. B **48**, 11638 (1993).
[19] D. Ceperley and B. J. Alder, Phys. Rev. Lett. **45**, 566 (1980).
[20] B. Tanatar and D. Ceperley, Phys. Rev. B **39**, 5005 (1989).
[21] D. Ceperley, G. V. Chester, and M. H. Kalos, Phys. Rev. B **16**, 3081 (1977).
[22] G. Baym and C. J. Pethick, Annu. Rev. Nucl. Sci. **25**, 27 (1975).

Published in English in the original Russian journal. Edited by Steve Torstveit.

Energy and number of particles in skyrmion excitations with odd filling of the Landau levels of a two-dimensional electron gas

S. V. Iordanskiĭ and S. G. Plyasunov
Landau Institute of Theoretical Physics, Russian Academy of Sciences, 117334 Moscow, Russia

(Submitted 25 December 1996; resubmitted 5 January 1997)
Pis'ma Zh. Éksp. Teor. Fiz. **65**, No. 3, 248–252 (10 February 1997)

It is shown that approximations employing projections of wave functions onto a single Landau level are inadequate for describing skyrmion-type excitations. Nonprojected functions give a clear physical picture and calculations are greatly simplified by their use. The expression for the energy of skyrmion excitations differs substantially from the expressions obtained in the approximation of globally projected functions by a series of terms which have a very simple meaning. [S0021-3640(97)00503-3]

PACS numbers: 73.20.Mf, 71.70.Di, 12.39.Dc

The question of the existence of skyrmion-type excitations for oddly filled Landau levels of two-dimensional electrons arose a comparatively long time ago,[1,2] but a specific calculation of their energies was made only recently. In Ref. 3 the phenomenological approach of the Chern–Simons theory was used, and it was shown that skyrmions must exist in this case and their energy was calculated. Next, the skyrmion energies were determined numerically in Ref. 4 by the Hartree–Fock method on the basis of wave functions projected onto the lowest Landau level. In Ref. 5 the gradient-expansion method was used and the number of particles and the energy were calculated in the lowest approximation in the gradients. The results of Ref. 5 were refined in Ref. 6, where a technique was also developed for performing calculations in any order of the gradient expansion. The gradient-expansion technique is very unwieldy and the final results appear only after tedious calculations, even in the lowest order. The projected-function approximation is ordinarily justified by the large value of the cyclotron energy $\hbar\omega_c$ compared with the Coulomb energy, which is of order $e^2/\kappa l_H$, where $l_H^2=c\hbar/eH$ and κ is the dielectric constant.

In the present letter we show that this assertion is incorrect and that taking account of other Landau levels leads to corrections in the energy in zeroth order in $1/\hbar\omega_c$ and to terms of order $\hbar\omega_c$ in the skyrmion energy. At the same time, the calculations simplify substantially and have a simple physical interpretation.

Skyrmions correspond to a nonuniform rotation of the second-quantization spinor operators with the aid of the rotation matrix $U(\mathbf{r})$. This corresponds to the transformation $\Psi(\mathbf{r})=U(\mathbf{r})\chi(\mathbf{r})$, where $\chi(\mathbf{r})$ are new spinors. The matrix $U(\mathbf{r})$ is parameterized by three Euler angles:

$$U(\mathbf{r})=U(\gamma(\mathbf{r}))U(\beta(\mathbf{r}))U(\alpha(\mathbf{r})),$$

$$U(\alpha)=\cos\frac{\alpha}{2}+i\sigma_z\sin\frac{\alpha}{2};\quad U(\beta)=\cos\frac{\beta}{2}+i\sigma_y\sin\frac{\beta}{2};$$

$$U(\gamma)=\cos\frac{\gamma}{2}+i\sigma_z\sin\frac{\gamma}{2}.$$

For the energy to be finite with a finite g-factor, the angle β corresponding to a deviation of the spin direction away from the z axis, along which the spin is directed in the limit $r\to\infty$, must go to zero at large distances. It is assumed that the matrix $U(\mathbf{r})$ has no singularities anywhere. This corresponds to the absence of singularities in the matrix

$$\mathbf{A}_\mu=-iU^\dagger\partial_\mu U=\Omega_\mu^i\sigma_i,$$

where σ_i are the Pauli matrices, $i=x, y, z$ and $\mu=x, y$. The expressions for Ω^x, Ω^y, and Ω^z can be easily obtained by direct differentiation:

$$\Omega_\mu^z=\frac{1}{2}(\partial_\mu\alpha+\cos\beta\partial_\mu\gamma),$$

$$\Omega_\mu^x=\frac{1}{2}(\partial_\mu\gamma\sin\beta\cos\alpha-\partial_\mu\beta\sin\alpha),$$

$$\Omega_\mu^y=\frac{1}{2}(\partial_\mu\beta\cos\alpha+\partial_\mu\gamma\sin\beta\sin\alpha).$$

The nontrivial topology of the matrix U is due to the properties of the mappings $\gamma(\mathbf{r})$ and $\alpha(\mathbf{r})$, where $\mathbf{r}$ runs over a circle of large radius. The degree of the mapping of the two-dimensional plane onto a sphere, parameterized by the angles γ and β, is equal to the degree of the mapping of a circle onto a circle, i.e., a vortex singularity of $\gamma(\mathbf{r})$. For Ω_i to be nonsingular, the singularity of $\gamma(\mathbf{r})$ must coincide with the corresponding singularity of $\alpha(\mathbf{r})$, located at the point where $\cos\beta=-1$. Therefore, the rotation matrix $U(\mathbf{r})$ must be determined by all three Euler angles, and the corresponding spinor Ψ possesses an integral quantization of the circulation integral at large distances.

Therefore, it would be more accurate to talk about nonsingular vortices whose core is given by a skrymion (by analogy to ^{3}He-A (Ref. 7)). The vortex numbers can be arbitrary integers, in contrast to ^{3}He-A, where they are even. The Hamiltonian of the electronic system in a magnetic field is

$$H=\int\frac{1}{2m}\Psi^\dagger(\mathbf{r},t)\left(-i\frac{\partial}{\partial r_\mu}-A_\mu\right)^2\Psi(\mathbf{r},t)d^2r$$
$$+\frac{1}{2}\int\int V(r-r')\Psi^\dagger(\mathbf{r},t)\Psi^\dagger(\mathbf{r}',t)\Psi(\mathbf{r}',t)\Psi(\mathbf{r},t)d^2\mathbf{r}d^2\mathbf{r}', \tag{1}$$

where $V(\mathbf{r})$ is the Coulomb potential. After the substitution $\Psi=U(\mathbf{r})\chi$ the Hamiltonian assumes the form (without any approximations)

$$H=\int \frac{1}{2m}\chi^{\dagger}(\mathbf{r},t)\left(-i\frac{\partial}{\partial r_{\mu}}-A_{\mu}-iU^{\dagger}\partial_{\mu}U\right)^{2}\chi(\mathbf{r},t)d^{2}r$$
$$+\frac{1}{2}\int\int V(r-r')\chi^{\dagger}(\mathbf{r},t)\chi^{\dagger}(\mathbf{r}',t)\chi(\mathbf{r}',t)\chi(\mathbf{r},t)d^{2}\mathbf{r}d^{2}\mathbf{r}', \quad (2)$$

i.e., for new spinors a spin-dependent vector potential appears in the kinetic energy. For purposes of simplification, the Zeeman energy is not included in this Hamiltonian; this will be done later.

It is easy to show that the representation of a spinor χ in the form of a spinor projected onto a single Landau level is inadequate, since after expansion in powers of $U^{\dagger}\partial_{\mu}U$ which induce transfers to higher and lower Landau levels are present in Eq. (2), and they give corrections of the same and lower order of magnitude as the terms which were taken into account in Refs. 4 and 5.

We shall assume that because of the smallness of the g factor, which determines the size of the region where the spins possess an unfavorable orientation from the standpoint of the Zeeman energy, the matrix U changes little over distances of the order of l_H. As usual, on account of the gradient invariance, only the vector $\nabla\times\vec{\Omega}^{i}$ is important. The main assumption of the further conclusions is that locally we have a filling of a Landau level with a definite projection of the spin in a local magnetic field, just as in the case of a matrix U which is uniform in all space. This assumption makes it possible to use the Hartree–Fock expression for the energy density of a filled level to terms $V_{\rm int}/\hbar\omega_c$. Then the energy is diagonalized locally by the spinor components $\chi_{\downarrow}$ and $\chi_{\uparrow}$, which makes it possible to retain in the additional vector potential only the diagonal part $\mathbf{A}'\approx\vec{\Omega}_z\sigma_z$. The effective magnetic field for the up spins is

$$\mathbf{H}_{\rm eff}^{+}=\mathbf{H}_0-\nabla\times\vec{\Omega}_z. \quad (3)$$

The magnetic field for the down spins is

$$\mathbf{H}_{\rm eff}^{-}=\mathbf{H}_0+\nabla\times\vec{\Omega}_z. \quad (4)$$

All local Landau levels are filled in the field $\mathbf{H}_{\rm eff}^{+}$ (3), and the electron spins are oriented according to a local average spin. The density of electrons filling a local Landau level is

$$\rho=\frac{1}{2\pi l_{H_{\rm eff}}^{2}}=\frac{1}{2\pi}\frac{eH_{\rm eff}^{+}}{c\hbar}=\frac{1}{2\pi}\frac{e}{c\hbar}(H_0-\nabla\times\Omega_z). \quad (5)$$

We can choose a system of units such that $eH_0/\hbar c=1$ and $H_0=1$. Then

$$\rho=\frac{1}{2\pi}+\frac{1}{2\pi}\nabla\times\Omega_z. \quad (6)$$

The same result is obtained in the approximation of a global projection on one Landau level.[4,5] Therefore, the nonzero average magnetic flux of the additional magnetic field changes the total number of electrons on the lower Landau level. The quantity $Q=(1/2\pi)\int\nabla\times\Omega_z d^{2}\mathbf{r}$ is a topological invariant (the degree of the mapping of the plane onto a sphere $S^{2}\to S^{2}$), which assumes integer values. In the case when the number

of particles is given, all particles cannot fit on the lowest Landau level, since $(1/2\pi)\int(1-\nabla\times\Omega_z)d^2\mathbf{r}=N_0-Q$, and Q particles must occupy a state on the second spin sublevel (we assume that the spin splitting is much less than $\hbar\omega_c$ and $Q>0$). If, however, the chemical potential μ is given, then the number of particles should simply decrease by Q, since the states on the second spin sublevel lie above the chemical potential. Similarly, the case $Q<0$ leads to the appearance of a hole in the local filling of the lower spin sublevel.

We shall assume below that the case of a fixed chemical potential is realized and the zeroth Landau level (LL) is filled. The Hartree–Fock energy is an integral of the local Hartree–Fock energy density, calculated for a completely filled Landau level in the local effective magnetic field. For a fixed interaction, this energy depends only on the magnetic field, which according to Eq. (4) is uniquely related with the density ρ and has the form

$$\mathcal{H}(\mathbf{r})=\frac{\hbar\omega_c}{2}\rho+\frac{\widetilde{E}(\rho)}{2}\rho^2-\frac{E(\rho)}{2}\mathbf{S}^2\rho^2+\frac{E_1(\rho)}{2}\rho^2(\vec{\nabla}\cdot\mathbf{S})^2+g\mathbf{H}\cdot\mathbf{S}\rho+E_c(\rho). \tag{7}$$

The expressions for the coefficients E, $\widetilde{E}$, and E_1 are of order of $e^2/\kappa l_H$ and are presented in Ref. 6; **S** is the average spin. We confine our attention to the first two terms of the expansion in $\nabla\times\Omega_z$:

$$\mathcal{H}(\mathbf{r})\approx\frac{1}{2\pi}\frac{\hbar\omega_c}{2}+\frac{\widetilde{E}(\rho_0)}{2(2\pi)^2}-\frac{E(\rho_0)}{2(2\pi)^2}\mathbf{S}^2+\frac{\hbar\omega_c}{2\pi}\nabla\times\vec{\Omega}_z+\frac{\left(\widetilde{E}(\rho_0)+\frac{1}{2}\frac{\partial\widetilde{E}}{\partial\rho_0}\rho_0\right)}{(2\pi)^2}\nabla\times\vec{\Omega}_z$$
$$-\frac{\left(E(\rho_0)+\frac{1}{2}\frac{\partial E}{\partial\rho_0}\rho_0\right)}{(2\pi)^2}\mathbf{S}^2\nabla\times\vec{\Omega}_z+\frac{1}{2\pi}g\mathbf{H}\cdot\mathbf{S}+\frac{E_1(\rho_0)}{2(2\pi)^2}(\vec{\nabla}\mathbf{S})^2+E_c(\rho). \tag{8}$$

Here $\rho_0=1/2\pi$ is the electron density in the completely filled Landau level in an external magnetic field; in the Zeeman term, we neglected the change in the density. The change in the total free energy of the electrons on the lower spin sublevel accompanying the appearance of a nonsingular skrymion vortex with vortex number Q is expressed by the formula

$$\Omega=\int d^2\mathbf{r}(\mathcal{H}(\mathbf{r})-\mu\rho(\mathbf{r}))=\frac{\hbar\omega_c^0}{2}Q+\left(\frac{\widetilde{E}'(\rho_0)}{2\pi}-\frac{E'(\rho_0)}{2\pi}\right)Q+g\int\frac{d^2\mathbf{r}}{2\pi}\mathbf{H}\cdot\mathbf{S}(\mathbf{r})$$
$$+\frac{E_1(0)}{4\pi}\int(\vec{\nabla}\cdot\mathbf{S})^2d^2\mathbf{r}+\int E_c d^2\mathbf{r}, \tag{9}$$

where

$$E'(\rho_0)=E(\rho_0)+\frac{1}{2}\frac{\partial E}{\partial\rho_0}\rho_0,\quad \widetilde{E}'(\rho_0)=\widetilde{E}(\rho_0)+\frac{1}{2}\frac{\partial\widetilde{E}}{\partial\rho_0}\rho_0.$$

We can see that additional terms, which are proportional to Q and are absent in the expressions obtained previously in Refs. 5 and 6, appear in the total energy.[5,6] We

assumed that the chemical potential corresponds to half the spin-splitting gap. The energies of the single-particle excitations correspond to the variational derivative of H with respect to the densities $n_{\uparrow}(\mathbf{r})$ and $n_{\downarrow}(\mathbf{r})$ and have the form

$$\epsilon^{+} = -\frac{E(0)}{2\pi} + \hbar\omega_c \nabla\times\Omega_z + \left(\frac{\widetilde{E}'}{2\pi} - \frac{E'}{2\pi}\right)\nabla\times\Omega_z + g\mathbf{H}\cdot\mathbf{S} + \frac{E(0)}{2\pi}(\triangle\mathbf{S})\cdot(U^{\dagger}\vec{\sigma}U), \tag{10}$$

$$\epsilon^{-} = \frac{E(0)}{2\pi} - \hbar\omega_c \nabla\times\Omega_z - \left(\frac{\widetilde{E}'}{2\pi} - \frac{E'}{2\pi}\right)\nabla\times\Omega_z - g\mathbf{H}\cdot\mathbf{S} - \frac{E(0)}{2\pi}(\triangle\mathbf{S})\cdot(U^{\dagger}\vec{\sigma}U) \tag{10$'$}$$

(the chemical potential was subtracted from the values of the energies).

We can see that a skyrmion possesses many attributes of a composite fermion: an integral charge and an integral number of magnetic-flux quanta. In our approximation there is one flux quantum per charge. This could be due to the fact that we employed the small-gradient approximation and the change in the magnetic field $H^{+} - H_0$ was assumed to be small, so that the following Landau levels in the field H^{+} are located at a distance $\hbar\omega_c$. The real magnitude of the additional field depends on its region of localization, since the flux is a topological characteristic. For a small localization region, the additional field increases and H^{+} decreases. Moreover, the additional field increases with Q. Also, the value of the g factor itself is not too small, so that the eigenvalue ϵ^{+} for negative Q can drop below the chemical potential not only for the first but also for the second Landau level. If this were to occur for a vortex with $Q=-2$, then the flux would equal two quanta per unit charge, as happens in composite fermions. Of course, to explain this fact it is necessary to go beyond the framework of our analysis, since in this case the ''local'' approximation is invalid and numerical methods must be used.

We thank G. E. Volovik for many discussions of a number of questions touched upon in this work. We also thank Yu. A. Bychkov for familiarizing us with his work prior to publication. This work was supported by the Russian Fund for Fundamental Research Grant 95-02-05883 and CRDF Grant No. 452.

[1] D. H. Lee, and C. L. Kane, Phys. Rev. Lett. **64**, 1313 (1990).
[2] Yu. A. Bychkov, JETP Lett. **55**, 170 (1992).
[3] S. L. Sondhi, A. Kalrede, S. A. Kivelson, and E. H. Rezai, Phys. Rev. B **47**, 16418 (1993).
[4] H. A. Fertig, L. Brey, R. Cote, and A. H. MacDonald, Phys. Rev. B **50**, 11018 (1994).
[5] K. Moon, H. Mori, Kun Yang *et al.*, Phys. Rev. B **51**, 5138 (1995).
[6] Yu. A. Bychkov, T. Maniv, and I. Vagner, Phys. Rev. B **53**, 10148 (1996).
[7] M. M. Salomaa and G. E. Volovik, Rev. Mod. Phys. **59**, 533 (1987).

Translated by M. E. Alferieff

Current filamentation and macroturbulence in superconductors in rotating magnetic fields

V. Vlasko-Vlasov,[a)] V. Kabanov, and V. Nikitenko
Institute of Solid-State Physics, Russian Academy of Sciences, 142432 Chernogolovka, Moscow District, Russia

U. Welp and G. Crabtree
Argonne National Laboratory, 9700 South Cass Avenue, Argonne, IL 60439, USA

(Submitted 27 December 1996)
Pis'ma Zh. Éksp. Teor. Fiz. **65**, No. 3, 253–257 (10 February 1997)

The onset of specific magnetic structures associated with the formation of extended current filaments is observed in YBCO single crystals in a rotating magnetic field. Like current filaments in a plasma, they are unstable and decay into current macrovortices. The appearance of filaments is explained by the formation of closed flux rings along magnetization-reversal fronts and collapse of these rings with formation of Meissner cylinders. The total current along the surface and in the vortex shell of the cylinder (the latter current dominates in high-T_c superconductors) exceeds the critical current in the same volume located far from a filament. © *1997 American Institute of Physics.* [S0021-3640(97)00603-8]

PACS numbers: 74.60.−w, 74.72.Yg, 74.25.Ha, 74.25.Fy

Magnetization reversal in type-II superconductors is ordinarily studied on the basis of critical-state models[1,2] developed for finite samples (plates and cylinders) in a longitudinal field. In this case, the magnetization-reversal front is a two-dimensional surface oriented parallel to the field and the straight flux lines are oriented along the front. In real samples edge effects cause a strong curvature of the flux lines and give rise to specific current structures and instabilities.[3] In the present work, we observed the formation of current filaments and decay of these filaments into macrovortex formations in high-T_c superconducting plates with the field rotating in the plane of the plates. The characteristic features observed make it possible to explain the magnetization instability in superconductors in rotating fields, which has been observed in macroscopic measurements over the last twenty years.[4]

The structure of the magnetic flux in YBCO single crystals (20–110 μm thick, with dimensions of 0.5–1 mm in the plane, and with width-to-thickness ratios from 5 to 40) was investigated with the aid of magnetooptic indicator films consisting of bismuth-containing iron garnets, which made it possible to visualize and measure the normal component of the induction at the superconductor surface.[5,6] The field rotated slowly in the developed plane **ab** of the crystal, normal to the optic axis. In the process, only the deviation of the magnetic flux from the direction of the field in a direction perpendicular to the surface of the sample was revealed. In slightly crossed polarizers of a microscope,

the oppositely directed normal components of the induction gave rise to a decrease or increase in the background intensity and to the appearance of black–white contrast.

In the initial state, with a field imposed on a cooled sample, the standard magnetooptic contrast[3,5,6] due to partial bending of the flux lines around the superconductor was observed at the edges of the plates which were oriented in a direction normal to the applied planar field. The contrast at these edges changed substantially in a rotating field. This is due to a change in the character of the bending of the flux lines near the edges (when a field is applied the flux lines bend around the corners of the sample, and when the field rotates, the curvature of the lines of the previously trapped flux changes sign). At the same time, contrast appears at the edges which are oriented in a direction normal to the new direction of the field, where the newly entering flux lines bend around the center of the crystal. The flux distribution remains practically unchanged in the central region of the sample, and periodic narrow stripes of brighter contrast appear at the boundary between the central region and the periphery, where the bending of the flux lines changes. They correspond to deflections of the flux lines out of the plane of the sample at these locations. Such periodic deflections can be attributed to helicoidal disturbances of the flux lines. As the field rotates, currents perpendicular to the currents induced in the initial field H, i.e., parallel to the previously penetrating flux lines, appear in the peripheral zone. In this case, the trapped flux lines are unstable with respect to helicoidal disturbances of their shape,[7,8] which produces a modulation of the normal component of the induction at the surface of the sample. We note that the period of the observed stripes is close to the helicoid spacing estimated according to the theory of Ref. 8.

When the field is rotated by $\sim 90°$, new features arise at the edges oriented along H (normal to the direction of the initial field). Here lines of bright contrast with edges of a different color (Fig. 1a), corresponding to opposite normal components of the induction at the edges, appear. This picture is characteristic for a field around a current-carrying wire and corresponds to the current density on these lines. In short narrow samples contrast arises along one continuous line. Lines with steps (as in Fig. 1a) making an angle with the edge of the sample appear in crystals with quite long sides. As the field is further rotated, they merge into a continuous structure (Fig. 1b). The profile of the normal component B_n of the induction, measured across the lines, gives $B_n \cong \pm 80$ Oe at the edges of the line (with an ~ 1.5 kOe in-plane field and $T \sim 50$ K). Fitting of the profile with model current distributions showed that the profile is best described by three parallel current filaments in the plate carrying a current of some average density. The current along the central filament is maximum and flows in the direction of the critical current in the surrounding volume. In the satellite filaments the current is ~ 3 times weaker and is oppositely directed. This corresponds to an increase of the current along the center of the observed bright lines and a decrease of the current on the edges of the lines.

The formation of lines of current can be explained by taking account of flux-line bending accompanying a rotation of the field. When a field is applied, the ends of the flux lines drop downward (toward the central plane) at the edges of the sample (Fig. 2a). As H rotates, the magnitude of the field component giving rise to their appearance decreases (right down to zero) and the flux lines start to move in the opposite direction — toward the surface of the crystal. In the process, half-loops (Fig. 2b) or closed loops form near the surface. This occurs along fronts which make an angle with the edge. Subsequently,

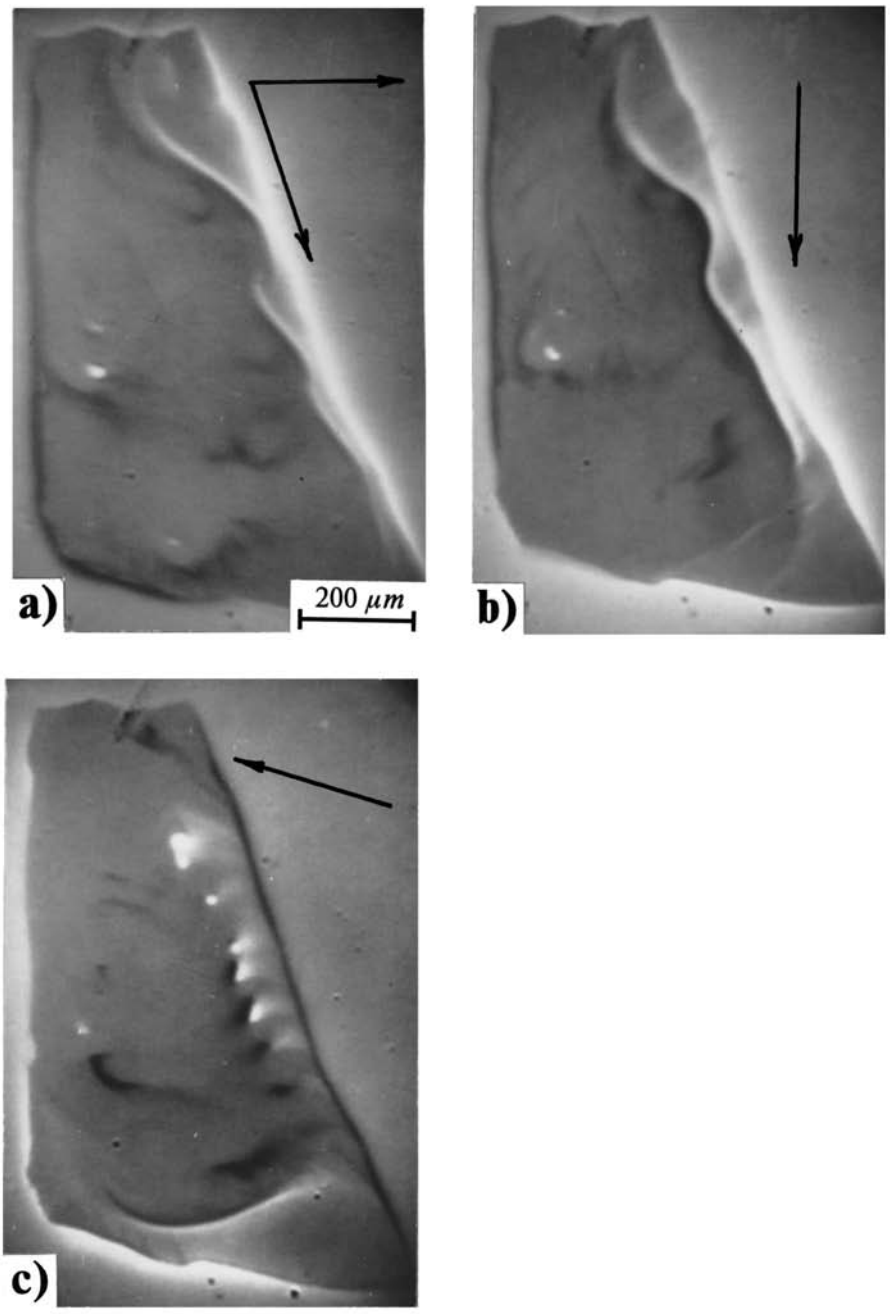

FIG. 1. Magnetooptic contrast due to lines of current arising and decaying in a YBCO plate with clockwise rotation of an external magnetic field in the plane of the plate. $T = 43$ K, $H = 1$ kOe. The light and dark contrasts correspond to normal components of induction of opposite polarity. The solid arrows show the corresponding field directions. The dashed arrow indicates the initial direction of the field.

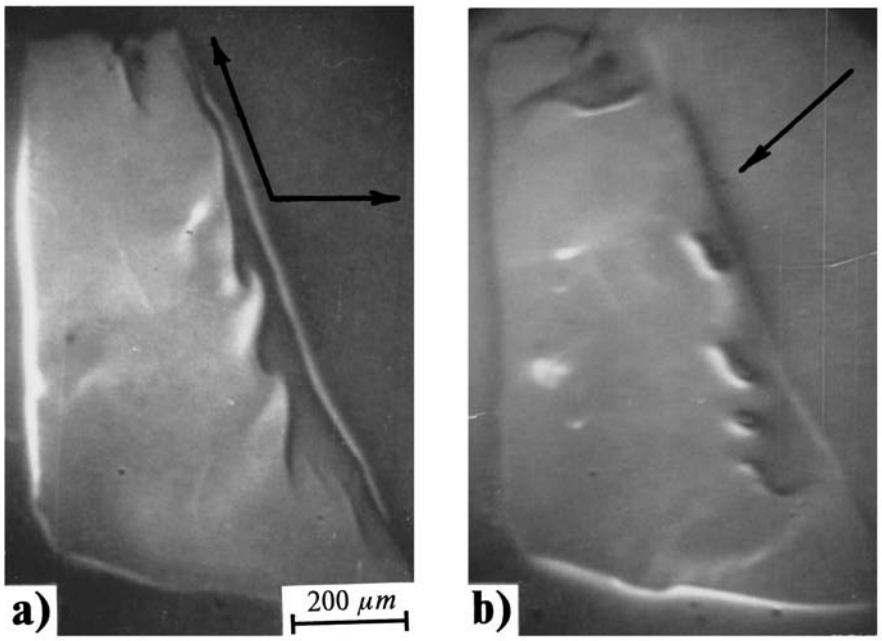

FIG. 2. Diagrams of the flux distribution in the central transverse section of the high-T_c plate: a — with an external magnetic field imposed parallel to the plate surface, b — after the field rotates by 90° (flux lines perpendicular to the plate section are not shown).

the half-loops and loops of small radius collapse as a result of the linear tension in the flux lines when this force exceeds the pinning force opposing this process. As a result, flux-free cylinders are obtained. A high magnetization current i_M flows along their surface separating the Meissner and the mixed state, and it can exceed the losses of the critical current $-i_c$ inside a cylinder. The appearance of such ''Meissner holes'' was first discussed in Refs. 9 and 10. Numerical estimates show that in high-T_c superconductors a large contribution to the total current along a ''Meissner hole'' is associated with an increase of the critical current in the cylinder shell. At locations where the segments of flux loops lie in the basal plane the critical current density is higher than the average critical current J_c in the surrounding volume. Conversely, however, the current density is less than J_c on the sides of the cylinder, where the flux lines are oriented along the c axis. As a result, an excess positive current appears at the center of a ''Meissner hole'' and negative satellites form along the sides. Such a three-current model makes gives a good fit of the induction profiles measured across the lines of strong contrast.

As H turns further, the lines of bright contrast decompose into small regions with flux lines perpendicular to the surface (Fig. 1c). They correspond to the formation of closed current loops (macrovortices), which then move through the crystal, change shape and sign, and partially annihilate. Furthermore, the new lines on which current is concentrated appear at neighboring edges of the sample (Fig. 1c) and the process repeats. As

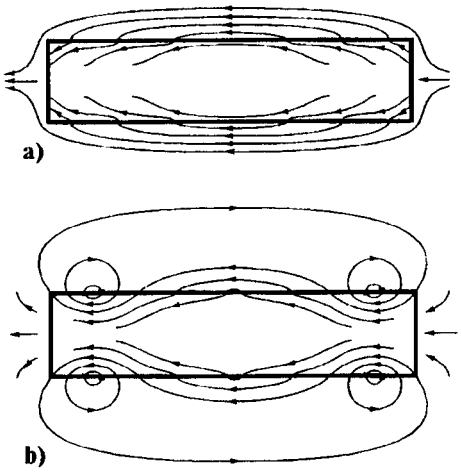

FIG. 3. Magnetooptic contrast due to lines of current arising in a YBCO plate with counterclockwise rotation of the magnetic field in the plane of the plate.

a result, complicated distributions of the induction form. These distributions characterize the dynamic structure of the flux in a rotating field.

When the field rotates in the opposite direction, the direction of the current lines changes symmetrically (Fig. 3). In other respects, the details of the process recur. We note that this picture was observed in all the experimental samples, all the way up to plates with a width-to-thickness ratio of ~ 40, where it would appear that the one-dimensional Bean picture of magnetization reversal[1] could have been realized.

It is obvious that the formation and decay of current filaments as well as the subsequent motion of macrovortices should give rise to local electric-field spikes, which have often been observed in superconductors in rotating fields.[4] It appears that the characteristic formation and transformation times of the observed structures, together with the helicoidal disturbances, determine the experimentally observed periodic changes in the local potential (see citations in Ref. 4).

The authors from the Institute of Solid-State Physics are grateful to the International Science Foundation (Grants RF1000 and RF1300) and the Fund of the Russian State Scientific and Technical Program ''Topical Problems in Condensed-Matter Physics'' (Program ''Superconductivity'') for support. This work was also supported by US DOE, BES-MS, contract No. W-31-109-ENG-38.

[a)]e-mail: vlasko@issp.ac.ru

[1] C. Bean, Phys. Rev. Lett. **8**, 250 (1962); Rev. Mod. Phys. **36**, 31 (1964).
[2] Y. B. Kim, C. F. Hempstead, and A. R. Strand, Phys. Rev. **129**, 528 (1963).
[3] V. K. Vlasko-Vlasov, V. I. Nikitenko, A. A. Polyanskii *et al.*, Physica C **222**, 361 (1994).

[4] E. H. Brandt, Rep. Prog. Phys. **58**, 1465 (1995), §7.2.
[5] L. M. Dorosinskii, M. I. Indenbom, V. I. Nikitenko *et al.*, Physica C **203**, 149 (1992).
[6] V. K. Vlasko-Vlasov, L. M. Dorosinskii, A. A. Polyanskii *et al.*, Phys. Rev. Lett. **72**, 3246 (1994).
[7] J. Clem, Phys. Rev. Lett. **38**, 1425 (1977).
[8] E. H. Brandt, Phys. Lett. A **79**, 207 (1980).
[9] H. Koppe, Phys. Status Solidi **17**, K229 (1966).
[10] J. E. Evetts and A. M. Campbell, in *Proceedings of the 10th International Conference on Low-Temperature Physics* (Moscow, USSR, Aug. 31–Sept. 6, 1966), Moscow, VINITI, 1967.

Translated by M. E. Alferieff

Disordering effects in superconductors with anisotropic pairing: from Cooper pairs to compact bosons

M. V. Sadovskiĭ[a)] and A. I. Posazhennikova
Institute of Electrophysics, Ural Branch of the Russian Academy of Sciences, 620049 Ekaterinburg, Russia

(Submitted 27 December 1996)
Pis'ma Zh. Éksp. Teor. Fiz. **65**, No. 3, 258–262 (10 February 1997)

In the weak-coupling BCS-theory approximation, normal impurities do not influence the superconducting transition temperature T_c in the case of isotropic s pairing. In the case of d pairing they result in a rapid destruction of the superconducting state. This is at variance with many experiments on the disordering of high-T_c superconductors, assuming that d pairing is realized in them. As the interelectronic attraction in a Cooper pair increases, the system transforms continuously from a BCS-type superconductor with ''loose'' pairs to a picture of superconductivity of ''compact,'' strongly coupled bosons. Near such a transition substantial deviations can be expected from the universal disorder dependence of T_c, as determined by the Abrikosov–Gor'kov equation, and T_c becomes more stable against disordering. Since high-T_c superconducting systems fall into the transitional region from BCS-type pairs to compact bosons, these results can explain their relative stability against disordering. © *1997 American Institute of Physics.* [S0021-3640(97)00703-2]

PACS numbers: 74.72−h, 74.20.Fg, 74.20.Mn

It is well known that in the standard weak-coupling BCS-theory approximation, normal impurities do not strongly influence the superconducting transition temperature T_c in the case of isotropic s pairing (Anderson's theorem).[1] The suppression of T_c by disorder is also quite weak in the case of so-called anisotropic s pairing.[2,3] At the same time, for d pairing normal impurities destroy superconductivity very rapidly,[2–4] and the disorder dependence of T_c is determined by the universal Abrikosov–Gor'kov equation

$$\ln\left(\frac{T_{c0}}{T_c}\right)=\left[\Psi\left(\frac{1}{2}+\frac{\gamma}{2\pi T_c}\right)-\Psi\left(\frac{1}{2}\right)\right], \tag{1}$$

where $\Psi(x)$ is the digamma function, $\gamma=\pi n_{\rm imp}v^2N(E_F)$ is the standard rate of scattering of electrons by point defects with potential v which are distributed randomly with some density $n_{\rm imp}$ in space, and $N(E_F)$ is the density of states at the Fermi level E_F. It follows directly from Eq. (1) that T_c is suppressed completely at some critical scattering rate $\gamma=0.88T_{c0}$, which determines the corresponding critical impurity density and the residual normal-state resistance:

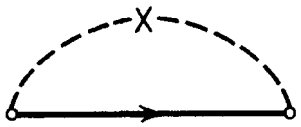

FIG. 1. Boson self-energy due to impurity scattering.

$$\rho_{AG}=\frac{2m\gamma_c}{ne^2}=\frac{8\pi\gamma_c}{\omega_p^2}, \tag{2}$$

where n and m are, respectively, the electron density and mass and ω_p is the plasma frequency.[4]

It is now becoming increasingly more certain that d-type pairing occurs in copper-oxide high-T_c superconductors.[5] However, the characteristic scale of the critical scattering frequency $\gamma_c \sim T_{c0}$ is at serious variance with a large number of experimental data on T_c suppression by disorder for these systems.[6] These data apparently indicate that the superconducting state persists all the way up to the disorder-induced metal–insulator transition, i.e., up to $\gamma \sim E_F \gg T_{c0}$. The purpose of this letter is to give a qualitative explanation for this discrepancy.

Let us consider the limit of a very strong pairing interaction (opposite to the standard BCS approximation), leading to the formation of compact bosons.[7] In this case T_c is determined by the Bose condensation temperature of free bosons. In the case of a system with impurities, the Bose condensation point is determined by the equation:[8]

$$\mu_p-\sum(0)=0, \tag{3}$$

where μ_p is the chemical potential of the pairs and $\Sigma(0)$ is the zero-frequency limit of the self-energy of a boson in the field of the impurities. In the case of weak scattering the self-energy is determined by the diagram displayed in Fig. 1:

$$\sum(\epsilon_n)=n_{\mathrm{imp}}v^2\int\frac{d^3\mathbf{p}}{(2\pi)^3}\,\frac{1}{i\epsilon_n-\mathbf{p}^2/2m^*+\mu_p}, \tag{4}$$

where $\epsilon_n=2\pi nT$ are the even Matsubara frequencies, $m^*=2m$ is the mass of a pair, and we assume that $T>T_c$. In what follows we shall confine our attention to three-dimensional systems. Direct calculations give

$$\sum(0)=\mathrm{Re}\,\tilde{\Sigma}(0)+E_{0c}, \tag{5}$$

where $E_{0c}=-(m^*/\pi^2)n_{\mathrm{imp}}v^2p_0$ is the impurity scattering induced shift in the band edge[9] (p_0 is the momentum cutoff parameter of the order of the reciprocal a^{-1} of the lattice constant), and

$$\mathrm{Re}\,\tilde{\Sigma}(0)=\frac{1}{\sqrt{2}\pi}n_{\mathrm{imp}}v^2m^{*3/2}\sqrt{|\mu_p|}. \tag{6}$$

The quantity E_{0c} results in a simple renormalization of the chemical potential $\tilde{\mu}=\mu_p-E_{0c}$, so that Eq. (3) in the renormalized form reduces to

$$\tilde{\mu}\left(1-\frac{1}{\sqrt{2|\tilde{\mu}|}\pi}n_{\text{imp}}v^2m^{*3/2}\text{sign}\tilde{\mu}\right)=0 \tag{7}$$

with only one root of importance for us ($\tilde{\mu}<0$ for bosons at temperature $T>T_c$): $\tilde{\mu}=0$, i.e., $\mu_p-E_{0c}=0$. Accordingly, the Bose condensation temperature in an impure system is determined by the standard equation

$$\frac{n}{2}=g\int_{-\infty}^{\infty}d\epsilon N(\epsilon)\frac{1}{e^{\epsilon/T_c}-1}, \tag{8}$$

where $g=2s+1$ (for bosons with spin s) and $N(\epsilon)$ is the impurity-averaged density of states, which in the simplest approximation (4) reduces to $N(E-E_{0c})$ — the density of states of free particles with energy ϵ, measured from the shifted band edge. It is obvious that this gives the standard expression for T_c:[10]

$$T_c=\frac{3.31}{g^{2/3}}\frac{(n/2)^{2/3}}{m^*}, \tag{9}$$

which is *independent of the disorder*. Disorder could only have an effect due to the exponentially small ''Lifshitz tail'' in the density of states in Eq. (8); this tail is due to localization[11] and does not arise in our very simple approximation (4). We therefore conclude that in the approximation of a very strong pairing interaction (compact-pair superconductivity), T_c is virtually independent of disorder for *any* value of the spin of a Cooper pair, i.e., for pairs of the *s*-, *d*-, etc., types.

In a quite old paper by Nozières and Schmitt-Rink,[7] devoted to ideal superconductors with no impurities, it was shown that as the pairing interaction increases, a continuous transition occurs from expressions for T_c in the weak-coupling BCS theory approximation to expressions determined by the picture of Bose condensation of compact pairs. A corresponding analysis for T_c in a system with impurities can be performed by solving a system of coupled equations which generalizes the analogous equations of Ref. 7 — the standard equation for BCS instability

$$1-\chi(0,0)=0 \tag{10}$$

and an equation for the fermion density (chemical potential μ of the electrons)

$$\frac{1}{2}(n-n_f)=\int\frac{d^3\mathbf{q}}{(2\pi)^3}\int\frac{d\omega}{\pi}\frac{1}{\exp(\omega/T_c)-1}\frac{\partial}{\partial\mu}\delta(\mathbf{q},\omega), \tag{11}$$

where $n_f(\mu, T_c)$ is the free-fermion density,

$$\delta(\mathbf{q},\omega)=\arctan\frac{\text{Im}\chi(\mathbf{q},\omega)}{1-\text{Re}\chi(\mathbf{q},\omega)}, \tag{12}$$

and the Cooper susceptibility $\chi(\mathbf{q}, \omega)$ is determined by the diagrams shown in Fig. 2. In this figure the corresponding symmetry factors for different types of pairing stand in the vertices. For example, for a cubic lattice[12]

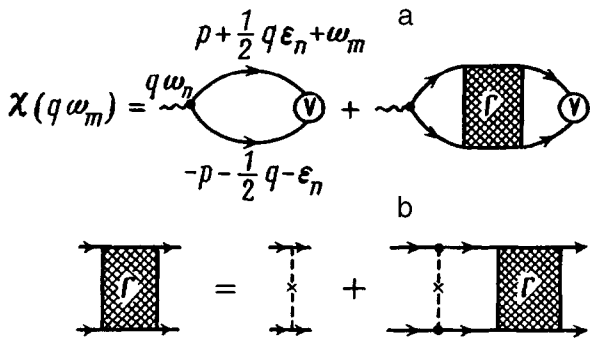

FIG. 2. a) Diagrammatic representation of the Cooper susceptibility $\chi(\mathbf{q}, \omega)$, V — pairing interaction potential, Γ — vertex part of impurity scattering in the Cooper channel, as determined in the ''ladder'' approximation (b).

$$\psi_s(\mathbf{p})=1(\text{isotropic } s\text{-pairing}),$$

$$\psi_{s'}(\mathbf{p})=\cos p_x a+\cos p_y a+\cos p_z a(\text{ anisotropic } s\text{-pairing}),$$

$$\psi_{d_{x^2-y^2}}(\mathbf{p})=\cos p_x a-\cos p_y a(d\text{-pairing}),$$

$$\psi_{d_{3z^2-r^2}}(\mathbf{p})=2\cos p_z a-\cos p_x a-\cos p_y a, \text{ and so on,} \tag{13}$$

and the following model expression can be used for a pairing interaction:

$$V_i(\mathbf{p},\mathbf{p}')=V_{\mathbf{pp}'}\psi_i(\mathbf{p})\psi_i(\mathbf{p}'), \tag{14}$$

where $\psi_i(\mathbf{p})$ were determined above, and the potential

$$V_{\mathbf{pp}'}=-\frac{V_0}{\sqrt{(1+p^2/p_0^2)(1+p'^2/p_0^2)}} \tag{15}$$

is analogous to that employed in Ref. 7, where $p_0\sim a^{-1}$.

The system of equations (10) and (11) is very time-consuming to solve numerically, even for systems with no impurities.[7] At the same time, it is perfectly obvious that even in the impurity case these equations will give a continuous transition from disorder as a function of T_c, interpolating between the limiting cases of weak coupling and the compact-boson picture which were discussed above. In the case of isotropic s-pairing T_c remains virtually disorder-independent, i.e., Anderson's theorem holds even in the strong-coupling case. In the d-pairing case, however, the universal disorder dependence of T_c determined by Eq. (1) will no longer hold in the region of the transition from Cooper pairs to compact bosons. The physical reason for this phenomenon is quite obvious — the mechanism of T_c suppression by ''depairing'' no longer works as the attraction in pairs increases and in the very strong coupling regime T_c will be determined by the Bose condensation temperature of pairs in the impure system. The qualitative behavior of T_c as a function of the disorder is shown in Fig. 3. This figure illustrates the continuous transition in the normal-state resistance dependence of T_c given by the universal Abrikosov–Gor'kov relation (curve d) to disorder-independent T_c (curve s). The

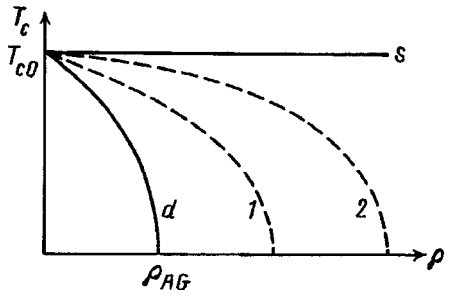

FIG. 3. Qualitative disorder dependence of the transition temperature T_c (residual normal-state resistivity ρ). Curve *d* — universal Abrikosov–Gorkov relation determined by Eq. (1). Curve *s* — isotropic *s*-pairing. Dashed curves — *d*-pairing in the transitional region from BCS theory pairs to compact bosons.

dashed curves correspond to *d* pairing in the transitional region (the coupling constant V_0 increases from curve *1* to curve *2*). Therefore, for a *d*-pairing system in the transitional region it is easy to obtain a superconducting state with quite strong disorder, corresponding to $\rho > \rho_{AG}$.

The transitional region is determined qualitatively by a simple inequality introduced in Ref. 13: $\pi^{-1} < p_F \xi < 2\pi$, where p_F is the Fermi momentum and ξ is the coherence length of the superconductor. In the so-called Uemura plot[14] the high-T_c superconductors lie near the ''instability'' line $p_F \xi = 2\pi$.[13] This fact can easily explain the deviation observed in high-T_c superconducting systems away from the universal disorder-dependence of T_c and the relative stability of such systems with respect to disorder,[6] despite the fact that *d* pairing is realized in them.

We thank A. V. Mirmel'shteĭn who insisted that these simple considerations be published. This work was partially supported by Russian Fund for Fundamental Research, Grant 96-02-16065 and Grant IKh.1 of the program ''Statistical Physics'' of the Russian State Committee on Science and Technology.

[a)]e-mail: sadovski@ief.intec.ru

[1] P. G. de Gennes, *Superconductivity of Metals and Alloys*, Benjamin, New York, 1966 [Russian translation, Mir, Moscow, 1968].
[2] L. S. Borkovski and P. J. Hirschfeld, Phys. Rev. B **49**, 15404 (1994).
[3] R. Fehrenbacher and M. R. Norman, Phys. Rev. B **50**, 3495 (1994).
[4] R. J. Radtke, K. Levin, H. B. Schuttler, and M. R. Norman, Phys. Rev. B **48**, 653 (1993).
[5] D. J. Van Harlingen, Rev. Mod. Phys. **67**, 515 (1995).
[6] M. V. Sadovskiĭ, SFKhT **8,** 337 (1995); Phys. Rep. (1996).
[7] P. Nozieres and S. Schmitt-Rink, J. Low Temp. Phys. **59**, 195 (1985).
[8] A. Z. Patashinskiĭ and V. L. Pokrovskiĭ, *Fluctuation Theory of Phase Transitions*, Pergamon Press, New York, 1979 [Russian original, Nauka, Moscow, 1982].
[9] M. V. Sadovkiĭ, Zh. Éksp. Teor. Fiz. **83,** 1418 (1982) [Sov. Phys. JETP **56**, 816 (1982)].
[10] L. D. Landau and E. M. Lifshitz, *Statistical Physics*, Pergamon Press, New York, Part 1 [Russian original, Nauka, Moscow, 1976].
[11] I. M. Lifzhits, S. A. Gredeskul, and L. A. Pastur, *Introduction to the Theory of Disordered System*, Wiley, New York, 1988 [Russian original, Nauka, Moscow, 1982].

[12] D. J. Scalapino, E. Loh, and J. E. Hirsch, Phys. Rev. B **35**, 6694 (1987).
[13] F. Pistolesi and G. C. Strinati, Phys. Rev. **49**, 6356 (1994).
[14] Y. J. Uemura, L. P. Le, G. M. Luke *et al.*, Phys. Rev. Lett. **66**, 2665 (1991).

Translated by M. E. Alferieff

Self-cooling of weak solutions of ^{3}He in ^{4}He during adiabatic melting

A. P. Sebedash[a)]

P. L. Kapitsa Institute of Physics Problems, Russian Academy of Sciences, 117334 Moscow, Russia; P. N. Lebedev Physics Institute, Russian Academy of Sciences, 117924 Moscow, Russia

(Submitted 27 December 1996)
Pis'ma Zh. Éksp. Teor. Fiz. **65**, No. 3, 263–267 (10 February 1997)

A new method of pressure regularization in the measuring cell is proposed for experiments on self-cooling of weak solutions. Preliminary results are presented for solutions with concentrations of 2% and 7%. Cooling by a factor of 1.5–2 was observed in the starting-temperature range 40–140 mK. © *1997 American Institute of Physics.* [S0021-3640(97)00803-7]

PACS numbers: 67.60−g, 67.80.Gb

The possibility of cooling of solutions of ^{3}He in ^{4}He during adiabatic melting was predicted in Refs. 1 and 2 on the basis of a number of assumptions about the characteristic features of the crystal–liquid phase equilibrium below 0.1 K, later confirmed in measurements[3,4] and calculations[5] of the phase diagrams. The most important feature is that the equilibrium concentration of ^{3}He in the solid phase (x_s) is negligibly small at these temperatures.[6,7] Therefore, in the process of crystallization of a solution the concentration of the liquid phase continuously increases up to ~8%, when a second liquid phase — virtually pure ^{3}He — appears. At this point the system emerges onto the triple line and the concentrations of all three phases and the pressure depend only on the temperature. Further growth of the ^{4}He crystal results in complete vanishing of the dilute solution, and only spatially separated ^{4}He (crystal) and ^{3}He (liquid) remain in the cell. When solid ^{4}He melts, the only important thermal process in the system is dissolution of ^{3}He in ^{4}He, since the phonon entropies of ^{4}He in both the liquid and solid phases as well as the entropy of ^{3}He in the solid phase ($S_3 = x_s R \ln 2$) are negligibly small. Thermodynamically, this process is similar to one-time dissolution at zero pressure, studied in Ref. 8 in the temperature range 100–5.7 mK. When ^{3}He was diluted with liquid ^{4}He through a superfluid filter to a final concentration of 6.6%, degrees of cooling η equal to 3.6 with a theoretically maximum value of 4.56 were obtained ($\eta = T_i/T_f$, where T_i and T_f are the initial and final temperatures of the process). In the case of adiabatic melting of a solution with an initial concentration of 2% it is possible to obtain (as in Ref. 8) a degree of cooling $\eta = T_F(100\%)/T_F(2\%) = 7.3$, where $T_F(x)$ is the Fermi temperature for a solution with concentration x (for pure ^{3}He — $T_F(100\%) = 1.2$ K at $P = 2.5$ MPa).

Both methods are most promising for cooling solutions to extremely low temperatures, which is important in connection with the search for a superfluid transition of the impurity component of the solutions. Indeed, if $T_i < T_c$, where T_c is the superfluid transition temperature in ^{3}He (equal to 2.4 mK at a pressure of 2.5 MPa), the degree of

cooling increases substantially. According to estimates, in the case of adiabatic melting of a 1% solution from the starting temperature $T_i = 1$ mK the degree of cooling $\eta \approx 70$ and the final temperature $T_f \approx 15$ μK. The source of the cold is the solution itself, while the efficiency of cooling by nuclear demagnetization decreases rapidly because of the large Kapitsa jump. The minimum solution temperature achieved to date is approximately 100 μK.[9,10]

The practical observation of adiabatic melting of solutions is limited to the two attempts made in Ref. 3. For the initial temperatures of 57 and 217 mK the final temperatures were equal to 55 and 184 mK, and after repeated crystallization these temperatures increased to 80 and 221 mK, respectively. The authors concluded that as the temperature decreases, the refrigeration capacity, which decreases as T^2, rapidly drops below the heat release due to irreversible processes. Indeed, in n the case of solutions the Pomeranchuk cells ordinarily employed[11] for crystallizing ^{3}He result in dissipation due to plastic deformation and friction of the crystals against one another, since even at the start of the process the fraction of the solid phase is close to 1 and the cell volume must increase by 10% for complete melting of the crystal. In the present work we were able to employ a cell with a constant geometry for crystallization and melting of solutions at low temperatures. This was made possible by an additional line, equipped with a superfluid filter (SF), for filling the cell. At pressures for which the conventional filling line was blocked by the solid phase, the SF made it possible to transport liquid ^{4}He into and out of the chamber.[b)] The ^{4}He crystallization pressure in the pores of the SF was much higher than in the volume of the liquid (see, for example, Ref. 12 — $\Delta P \sim 0.2$–0.3 MPa for $d \sim 1$ μm). The use of a cell with a SF instead of a Pomeranchuk cell not only simplifies the construction of the low-temperature part of the apparatus, but it also eliminates the problem of heat release accompanying a change in geometry.

The experiments were performed in a 3.3 cm^3 cell (Fig. 1). The superfluid filter consisted of a Melchior capillary tightly plugged with a fine Fe_2O_3 powder (crocus). Special experiments showed that the SF is not plugged with solid ^{4}He at least up to 2.8 MPa. One end of the SF was located in the experimental cell and contained a packing (sp) consisting of sintered silver powder in order to increase the geometrical area through which pressure is transmitted to the chamber. The temperature at the second end of the SF at the location where it connects with the capillary tube running to the valve on the Dewar cup was maintained in the range $T_m < T < T_\lambda$, where T_m and T_λ are the crystallization temperature and λ-point temperature of ^{4}He at the working pressure. The first condition is that solid ^{4}He is not formed in the capillary and the second condition is that He II is present in the powder. The heat exchangers (*he*), consisting of ultradisperse silver powder baked onto copper foil, had an effective area (computed) of the order of 1 m^2. The temperature was measured according the susceptibility of the powdered cerium–magnesium nitrate, diluted to 50% with lanthanum (*LCMN*), pressed into the shape of a cylinder ($D = 5.5$ mm, $H = 5.5$ mm) with a filling factor of 90%. The working frequency of the oscillator equalled approximately 227 kHz. The sensitivity at $T = 0.1$ K was equal to $dT/df = 0.5$ mK/Hz. The thermometer *LCMN* was calibrated acccording to a 100-Ω rated Speer thermometer (t) placed in the mixing cell (mc) and serving as a sensitive element of an electronic temperature stabilizer. The measuring coil (c), which is in resonance with the oscillator circuit, was secured to the cell on three thin Stycast rods

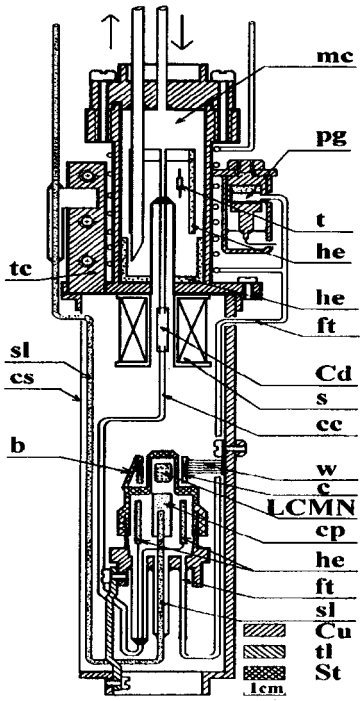

FIG. 1. Low-temperature part of the apparatus: Cu — copper, *tl* — textolite, *St* — Stycast, *cc* — cold conduit, *ft* — filling tube , *cs* — copper screen, *tc* — vise for thermal contact of SF on the mixing cell. The rest of the designations are explained in the text.

(*b*). To remove the heat released in the coil, copper insulated wires (50 μm) (*cw*) were glued onto it. The pressure in the cell was measured through the filling tube (*ft*) with the aid of a capacitive pressure gauge (*pg*) with a sensitivity of 2.9 kHz/atm, placed on the mixing cell. The superconducting thermal switch consisted of a cadmium rod (Cd) ($D=1.5$ mm, $L=9$ mm) placed in the field of a superconducting solenoid (*s*). After condensation of the mixture through the filling tube this line was cut off from external connections by a valve on the cap and the pressure in the cell was increased with the aid of a ^{4}He high-pressure tank through the SF. The concentration of the experimental mixture was calculated according to molar-volume data[13] and according to the known concentration of the initial mixture, the cell volumes, and the filling and SF lines. After the starting temperature was reached a crystal was grown in the cell over a time of the order of 30 min. The heat released in the process was removed into the mixing chamber. With the thermal switch open, the pressure was lowered with the aid of a fine-regulation valve. The excess ^{4}He (approximately 0.3 cm^3 of liquid) was collected into a bottle with a volume $V=1.50$ liters, and the amount of melted crystal was monitored according to the pressure in the bottle.

The results of several coolings for 2% and 7% solutions with different rates of melting and different starting temperatures are presented in Table I (x_3 — solution

TABLE I.

x_3, %	$T_F(x)$, K	n_3, mmole	$\dot{n}_L$, mmole/s	δt, min	T_i, mK	T_f, mK	η_e	η_t
			1.1	~2	142	70	2	
			0.56	4	95	50.3	1.9	
2	0.16	3.4	0.056	41	100	61	1.6	7.3
			0.39	6	56	43	1.3	
			—	—	42	29	1.4	
			0.36	6.5	57	39	1.5	
7	0.37	12	0.51	4.6	55	36	1.5	3.1

concentration, n_3 — number of ^{3}He moles in the cell, $\dot{n}_L$ — rate of formation of the liquid solution, δt — melting time of the crystal, T_i — initial temperature, T_f — final temperature, η_e — experimental degree of cooling, and η_t — theoretical degree of cooling).

The data are of a strongly preliminary character, since in the first experiments a strong thermal coupling was found between the experimental and mixing cells. According to data obtained from special measurements, the thermal resistance between them with the thermal switch open was two orders of magnitude lower than the computed value. This is due, in all probability, to an incomplete transition of the cadmium into the superconducting state. Nonetheless, the cooling effect was much stronger than that observed in Ref. 3: The degree of cooling in the range 40–140 mK was equal to 1.3–2. According to the data in Table I, for $x=2\%$ the value of η clearly tends to decrease as the initial temperature decreases. The relation of η with the rate of melting of the crystal is not as strict: For a 2% solution (second and third rows in Table I) a tenfold decrease of $\dot{n}_L$ resulted only in a small decrease in η (from 1.9 to 1.6), and for $x=7\%$ an increase in $\dot{n}_L$ by a factor of 1.4 had no effect at all on the value of η. These qualitative features cannot be explained by the effect of a heat inflow which is constant in time (or one which depends uniquely on the temperatures of the mixing and experimental cells); it is possible, that the heat inflow changed randomly from one measurement to another. The possibility that adiabatic conditions break down as a result of the melting itself of the crystal also cannot be ruled out. The characteristic time dependences of the temperature are shown in Fig. 2 for two coolings with a starting temperature of the order of 0.1 K. The first arrow corresponds to opening of the thermal switch. The sharp jump in the temperature derivative corresponds to melting onset. The second arrow indicates the moment when the third phase (pure liquid ^{3}He) vanished in the cell. This corresponds to melting of the crystal in one-fourth of the cell volume. It is evident in the curves that at this moment the rate of cooling decreases (Fig. 2a) or even that cooling is replaced by heating (Fig. 2b). This is qualitatively explained by the fact that the refrigeration efficiency in a three-phase system does not depend on the concentration, while in a two-phase system the refrigeration efficiency decreases as $\dot{q}\sim x_L^{1/3}T^2$ (Ref. 14), where x_L is the ^{3}He concentration in the diluted phase. When the entire crystal has melted (third arrow),

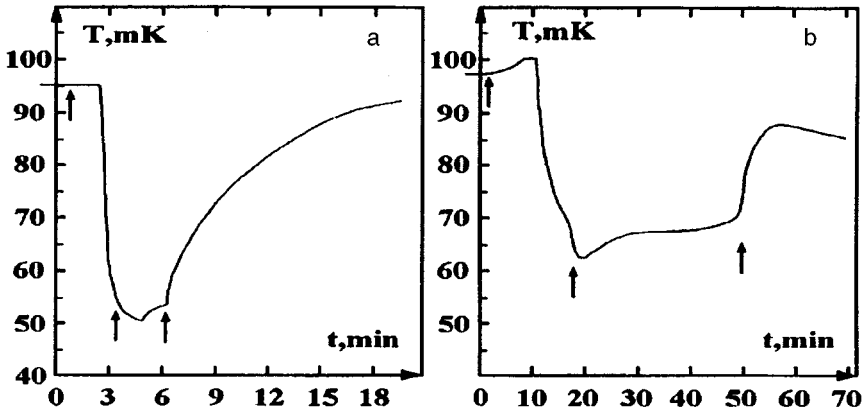

FIG. 2. Time dependence of the temperature during adiabatic melting with concentration $x=2\%$: a) $T_i=100$ mK, b) $T_i=95$ mK.

which can be judged according to the indications of the pressure gauge, the system starts to heat up as a result of parasitic heat inflow.

In closing, we note that the SF makes it possible to perform experiments with solutions at temperatures below the minimum on the crystallization curves. Furthermore, this structure is technically much simpler than the Pomeranchuk cells customarily used. At this stage it is impossible to say anything about the presence of internal dissipation sources characteristic of the melting process itself. Nonetheless, it can be expected that under adiabatic conditions the method employed makes it possible to approach the theoretical degrees of cooling.

I wish to thank the directors of the Institute of Physics Problems of the Russian Academy of Sciences and K. N. Zinov'eva for making it possible to perform this work, Yu. D. Anufriev for formulating the problem, and S. T. Boldarev for helpful discussions and suggestions.

[a)]e-mail: sebedash@kapitza.ras.ru
[b)]This possibility was pointed out to me by Yu. D. Anufriev.

[1] A. S. Greenberg, B. Hebral, M. Papoular *et al.*, J. de Physique (Paris) **41**, Colloq. C7–79 (1980).
[2] B. Castaing, A. S. Greenberg, and M. Papoular, J. Low Temp. Phys. **47**, 191 (1982).
[3] B. van den Brandt, W. Griffioen, G. Frossati *et al.*, Physica B **114**, 295 (1982).
[4] Yu. D. Anufriev, V. N. Lopatik, and A. P. Sebedash, JETP Lett. **37**, 45 (1983); V. N. Lopatik, Zh. Éksp. Teor. Fiz. **86**, 487 (1984) [Sov. Phys. JETP **59**, 284 (1984)].
[5] D. O. Edwards and S. Balibar, Phys. Rev. B **39**, 4083 (1989).
[6] P. M. Tedrow and D. M. Lee, Phys. Rev. **181**, 399 (1969).
[7] V. L. Vvedenskiĭ, JETP Lett. **24**, 132 (1976).
[8] A. P. J. Voncken and A. T. A. M. de Waele, J. Low Temp. Phys. **100**, 463 (1995).
[9] R. König, A. Betat, and F. Pobell, J. Low Temp. Phys. **97**, 311 (1994).
[10] G.-H. Oh, Y. Ishimoto, T. Kawae *et al.*, J. Low Temp. Phys. **95**, 525 (1994).
[11] V. Lounasmaa, *Experimental Principles and Methods Below 1 K*, Academic Press, N. Y., 1974 [Russian translation, Mir, Moscow, 1977, p. 92].

[12] E. N. Smith, D. F. Brewer, J. D. Reppy *et al.*, Physica B **107**, 585 (1981).
[13] B. N. Esel'son, V. G. Ivantsov, V. A. Koval' *et al.*, *Properties of Liquid and Solid Helium:* ^3He–^4He *Solutions* [in Russian], Naukova Dumka, Kiev, 1982.
[14] R. Radebaugh, NBS (US) Tech. Note No. 362 (1967).

Translated by M. E. Alferieff

Two-dimensional microclusters of vortices: shell structure and melting

Yu. E. Lozovik[a)] and E. A. Rakoch

Institute of Spectroscopy, Russian Academy of Sciences, 142092 Troitsk, Moscow Region, Russia

(Submitted 20 December 1996; resubmitted 30 December 1996)
Pis'ma Zh. Éksp. Teor. Fiz. **65**, No. 3, 268–273 (10 February 1997)

The melting of two-dimensional microclusters of ''particles'' which repel one another according to a logarithmic law and are confined by an external quadratic potential is investigated. The model describes Abrikosov vortices in a superconducting island of vortices in a rotating superfluid liquid and electrons in a semiconductor nanostructure surrounded by a low-permittivity medium. The structure of clusters and its dependence on temperature and melting are investigated. *The melting of microclusters of vortices* proceeds in *two stages*: 1. A transition from a frozen phase into a state corresponding to *rotational reorientation of crystal shells* relative to one another. 2. At a higher temperature, the radial order vanishes. This is connected with the fact that the barrier for rotation of the shells is much lower than the barrier for radial breakup of the shells.
[S0021-3640(97)00903-1]

PACS numbers: 74.60.−w, 64.70.Dv, 47.32.−y, 47.37.+q

INTRODUCTION

A magnetic field $H>H_{c_1}$ penetrates into a type-II superconductor in the form of Abrikosov vortices, which at low temperatures form an ideal triangular lattice (in the absence of pinning centers).[1] As the temperature increases, melting of this lattice and formation of a liquid phase from vortices can occur, as has been observed in high-T_c superconductors (see the review in Ref. 2).

The question of the structure of a mesoscopic system consisting of a *small* number of Abrikosov vortices confined in islands of a superconducting phase is of great interest. The system is equivalent to the problem of the *two-dimensional analog* (compare Ref. 3) of a classical Thompson atom[4] with ''charges'' which satisfy the laws of two-dimensional electrostatics and compensated by an incompressible background. This model also describes vortices in a rotating superfluid liquid as well as electrons in a semiconductor quantum dot embedded in a medium with a much lower permittivity (see below). A small system of vortices should behave like a *microcluster*. This means that the shell structure of the cluster can change sharply when only a single ''particle'' is added (structural sensitivity) right up to some number N of ''particles'' when a region with the structure of a ''volume'' phase — a region with a triangular lattice — appears inside this

cluster and melting of the microcluster can exhibit interesting specific features compared with melting of a volume phase.[3,5]

In the present work we studied the temperature dependence of the structure of microclusters of vortices. We have shown that the *melting of a two-dimensional microcluster of vortices proceeds in two stages*: First, intershell (''orientational'') melting occurs and at a much higher temperature the shells dissipate. We have also shown that this is due to the fact that the energy barrier for reorientation of the shells is much higher than the barrier for radial hops of the particles.

PHYSICAL MODEL

Let us now consider an island of a type-II superconductor in a transverse magnetic field. If the thickness d of the island in the temperature range studied is less than the coherence length $\xi(T)$ of the superconductor, then from the standpoint of the superconducting properties the island can be viewed as being *two-dimensional*. The magnetic field penetrates into the system in the form of two-dimensional (2D) vortices. The interaction potential between the 2D vortices has the form (see Ref. 6)

$$U(r)=-q^2\ln\frac{r}{a},\quad a\ll r\ll\lambda_\perp;\quad U(r)=q^2\frac{\lambda_\perp}{r}+\text{const},\quad r\gg\lambda_\perp,$$

where q is the ''charge,'' which is proportional to the density of the superfluid component; r is the distance between vortices; a is the radius of the core of a vortex, $a\sim\xi(T)$; $\lambda_\perp=\lambda^2/d$ is the penetration depth of the perpendicular magnetic field into a 2D superconductor; and, λ is the London penetration depth of the magnetic field in a three-dimensional superconductor. For example, for films of thickness $d\simeq 100$ Å and $\lambda\simeq 2000$ Å we have $\lambda_\perp\simeq 4$ μm.

Let $\xi\ll R\ll\lambda_\perp$. Then vortices in the island can be regarded as point-like ''particles'' repelling one another according to a logarithmic law. Stabilization of the density of vortices in superconductors in an external magnetic field is taken into account in this model by introducing an effective confinement potential $U_{\text{eff}}=\alpha r^2$ corresponding to a uniform compensating background. The image forces for vortices do not qualitatively change the properties of the system (the problem of taking account of the image forces will be discussed in a more detailed paper).

Therefore we arrive at a model of a 2D cluster consisting of N classical particles ($N=1-50$) repelling one another according to the law $U(r_{ij})=q^2\ln(r_{ij}/a)$ and confined by an external potential $U_{\text{ext}}(r_i)=\alpha r_i^2$.

After the scaling transformations

$$r\to(\alpha^{1/2}/q)r,\quad T\to(k_B/q^2)T,\quad U\to(1/q^2)U$$

the potential energy of the system assumes the form, to within the constant $C_N^2\ln(q/\alpha^{1/2}a)$,

$$U=-\sum_{i>j}\ln r_{ij}+\sum_i r_i^2. \tag{1}$$

The cluster properties studied here do not change qualitatively even for a small anisotropy of $U_{\text{eff}}(r)$.

A system of classical particles with the indicated potential energy (2) is equivalent to the 2D analog (compare with Ref. 3) of a classical Thomson atom.[4] This model describes not only vortices in a superconducting island, but also *vortices in a rotating vessel* with superfluid helium (see Refs. 7–11). It is also describes an *electronic cluster* in a semiconductor nanostructure (2D quantum dot), surrounded by a medium with a much lower permittivity $\epsilon \ll \epsilon_{\text{qdot}}$ (if the interelectronic distances r are such that $D \ll r \ll D/k$; D is the thickness of the nanostructure and $k = \epsilon/\epsilon_{\text{qdot}}$; like charges of the images of the electrons ''are aligned'' in charged lines, which results in an effective logarithmic interaction between the particles.

EQUILIBRIUM CLUSTER CONFIGURATIONS

To find the equilibrium particle configurations a random search for the minimum of the potential energy of the system with random motion of all other shells as a whole and random motion of the particles was employed.

The local and global minima of the potential energy were found. At low temperatures small logarithmic clusters (just as Coulomb clusters, see Refs. 3, 5, 12, and 13) have a shell structure. When the number of particles is sufficiently large, a region with a triangular structure nucleates inside a cluster (see Refs. 3, 5, and 7–11).

The occupation numbers of the shells and the corresponding potential energies (measured from $C_N^2 \ln(q/\alpha^{1/2}a)$, see above) for global minima of 2D logarithmic clusters are presented in Table I. The sequential filling of the shells is reminiscent of the ''periodic table'' of the elements (compare the filling of shells in the 2D classical system of particles with the *three-dimensional* Coulomb interaction[3]). Each shell can contain no more than a definite number of particles.

We employ the following concept of a shell (different from the previously employed definitions, which are not universal for a different number of particles; see, for example, Ref. 9). We define a shell as a convex polygon consisting of the maximum possible number of particles (and it contains the preceding shell) that satisfies the following rule: The maximum distance from the center of the system to a particle belonging to a given shell must be less than the minimum distance from the center of the system to a particle belonging to a shell which is external with respect to the first shell. The filling rules which we obtained for shells in clusters from our calculations using the above-mentioned definition are similar to the filling rule for shells in the periodic system of the elements.[3,5] Specifically, in contrast to Ref. 9, the number of shells cannot *decrease* as the number of particles *increases*. Correspondingly, the distribution of the particles over the shells in our work is different from that obtained in Ref. 9.

Since the confining quadratic potential is centrosymmetric, one would think that the shells in a cluster must be regular polygons inscribed in a circle. However, this is true only for clusters consisting of one or two shells, the inner shell consisting only of one particle. As the number of particles in clusters with small N increases further, spontaneous breaking of the symmetry occurs. This effect is strongest for $N = 10$ and $N = 24$. In

TABLE I. Shell structure and potential energy of vortex microclusters.

Number of particles	Shell filling numbers	Potential energy	Number of particles	Shell filling numbers	Potential energy
1	1	$0.000000\cdot 10^{0}$	26	3,9,14	$-1.940569\cdot 10^{2}$
2	2	$5.000000\cdot 10^{-1}$	27	3,9,15	$-2.156137\cdot 10^{2}$
3	3	$8.918023\cdot 10^{-1}$	28	4,9,15	$-2.384294\cdot 10^{2}$
4	4	$1.090457\cdot 10^{0}$	29	4,10,15	$-2.625912\cdot 10^{2}$
5	5	$9.764052\cdot 10^{-1}$	30	4,10,16	$-2.881028\cdot 10^{2}$
6	1,5	$4.354169\cdot 10^{-1}$	31	4,10,17	$-3.149268\cdot 10^{2}$
7	1,6	$-7.512442\cdot 10^{-1}$	32	4,11,17	$-3.431329\cdot 10^{2}$
8	1,7	$-2.514746\cdot 10^{0}$	33	5,11,17	$-3.727473\cdot 10^{2}$
9	1,8	$-4.914510\cdot 10^{0}$	34	1,5,11,17	$-4.037308\cdot 10^{2}$
10	2,8	$-8.100414\cdot 10^{0}$	35	1,6,11,17	$-4.361606\cdot 10^{2}$
11	3,8	$-1.209333\cdot 10^{1}$	36	1,6,12,17	$-4.700331\cdot 10^{2}$
12	3,9	$-1.697858\cdot 10^{1}$	37	1,6,12,18	$-5.053534\cdot 10^{2}$
13	4,9	$-2.271610\cdot 10^{1}$	38	1,6,12,19	$-5.420929\cdot 10^{2}$
14	4,10	$-2.942793\cdot 10^{1}$	39	1,7,13,18	$-5.803155\cdot 10^{2}$
15	4,11	$-3.706118\cdot 10^{1}$	40	1,7,13,19	$-6.200430\cdot 10^{2}$
16	5,11	$-4.573707\cdot 10^{1}$	41	1,7,13,20	$-6.612310\cdot 10^{2}$
17	1,5,11	$-5.541308\cdot 10^{1}$	42	1,7,14,20	$-7.039416\cdot 10^{2}$
18	1,6,11	$-6.620692\cdot 10^{1}$	43	2,8,14,19	$-7.481666\cdot 10^{2}$
19	1,6,12	$-7.811655\cdot 10^{1}$	44	2,8,14,20	$-7.939606\cdot 10^{2}$
20	1,6,13	$-9.110199\cdot 10^{1}$	45	2,8,14,21	$-8.412619\cdot 10^{2}$
21	1,7,13	$-1.052696\cdot 10^{2}$	46	3,9,14,20	$-8.901514\cdot 10^{2}$
22	1,7,14	$-1.205683\cdot 10^{2}$	47	3,9,15,20	$-9.406122\cdot 10^{2}$
23	1,8,14	$-1.370647\cdot 10^{2}$	48	3,9,15,21	$-9.926554\cdot 10^{2}$
24	2,8,14	$-1.548203\cdot 10^{2}$	49	3,9,15,22	$-1.046250\cdot 10^{3}$
25	3,8,14	$-1.737968\cdot 10^{2}$	50	4,10,15,21	$-1.101460\cdot 10^{3}$

these cases, since the first shell (counting from the center) consists of two particles, it is advantageous for the second shell to assume the shape of an ellipse.

MELTING AND PHASE TRANSITIONS

We used the Monte Carlo method (MC) to study the dependence of the physical quantities on the temperature and melting of the system. After the equilibrium configurations were found, the system was heated by the amount ΔT (ΔT) ranging from ($1\cdot 10^{-4}$ to $5\cdot 10^{-3}$), after which the system was held at the new temperature for $2\cdot 10^{4}$ Monte Carlo steps until it reached equilibrium. Next, the statistical characteristics were calculated by averaging over $1\cdot 10^{6}$ Monte Carlo steps. After this, a further heating using the described procedure was performed. The following quantities were calculated.

1. Total potential energy U_{pot}.

2. Mean-square radial displacements (MSRD) — total

$$\langle \delta R^2 \rangle = \frac{1}{N}\sum_{i=1}^{N}\frac{\langle r_i^2\rangle - \langle r_i\rangle^2}{a^2} \tag{2}$$

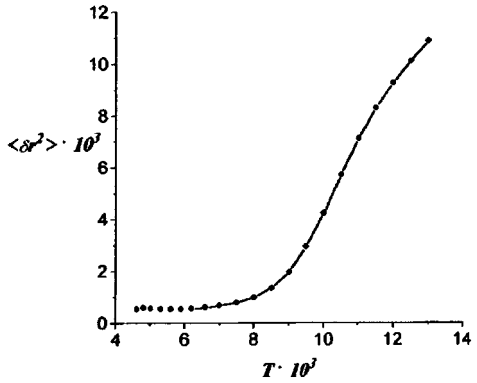

FIG. 1. Total mean-square radial displacement $\langle \delta r^2 \rangle$ as a function of temperature for a 2D logarithmic cluster with $N=37$ particles.

and for each shell separately

$$\langle \delta r^2 \rangle = \frac{1}{N_R} \sum_{i=1}^{N_R} \frac{\langle r_i^2 \rangle - \langle r_i \rangle^2}{a^2}, \tag{3}$$

where N_R is the number of particles in a shell and the averaging $\langle \ldots \rangle$ is performed over different Monte Carlo configurations.

3. The mean-square angular displacements (MSAD) relative to the nearest particles in the same shell

$$\langle \delta \phi_1^2 \rangle = \frac{1}{N_R} \sum_{i=1}^{N_R} \frac{\langle (\phi_i - \phi_{i_1})^2 \rangle - \langle (\phi_i - \phi_{i_1}) \rangle^2}{\phi_0^2} \tag{4}$$

and the MSAD relative to the closest particles of a neighboring shell

$$\langle \delta \phi_2^2 \rangle = \frac{1}{N_R} \sum_{i=1}^{N_R} \frac{\langle (\phi_i - \phi_{i_2})^2 \rangle - \langle (\phi_i - \phi_{i_2}) \rangle^2}{\phi_0^2}, \tag{5}$$

where i_1 and i_2 refer to the closest particle from the same and neighboring shells, respectively; $2\phi_0 = 2\pi/N_R$ is the average angular separation between neighboring particles in a given shell.

The temperature dependence of the total MSRD for a cluster with $N=37$ is shown in Fig. 1. The MSRD for all shells have a kink at the same temperature $T_c = 8 \cdot 10^{-3}$. One can see from Fig. 2 that for all shells the MSAD relative to the nearest particles in the same shell have a kink at the same temperature. Therefore a phase transition occurs at temperature $T_c = 8 \cdot 10^{-3}$ in a cluster with $N=37$ particles: The system becomes disordered. At $T > T_c$ the number of particles in the shells starts to change; the shells exchange particles and dissipate. It is impossible to distinguish any shells at temperatures $T \gg T_c$. Particles move about chaotically. The characteristic dimensionless parameter

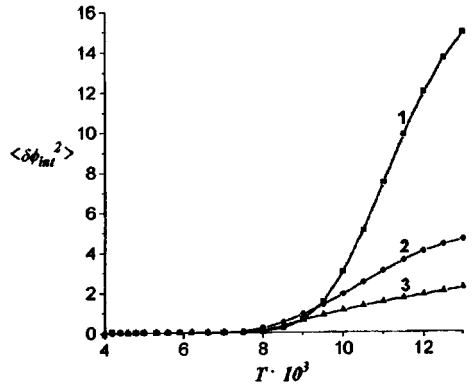

FIG. 2. MSAD $\langle \delta\phi_1^2 \rangle$ as a function of temperature for a 2D logarithmic cluster with $N=37$ particles relative to the closest particles from a given shell: *1* — MSAD of the outer shell relative to the closet particles from the given shell. *2* — MSAD of the middle shell relative to the closest particles from the given shell. *3* — MSAD of the inner shell relative to the closest particles from the given shell.

$\Gamma = q^2/k_B T_c$ for which a system with $N=37$ melts equals $\Gamma = 125$, which is almost identical to the value of Γ at which a system with a relatively large number of vortices melts ($\Gamma = \Gamma_c \simeq 130$).

It is found, however, that the MSAD of relatively close particles in *neighboring* shells possess a kink at *much lower* temperatures. For a cluster with 37 particles the MSAD of the outer shell relative to the closest particles in the middle shell start to grow

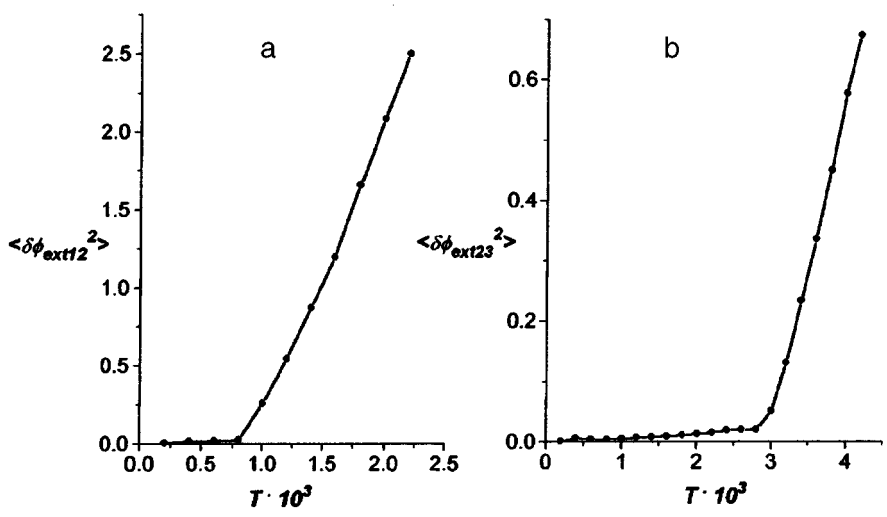

FIG. 3. MSAD $\langle \delta\phi_2^2 \rangle$ as a function of temperature for a 2D logarithmic cluster with $N=37$ particles with respect to the closest particles from the neighboring shell: a — MSAD of the middle shell relative to the closest particles from the outer shell; b — MSAD of the inner shell relative to the closest particles from the middle shell.

rapidly at $T_{c_1}=8\cdot 10^{-4}$ ($\Gamma=1/T_{c_1}=1250$, see Fig. 3a), and the MSAD of the middle shell relative to the closest particles of the inner shell start to grow rapidly at $T_{c_2}=3\cdot 10^{-3}$ ($\Gamma=1/T_{c_2}=333$, see Fig. 3b). This means that a specific *orientational* melting, characteristic for clusters with shell structure, occurs at these temperatures, i.e., in 2D clusters at some moment in time the shells the shells, *retaining their crystallinity, start to rotate relative to one another*.

We found the potential barrier U_1 for rotation and the potential barrier U_2 for a particle to hop from one shell to another. It turned out that the orientational barrier is much lower than the radial barrier. Together with the jump in the MSAD, this is another strong proof of the occurrence of orientational melting in 2D clusters of vortices (for example, for $N=11$, $U_1=2.32\cdot 10^{-6}\ll U_2=3.71\cdot 10^{-2}$).

It would be very interesting to observe experimentally the new orientational melting in a microcluster of vortices, for example, by observing the vortices using as a substrate a magnetooptic material whose local magnetization is studied with the aid of a polarization microscope (in this case, the reorientations of shells of vortices can be observed in real-time) or a scanning tunneling microscope or by means of decoration.

We thank S. A. Brazovskiĭ for a helpful discussion. This work was supported by Russian Fund for Fundamental Research grants, ''Physics of Solid-State Nanostructures'' and ''Surface Atomic Structures.''

[a)]e-mail: lozovik@isan.msk.su

[1] A. A. Abrikosov, Zh. Éksp. Teor. Fiz. **32**, 1442 (1957) [Sov. Phys. JETP **5**, 1174 (1957)].
[2] G. Blatter, M. V. Feigel'man, V. B. Geshkenbein *et al.*, Rev. Mod. Phys. **66**, 1125 (1994).
[3] Yu. E. Lozovik, Usp. Fiz. Nauk **153**, 356 (1987) [Sov. Phys. Usp. **30**, 912 (1987)].
[4] J. J. Thomson, Philos. Mag. **6, 7**, 238 (1904).
[5] Yu. E. Lozovik and V. A. Mandelshtam, Phys. Lett. A **145**, 269 (1990); Yu. E. Lozovik and V. A. Mandelshtam, Phys. Lett. A **165**, 469 (1992); F. M. Peeters, V. A. Schweigert, and V. M. Bedanov, Physica B **212**, 237 (1995); Yu. E. Lozovik, Izv. Ross. Akad. Nauk, Ser. Fiz. **60**, 85 (1996).
[6] Y. Pearl, Appl. Phys. Lett. **5**, 65 (1964).
[7] G. B. Hess, Phys. Rev. **161**, 189 (1967).
[8] D. Stauffer and A. L. Fetter, Phys. Rev. **168**, 156 (1968).
[9] L. J. Campbell and R. M. Ziff, Phys. Rev. B **20**, 1886 (1979).
[10] R. N. Ignat'ev and É. B. Sonin, Zh. Éksp. Teor. Fiz. **81**, 2059 (1981) [Sov. Phys. JETP **54**, 1087 (1981)].
[11] G. E. Volovik and U. Parts, JETP Lett. **58**, 774 (1993).
[12] H. Totsuji and J. L. Barrat, Phys. Rev. Lett. **60**, 2484 (1988).
[13] K. Tsuruta and S. Ichimaru, Phys. Rev. A **48**, 1339 (1993).

Translated by M. E. Alferieff

Luminescence of fluctuation tails of disordered solid solutions

A. A. Klochikhin
Institute of Nuclear Physics, Russian Academy of Sciences, 188350 Gatchina, St. Petersburg, Russia

S. A. Permogorov[a)] and A. N. Reznitskiĭ
A. F. Ioffe Physicotechnical Institute, Russian Academy of Sciences, 193021 St. Petersburg, Russia

(Submitted 5 January 1997)
Pis'ma Zh. Éksp. Teor. Fiz. **65**, No. 3, 274–279 (10 February 1997)

The form of the stationary luminescence spectra of excitons, localized by composition fluctuations, in disordered solid solutions under weak excitation is calculated. The tail states for which there are no nonradiative transition channels are distinguished by means of continuum percolation theory. Such states are responsible for the ''zero-phonon'' luminescence band. The shape of the short-wavelength luminescence band edge is determined mainly by the number of isolated localizing clusters and their smallest complexes, which decreases rapidly near the mobility threshold. The real luminescence spectrum is due to the simultaneous emission of phonons. The phonon emission determines the form of the long-wavelength wing of the emission band. The computed shape of the emission spectrum is compared with the experimental luminescence spectra of the solid solution $CdS_{(1-c)}Se_c$. © *1997 American Institute of Physics.* [S0021-3640(97)01003-7]

PACS numbers: 78.60.−b, 64.60.Ak, 64.60.Cn

The characteristic luminescence of many disordered systems[1] and, specifically, II–VI solid solutions,[2–6] is due to the recombination of excitons localized in the wells of the potential relief. A general feature of such systems is a large red shift of the luminescence relative to the excitonic absorption maximum, so that the main emission band falls into the region of low absorption coefficients and small values of the density of fluctuation states.

The origin of the red shift of the luminescence band and the ratio of the luminescence and absorption spectra are problems which are important for understanding the physical processes in disordered systems.

In this letter we report the results of a theoretical description of the position of the characteristic luminescence band contour relative to the absorption spectrum of fluctuation states, we give a qualitative justification of the approach to this problem with the aid of a classical continuum percolation theory, and we compare the theoretical and experimental results for II–VI solutions.

The density of states in the energy range where the tail states in the zeroth approxi-

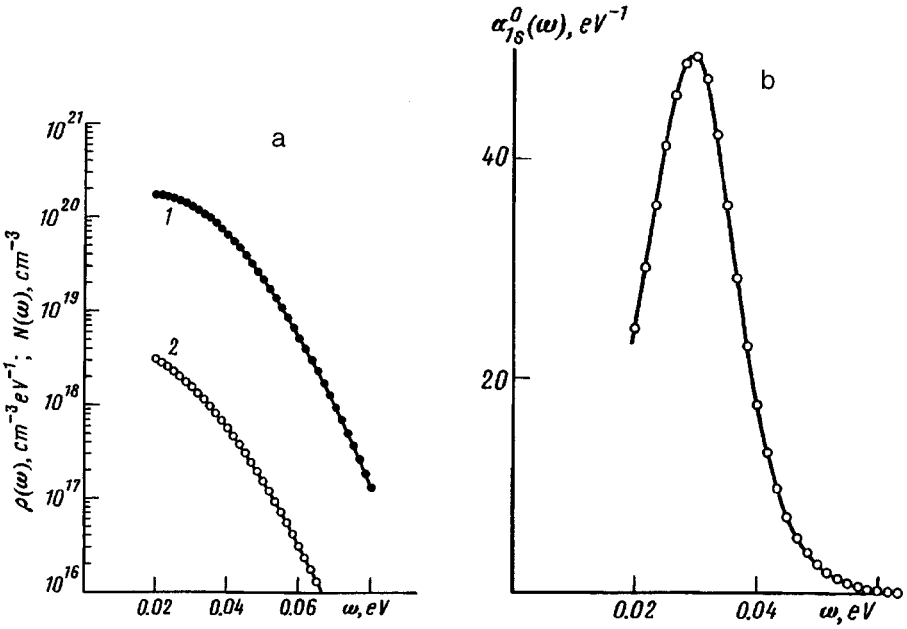

FIG. 1. a) Computed density of states $\rho(\omega)$ — *1* and integral density $\mathcal{N}(\omega)$ — *2* of the fluctuational tails of the ground state of an exciton in the solid solution $CdS_{(1-c)}Se_c$ with $c=0.2$. b) Spectral density $\alpha^0_{1s}(\omega)$ of an excitonic ground state in the solid solution $CdS_{(1-c)}Se_c$ with $c=0.2$ neglecting the interaction with phonons.

mation can be regarded as isolated from one another was calculated by a variational method which is a modification of the method described in Refs. 7 and 8. Next, a method which is not associated with a variational procedure and gives a normalization of the density of fluctuation states was used to calculate the total number of localized states. The calculation of the number of states was based on the assumption that localized excitonic states arise in fluctuations (clusters) which have the character of simply connected potential wells.

The results of the calculations of the density $\rho(\omega)$ and the integral density $\mathcal{N}(\omega)$ of states for $CdS_{(1-c)}Se_c$ with $c=0.2$ are displayed in Fig. 1a. The values obtained for the density of tail states lead to the zero wave vector spectral density presented in Fig. 1b. The band $\alpha^0_{1s}(\omega)$ obtained consists of the excitonic absorption spectrum in the region of the fluctuation states neglecting the interaction with lattice vibrations.

In the approach employed, the possibility of optical recombination is limited by the exciton lifetime with respect to a nonradiative transition into lower-lying tail states which is accompanied by phonon emission.[2–4] To calculate the zero-phonon luminescence band shapes it is necessary to find the energy distribution of states for which there are no nonradiative loss channels or such channels are strongly limited. In other words, it is necessary to know the distribution of spatially isolated localized states. In the general case this problem can be solved in the quantum theory of percolation.[9–16]

Isolated states in lattice models were studied in Refs. 9–11. As shown in Ref. 11,

two types of isolated localized states arise in the quantum percolation theory. The first type includes states belonging to isolated atoms[9–11] (in our case potential wells or clusters) and relatively small complexes (superclusters) which are formed with a random distribution of potential wells. Superclusters play an increasingly larger role as the mobility threshold is approached.

Isolated localized states of the other type are due to quantum interference effects.[11,13] In the presence of on-diagonal disorder, which in the problem at hand determines the energy distribution of the states, substantial suppression of interference effects should be expected. In the absence of interference effects the problem reduces to finding the distribution of tail states over superclusters in the continuous model, i.e., a problem which is substantially analogous to the problem of percolation along overlapping spheres.[17–20]

The relations which follow from the classical theory of percolation along overlapping spheres make it possible to find the distribution of states over superclusters and distinguish the fluctuation states which possess the maximum lifetime and form a zero-phonon luminescence band. This approach makes it possible to determine the position of the zero-phonon luminescence band relative to the maximum of the zero-phonon absorption band of the ground state of an exciton and the mobility threshold for classical percolation. We shall assume that for every localized state there exists a sphere of radius $R_{\rm int}$ such that if at a given density of localized states more than one potential well is present, on the average, in the volume $4\pi R_{\rm int}^3/3$, then a transition with phonon participation is possible between states in these wells. The quantity $R_{\rm int}$ cannot exceed the distance between two wells for which the exciton–phonon transition time between them equals the radiative lifetime of an exciton.

The stationary density $P(\omega)$ of occupied states with continuous and quite weak interband excitation is proportional to the density of states for given energy and lifetime. Taking account of the fact that for occupied states the emission probability is described by zero-phonon absorption coefficient $\alpha_{1s}^0(\omega)$ in the $1s$ state of an exciton, we can represent the zero-phonon luminescence band in the form

$$I_{1s}^0(\omega) \sim \alpha_{1s}^0(\omega) P(\omega), \tag{1}$$

where $P(\omega)$ is the total relative population of states with localization energy ω which belong to superclusters of different size. The main contribution of isolated wells and the ground states of pairs to $P(\omega)$ can be represented as

$$I^0(\omega) \sim \alpha_{1s}^0(\omega)\tau_{\rm rad}[\exp\{-2\mathcal{P}(\omega)\} + \mathcal{P}(\omega)\exp\{-3.073\mathcal{P}(\omega)\}], \tag{2}$$

where

$$\mathcal{P}(\omega) = \frac{1}{2}[R_{\rm int}/\overline{r(\omega)}]^3, \quad \overline{r(\omega)} = \left(\frac{3}{4\pi}\frac{1}{\mathcal{N}(\omega)}\right)^{(1/3)}.$$

The integral density of states $\mathcal{N}(\omega)$ gives a density of potential wells with localization energy limited by the quantity ω on one side and by Lifshitz's limit on the other.[21] The function $\mathcal{P}(\omega)$ is the density of localized excitons in units of the first virial coefficient. In the classical theory of percolation the data obtained by different authors for the critical density for percolation along spheres[20] fall in the range $1.17 \geqslant \mathcal{P}_{\rm cr}^{\rm cl} \leqslant 1.40$. In our calcula-

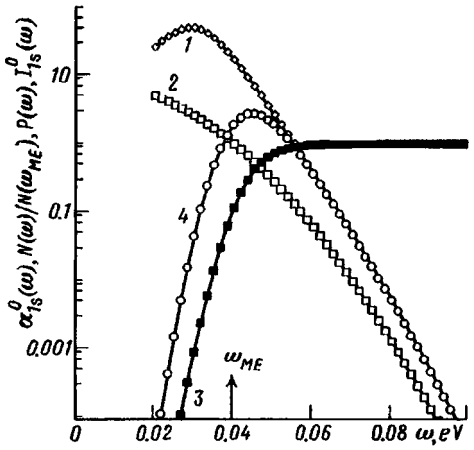

FIG. 2. Curve *1* — spectral density $\alpha^0_{1s}(\omega)$ of the excitonic ground state in the solid solution $CdS_{(1-c)}Se_c$ neglecting the interaction with phonons; curve *2* — relative integrated density of states $\mathcal{N}(\omega)/\mathcal{N}(\omega_{ME})$; curve *3* — relative occupancy $\mathcal{P}(\omega)$ of the states; *4* — zero-phonon luminescence band $I^0_{1s}(\omega)$; the arrow marks the position of the mobility threshold ω_{ME}, $c=0.2$.

tions we employed for the density of excitonic states at the percolation threshold the value $\mathcal{P}(\omega_{ME})=1.40$. Isolated potential wells and the smallest superclusters make the main contributions in all cases, while the higher-order terms give only small corrections both at low densities $\mathcal{N}(\omega)/\mathcal{N}(\omega_{ME})\ll 1$, as a result of the fact that their number is proportional to powers of the density[20] $\mathcal{P}(\omega)$ which increase with the supercluster size, as well as near the mobility threshold on account of additional exponentially small factors. The computational results for the zero-phonon luminescence band contour for the ground state of an exciton are presented in Fig. 2. The position of the percolation threshold corresponds to the point where the values of the curve *2* equal *1*.

The interaction with optical and acoustic phonons is taken into account on the basis of two models of localized excitons (models I and II). In the first model it is assumed that the electron can follow adiabatically the motion of the hole, and in the second model the electron interacts with a hole density distribution averaged over a fluctuation well. Both limits, as well as intermediate variants, are realized in the solid solution $CdS_{(1-c)}Se_c$.

Figure 3 displays the computational results and the experimental spectrum at concentration $c=0.2$, when model II makes the determining contribution. Satisfactory agreement with the experimental curves is achieved when up to four *LA*-phonon repetitions are taken into account. The maximum of the distribution of emitting states is red-shifted with respect to the absorption maximum, even when the interaction with the lattice vibrations is neglected; this agrees qualitatively well with existing experimental data for all disordered systems.[1] The interaction with phonons results in additional Stokes shifts of the emission and absorption bands in opposite directions.

Our model gives a good quantitative description of the experimental situation. Below the mobility threshold the form of the zero-phonon luminescence band is determined by an universal exponential dependence of the density of states and the occupancy func-

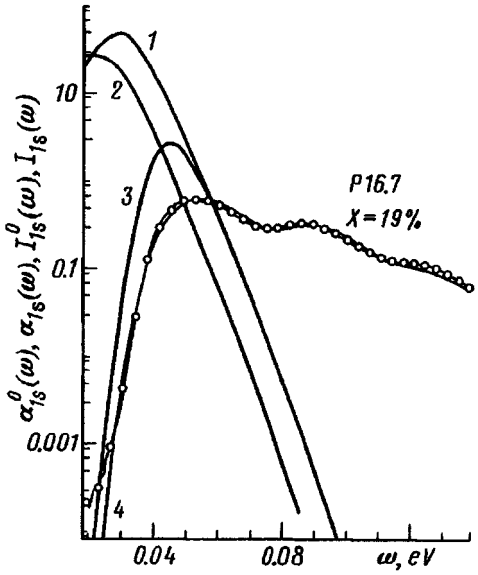

FIG. 3. Computed absorption and luminescence spectra taking account of the interaction with phonons for $c=0.20$. Curve *1* — zero-phonon absorption band $\alpha^0_{1s}(\omega)$ of the excitonic ground state; *2* — absorption band $\alpha_{1s}(\omega)$ taking account of the interaction with phonons; *3* — zero-phonon luminescence band $I^0_{1s}(\omega)$; *4* — luminescence band $I_{1s}(\omega)$ calculated taking account of the interaction with phonons. Dots — experimental luminescence spectrum of $CdS_{(1-c)}Se_c$ with band–band excitation.

tion $\mathcal{P}(\omega)$, calculated on the basis of the fundamental relations of the classical theory of percolation. This energy range makes the main contribution of the order of 80–90% of the integral luminescence intensity.

Above the mobility threshold the theory predicts a close-to-exponential decay of the luminescence intensity; this agrees qualitatively with a wide class of experiments. The computed value of the slope $\{[\ln(I^0_{1s}(\omega))]'_\omega\}^{-1}$ can be easily compared with the experimentally measured slope within 4 to 5 orders of the intensity.

As one can see from Fig. 3, the exciton–phonon interaction has practically no effect on the form of the long-wavelength absorption band edge and the short-wavelength edge of the luminescence spectrum. Therefore the experimentally measured exponential slopes of these sections of the spectra yield information about the zero-phonon luminescence band that can be used to determine the parameters characterizing disordered systems. It is also interesting that the ratio of the slope of the long-wavelength absorption band edge $\varepsilon_U(c)$ to the slope $\{[\ln(I^0_{1s}(\omega))]'_\omega\}^{-1}$ of the short-wavelength edge of the luminescence spectrum remains, to a good degree of accuracy, constant in the entire investigated range of concentrations.

In summary, the data presented in this letter show that new information about the states of excitons in disordered solid solutions can be obtained from a detailed analysis of the luminescence spectra.

This work is supported by the INTAS Foundation (Grants Nos. 94-324 and 94-481) and the Russian Fund for Fundamental Research (Grant No. 96-02-16933).

[a)]e-mail: PERM@prst.ioffe.rssi.ru

---

[1] R. A. Street, Adv. Phys. **30**, 593 (1981).
[2] S. Permogorov and A. Reznitsky, J. Luminescence **52**, 201 (1992).
[3] E. Cohen and M. Sturge, Phys. Rev. B **25**, 3828 (1982).
[4] A. Klochikhin, S. Permogorov, and A. Reznitsky, J. Cryst. Growth **159**, 848 (1996).
[5] A. Reznitsky, S. D. Baranovskii, A. Tsekoun *et al.*, Phys. Status Solidi B **184**, 159 (1994).
[6] A. Naumov, S. Permogorov, A. Reznitsky *et al.*, J. Cryst. Growth **101**, 713 (1990).
[7] A. A. Klochikhin and S. G. Ogloblin, Phys. Rev. B **48**, 3100 (1993).
[8] A. A. Klochikhin, Phys. Rev. B **53**, 10979 (1995).
[9] P. G. de Gennes, P. Lafore, and J. P. Millot, J. Phys. Chem. Solids **11**, 105 (1966); J. Phys. Radium **20**, 624 (1959).
[10] Y. Cho and Y. Toyozawa, J. Phys. Soc. Jpn. Suppl. **26**, 71 (1969).
[11] S. Kirkpatrick and T. P. Eggarter, Phys. Rev. B **6**, 3598 (1972).
[12] A. B. Harris and T. C. Lubensky, Phys. Rev. B **23**, 2640 (1981).
[13] Y. Shapir, A. Aharony, and A. B. Harris, Phys. Rev. Lett. **49**, 486 (1982).
[14] W. Y. Ching and D. L. Huber, Phys. Rev. B **25**, 1096 (1982).
[15] Y. Meir, A. Aharonyand A. B. Harris, Europhys. Lett. **10**, (3), 275 (1989).
[16] I. Chang, Zvi Lev, A. B. Harris *et al.*, Phys. Rev. Lett. **74**, 2094 (1995).
[17] D. F. Holcomb and J. J. Rehr Jr., Phys. Rev. **183**, 773 (1969).
[18] V. K. S. Shante and S. Kirkpatrick, Adv. Phys. **20**, 325 (1971).
[19] G. E. Pike and C. H. Seager, Phys. Rev. B **10**, 1421 (1974).
[20] S. W. Haan and R. Zwanzig, J. Phys. A: Math. Gen. **10**, 1547 (1977).
[21] I. M. Lifshitz, Usp. Fiz. Nauk **83**, 617 (1964) [Sov. Phys. Usp. **7**, 549 (1964)].

Translated by M. E. Alferieff

On the detection of finite-frequency current fluctuations

G. B. Lesovik
Institute of Solid State Physics, Russian Academy of Sciences, 142432 Chernogolovka, Moscow Region, Russia

R. Loosen
Bayer AG, 51368 Leverkusen, Germany

(Submitted 16 December 1996; resubmitted 16 January 1997)
Pis'ma Zh. Éksp. Teor. Fiz. **65**, No. 3, 280–284 (10 February 1997)

We consider a measurement of finite-frequency current fluctuations, using a resonance circuit as a model for the detector. We arrive at an expression for the measurable response in terms of the current–current correlators which differs from the standard (symmetrized) formula. The possibility of detection of vacuum fluctuations is discussed. © *1997 American Institute of Physics.* [S0021-3640(97)01103-1]

PACS numbers: 05.40.+j, 07.50.Hp, 72.70.+m

Finite-frequency (FF) current fluctuations at zero temperature (vacuum fluctuations, VFs) have been discussed for a long time[1] in connection with the analogous question of electromagnetic vacuum fluctuations. Recently there has been renewed interest in the noise at finite frequency in connection with the supposed possibility of observing the Fermi edge singularity in noninteracting[1,2] and interacting[3] systems.

In the present letter we consider a realistic model for an FF measurement and show that, in a very close analogy with the electromagnetic vacuum fluctuations, a certain measurability limitation appears.

There are different practical and theoretical approaches to FF measurements:

1. Making repeated measurements of the instantaneous values of the current over a long time interval and later Fourier transforming the data obtained.

2. Making a single measurement of the charge transmitted during a given time interval. In that case the information about the FF fluctuation appears through an integral over all frequencies. Ideally that can be done by making two measurements of the charge in the reservoir, the initial (during system preparation) and final. An alternative measurement can be made with a ''Larmor clock'' (the spin rotating in the magnetic field produced by the current); this method, which is described in Ref. 4, can perhaps be implemented.

3. Making a time-averaged measurement of the response of a resonance circuit, which can be an ordinary LC element, i.e., an inductive element coupled to the quantum wire, a capacitor whose charge is the quantity to be measured as a response, and the resistance of the circuit.

The last approach, we believe, is the most relevant for FF measurements.

We model our detector (the resonator, which we will refer to as LC) by an oscillator

and consider the response in the first nonvanishing order in the inductive coupling constant (we will outline the calculation at the end).

Finally, we arrive at the practical conclusion that the measurable response of such a model detector at a certain frequency Ω can be written in terms of the usual current–current correlators as follows:

$$S_{\text{meas}} = K\{S_+(\Omega) + N_\Omega[S_+(\Omega) - S_-(\Omega)]\}, \tag{1}$$

with the definitions

$$S_+(\Omega) = \int dt \langle I(0)I(t)\rangle \exp(i\Omega t),$$

and

$$S_-(\Omega) = \int dt \langle I(t)I(0)\rangle \exp(i\Omega t).$$

The frequency Ω in all the expressions is strictly positive. N_Ω stands for the Bose occupation number of the oscillator, i.e., $N_\Omega = [\exp(\hbar\Omega/k_B T_{LC}) - 1]^{-1}$, K is the effective coupling constant of the quantum wire with the resonator, $\langle A\rangle = \mathrm{Tr}\rho A$, where ρ is the density matrix of the electrons, and the time-dependent current operators are defined in the standard way: $I(t) = \exp(iHt) I \exp(-iHt)$.

The expression obtained here should be contrasted with the widely used formula[5]

$$S(\omega) = \int dt \, \exp(i\omega t) \left\langle \frac{1}{2}\{I(0)I(t) + I(t)I(0)\} \right\rangle. \tag{2}$$

Note that this formula contains the symmetrized current–current correlator. The necessity of such a symmetrization comes from the fact that in the general case the current operators at different times do not commute with each other, and it is motivated by the close correspondence with the classical expression.[5]

Using the definition (2), one arrives at the well-known expression for the spectral density of the current–current correlator for a conductor in equilibrium:[6]

$$S(\omega) = 2G\hbar\Omega \left[\frac{1}{2} + \frac{1}{\exp(\hbar\Omega/k_B T) - 1} \right]. \tag{3}$$

This expression tells us that at zero temperature one should expect fluctuations proportional to the frequency, which are interpreted as an analog of the vacuum fluctuations of the electromagnetic field.

Nevertheless, as is known from optical measurements, ordinary photodetectors do not react to the vacuum fluctuations, because it is not possible to take energy from the vacuum to excite atoms in the detector.[7]

Yet the vacuum fluctuations are observable, though less directly than are ordinary fluctuations, via the Lamb shift[8] or the Casimir effect[9] or by using a so-called quantum photocounter,[10] which is prepared in an excited state and can thus react to VFs.

As we will now show by analyzing Eq. (1), an LC detector may operate as a photodetector without any reaction to VFs or as an optical detector for VFs, but it never gives the standard Nyquist expression for FF noise (3), as one might naively expect.

If the detected frequency is higher than the LC temperature, the occupation N_Ω is exponentially small, and the only nonvanishing term in (1) is the ''positive part'' of the spectral density $S_+(\Omega)$, which describes the ''emission'' of energy by the conductor to the LC circuit, and in that case the LC circuit functions as an ordinary photodetector.

As an example, for $S_+(\Omega)$ in a coherent conductor with transmission D at zero temperature and a finite bias voltage one has

$$S_+(\Omega)=\frac{2e^2}{h}D(1-D)(eV-\hbar\Omega) \tag{4}$$

if $\hbar\Omega<eV$ and $S_+(\Omega)=0$ otherwise.

We have neglected the energy dependence of the transmission in the expression above, as well as an additional frequency dependence which has to come from the averaging over the coordinates (see below). Equation (4) coincides with the *excess* spectral density calculated in Ref. 1 using the symmetrized correlator (2).

If the frequency is much lower than the detector temperature, $\hbar\Omega\ll k_BT_{LC}$, one may replace the Bose occupation number N_Ω by $k_BT_{LC}/\hbar\Omega$.

The difference $S_+(\Omega)-S_-(\Omega)$ is *negative*, and in the case of a quantum conductor, provided that the transmissions D_n depend only weakly on the energy we find

$$S_+-S_-=-2\hbar\Omega G, \tag{5}$$

where $G=2e^2/h\Sigma_nD_n$ is the conductance.[11]

Note that the singular behavior of the spectral density at $\hbar\Omega=eV$ which was found in Ref. 2 for the symmetrized expression S_++S_- is not present in S_+-S_-, and we conclude that the measurable singularity at zero temperature and finite bias is due solely to the cutoff of the frequency by the voltage in $S_+(\Omega)$ (4).

Altogether, for $\hbar\Omega\ll k_BT_{LC}$ we have

$$S_{\text{meas}}=K\{S_+(\Omega)-2Gk_BT_{LC}\}. \tag{6}$$

The meaning of the negative part is clear—the LC circuit is ''cooled down'' by emitting energy into the conductor. So, in some sense, in this limit the vacuum fluctuations, represented by S_-, are detectable; note, however, that they appear in the answer in a way which is quite different from the Nyquist expression (3).

If the conductor is in equilibrium (aside from the weak interaction with the LC circuit), for low frequencies we find

$$S_{\text{meas}}\propto 2G(T_e-T_{LC}). \tag{7}$$

This expression vanishes if the electron temperature T_e is equal to the LC temperature T_{LC}, as is expected for overall equilibrium.

At intermediate frequencies, where $k_BT_e, eV_{\text{bias}}\ll\hbar\Omega\ll k_BT_{LC}$ the measurable response is negative:

$$S_{\text{meas}} = -2Gk_BT_{LC}. \tag{8}$$

Let us now outline briefly the derivation of Eq. (1). Our chosen detector can be regarded as a harmonic oscillator coupled linearly to the time derivative of the current to be measured:

$$M\ddot{x}(t) = -Dx(t) - \alpha\dot{I}(t). \tag{9}$$

In terms of the physical parameters of the counter (inductance L, inductive coupling, and capacitance C), we may write: $M=L$, $D=1/C$, resonance frequency $\Omega=\sqrt{D/M}=\sqrt{1/LC}$, while α is the inductive coupling itself.

Our goal is to calculate the change in x^2 due to current fluctuations in the first nonvanishing order of perturbation theory.

We must evaluate the expression:

$$\langle x^2(0)\rangle = (-i\alpha)^2 \int_{-\infty}^{0} dt_1 \int_{-\infty}^{t_1} dt_2 e^{\eta(t_1+t_2)} \langle [[x^2(0), x(t_1)\dot{I}(t_1)], x(t_2)\dot{I}(t_2)]]\rangle. \tag{10}$$

The angle brackets here stand for averaging over the unperturbed density matrix of the electrons and the oscillator. Evaluating the expression above, we get

$$\langle x^2(0)\rangle = \left(\frac{\alpha}{2M\Omega}\right)^2 \int_{-\infty}^{+\infty} dt\ \exp(-\eta|t| + i\Omega t)\left[\frac{1}{\eta} - \frac{1}{\eta - i\ \text{sign}(t)\Omega}\right]$$
$$\times\{\langle \dot{I}(0)\dot{I}(t)\rangle(1+N_\Omega) - \langle \dot{I}(t)\dot{I}(0)\rangle N_\Omega\}. \tag{11}$$

The derivation of Eq. (1) from this equation is not a straightforward procedure, the main problem being that the integral over frequencies ω of the Lorenzian $\eta/\eta^2+(\omega-\Omega)^2$, which is supposed to serve as a delta function, contains a factor of ω^2 and does not converge well. If we neglect that problem and replace the Lorenzian by a delta function, $\eta/\eta^2+(\omega-\Omega)^2=\pi\delta(\omega-\Omega)$, we end up with Eq. (1) with the coefficient K in it given by

$$K = \left(\frac{\alpha}{2L}\right)^2 \frac{1}{2\eta}. \tag{12}$$

The coefficient diverges as the width of the resonance η goes to zero, so we keep the latter small but finite.

The shape $F(\omega-\Omega)$ of the resonance in the LC circuit, when calculated more exactly, is in fact not a Lorenzian, and without specifying it we may write instead of Eq. (1)

$$S_{\text{meas}} = \int \frac{d\omega}{2\pi} F(\omega-\Omega)\{S_+(\omega) + N_\Omega[S_+(\omega) - S_-(\omega)]\}. \tag{13}$$

The function $F(\Delta\omega)$ can in principle be measured independently, by applying an alternating current. Afterwards the measured expression can be substituted into the formula above.

In general the current operator and its average over the density-matrix correlators at different times depends on the coordinates. The operators $I(t)$ used in this paper are in fact the total current operators averaged, in addition, over the length l of the inductive-coupling region,

$$I(t) \equiv 1/l \int_{X-l/2}^{X+l/2} I(r,t)dr.$$

Because of this symmetry with respect to the coordinates, the current operators stand as $I(r_1,t)+I(r_2,t)$, although we keep a certain order in time.

Apart from the symmetrization with respect to the coordinates, the problem of the ordering of the current operators stems from the presence of the vacuum fluctuation part. If discussion is limited to the low-frequency limit $\hbar\Omega \ll eV_{\text{bias}}, k_BT$, then it does not matter whether one uses $S_+(\Omega)$, $S_-(\Omega)$, or the Fourier-transformed symmetrized equation (2), the result will be the same up to small corrections of the order of $\hbar\Omega/eV,\ k_BT$.

We are indebted to Janosh Hajdu for many helpful discussions and for his participation in the initial stages of this work. We are also thankful to Christian Glattli for interesting discussions of the results and useful comments. The work of G. B. L. was done partly during his stay in Cologne ITP, Germany; Saclay, France; and ITP ETH Zürich, Switzerland and was supported by SFB 341 in Germany, the Swiss National Foundation, and in part by the Russian Academy of Sciences, RFFR Grant No. 96-02-19568.

[1)] J. Hajdu, private communication.

[1] G. B. Lesovik and L. S. Levitov, Phys. Rev. Lett. **72**, 538 (1994).
[2] S.-R. Eric Yang, Solid State Commun. **81**, 375 (1992).
[3] C. de C. Chamon, D. E. Freed, and X. G. Wen, Phys. Rev. B **51**, 2363 (1995).
[4] L. S. Levitov, H. Lee, and G. B. Lesovik, J. Math. Phys. **37**, 4845 (1996).
[5] L. D. Landau and E. M. Lifshitz, *Statistical Physics*, Pergamon Press, London, 1958.
[6] H. Nyquist, Phys. Rev. **32**, 110 (1928).
[7] See, for example: J. Perina, *Coherence of Light*, D. Reidel Publishing Co., Dordrecht, 1985.
[8] W. E. Lamb and R. C. Retherford, Phys. Rev. **72**, 339 (1947).
[9] H. B. G. Casimir, Proc. Kon. Ned. Akad. Wet. **51**, 793 (1948).
[10] L. Mandel, Phys. Rev. **152**, 438 (1966).
[11] R. Landauer, IBM J. Res. Dev. **32**, 306 (1988); D. S. Fisher and P. A. Lee, Phys. Rev. **23**, 6851 (1981).

Published in English in the original Russian journal. Edited by Steve Torstveit.

On a class of exactly solvable models of autowaves in active media with diffusion

V. M. Zhuravlev[a)]
Ul'yanovsk State University, 432700 Ul'yanovsk, Russia

(Submitted 9 December 1996)
Pis'ma Zh. Éksp. Teor. Fiz. **65**, No. 3, 285–290 (10 February 1997)

A class of autowave models in the form of nonlinear diffusion equations, closely related with the Liouville equation and two-dimensionalized Toda chains, is investigated. Exact solutions of these equations are constructed and analyzed. © *1997 American Institute of Physics.* [S0021-3640(97)01203-6]

PACS numbers: 66.10.−x, 66.30.−h, 66.90.+r

The investigation of autowave processes is an essential direction in the development of the theory of nonlinear wave processes in application to problems of the appearance of ordered structures in different types of physical, chemical, biological, and so on systems.[1–5] The standard model for such systems is an excitable medium described by equations of the ''reaction–diffusion'' type (RD)

$$\frac{d\mathbf{U}}{dt}=\mathbf{F}(\mathbf{U})+\mathbf{D}\Delta\mathbf{U}, \tag{1}$$

where **U** is the state vector of an element of the medium, for example, the concentrations of chemical substances entering into a reaction; $F(\mathbf{U})$ is a nonlinear function; and, **D** is a matrix of the diffusion coefficients of the components of the medium. The simplest model of this type that reproduces the main characteristic features of autowave propagation is the two-component ''activator–inhibitor'' (AI) system

$$\frac{\partial u}{\partial t}=F(u,v)+D_1\Delta u, \quad \frac{\partial v}{\partial t}=G(u,v)+D_2\Delta v \tag{2}$$

for the case of a two-dimensional medium: $\Delta=\partial_x^2+\partial_y^2$. Conventionally, u is the activator concentration and v is the inhibitor concentration; this is determined by the form of the zero isocline $F(u,\ v)=0$ and $G(u,\ v)=0$ and is related with the possible practical realization of such systems in chemical reactions. As a rule, models of this type are investigated with the aid of approximate analytical methods[6,7,4,5] or by numerical modeling.

This letter investigates systems of the type (2) with functions $F(u,\ v)$ and $G(u,\ v)$, which have a type of nonlinearity that is similar to the Liouville equation or the two-dimensionalized Toda chain (TDTC) (see, for example, Ref. 8), and multicomponent RD systems with a nonlinearity of a similar form. Two systems will be investigated in greatest detail. The first one has the form

$$F(u,v)=\mu+\frac{\nu_1 e^{u+v}-\lambda_1}{e^{-2u}},\quad G(u,v)=-\mu-\frac{\nu_2 e^{u+v}+\lambda_2}{e^{-2v}},\tag{3}$$

where λ_1, λ_2, μ, ν_1, and ν_2 are constants. In what follows we shall refer to this system as the Toda type-*V* activator–inhibitor system (TVAI). The second system is closely related with the first one and has a similar form:

$$F(u,v)=2\mu+\nu_1 e^{-u}-\nu_2 e^{u}-\lambda_1 e^{-u-v}-\lambda_2\frac{D_1}{D_2}e^{u-v},\tag{4}$$

$$G(u,v)=\nu_1 e^{-u}+\nu_2 e^{u}+\lambda_2 e^{u-v}-\lambda_1\frac{D_2}{D_1}e^{-u-v},$$

where λ_1, λ_2, μ_1, μ_2, ν_1, and ν_2 are the same constants as in Eq. (3). We shall refere to this system as the Toda type-*N* activator–inhibitor system (TNAI). The type of system is determined from the standpoint of the general classification given for excited systems in Ref. 5. For example, the TVAI system belongs to systems of the type *V* or Λ. This is determined by the three main types of asymptotic behavior of the zero-isocline curves $F(u, v)=0$:

$$v=\ln\left\{\frac{\lambda_1}{\nu_1}e^{-u}-\frac{\mu_1}{\nu_1}e^{u}\right\}.$$

In the case $\lambda_1/\nu_1>0$, $\mu_1/\nu_1<0$ the system (3) is a type-*V* system, in the cases $\lambda_1/\nu_1>0$, $\mu_1/\nu_1>0$ and $\lambda_1/\nu_1<0$, $\mu_1/\nu_1<0$ it is a type-Λ system, and in the case $\lambda_1/\nu_1<0$, $\mu_1/\nu_1>0$ the zero isocline is complex and the system has no real points of equilibrium. Similar curves also obtain for the equation $G(u, v)=0$ with the axes rotated by 90°. The equation for the stationary points of the system has the form

$$\mu(\mu^2-\nu_1\nu_2)U^4+[\lambda_1(\nu_1\nu_2-2\mu^2)+\lambda_2\nu_1^2]U^2+\mu\lambda_1^2=0,\quad V=\lambda_1 U^{-1}-\mu U,\tag{5}$$

where $U=e^u$ and $V=e^v$. The TNAI system is a type-*N* or -*I* system depending on the parameters. This is also determined by the form of the zero isocline $F(u, v)=0$:

$$v=\ln\frac{\lambda_1 e^{-u}+\lambda_2\dfrac{D_1}{D_2}e^{u}}{\nu_1 e^{-u}-\nu_2 e^{u}+2\mu}.$$

In Ref. 9 a simple method was proposed for constructing the solutions of the Liouville equation with the aid of quadratic forms. In the present letter this method is carried over to the system (2). This approach makes it possible to find an entire class of TAI solutions and to investigate their characteristic behavior. It is then applied in a general form to more general multicomponent systems whose functions **F(U)** have the form

$$F_i(u_1,u_2,\ldots,u_n)=e^{-2u_i}\left(\lambda_i+e^{u_i}\sum_{k=1}^{n}\mu_{ik}e^{u_k}\right)\tag{6}$$

or linear combinations of such functions, where λ_i and μ_{ij} are constant parameters of the model. We shall refer to such systems as Toda reaction–diffusion chains (TRDCs).

Systems of the types (3), (4), or (6) with an exponential nonlinearity have apparently not been studied in an explicit form in the theory of autowaves. This is because most examples of model equations for autowaves, for example, the Zhabotinskiĭ equations[10,3,5] (describing the Belousov–Zhabotinskiĭ reaction) or the Brusselator[11,2,3,5] and similar models (see Refs. 3 and 5), include a power-law nonlinearity. However, models of the type (6) can have a direct bearing on models of autowaves with thermal diffusion, when the diffusion coefficient of the material and the thermal conductivity become nonlinear functions of the parameters of the systems, i.e., u_i (Ref. 3 and 5). Indeed, the equations (2) with the relations (3) and (4) for the functions $\Psi = e^u$ and $\Phi = e^v$ can be written in the following form:

$$\Psi_t - D_1 \Psi \sum_{\alpha=1}^{2} \partial_\alpha \left(\frac{1}{\Psi} \partial_\alpha \Psi \right) = \mu \Psi + \frac{\nu_1 \Psi \Phi - \lambda_1}{\Psi},$$

$$\Phi_t - D_2 \Phi \sum_{\alpha=1}^{2} \partial_\alpha \left(\frac{1}{\Phi} \partial_\alpha \Phi \right) = -\mu \Phi - \frac{\nu_2 \Psi \Phi + \lambda_2}{\Phi},$$

which corresponds to a system of equations describing diffusion of matter and heat conduction with a special choice of the dependence of the diffusion coefficient and thermal conductivity on the unknown functions of the model. On the other hand, the functions $F(v,u)$ and $G(u,v)$ in the regions where the model functions u and v are close to the equilibrium values U_0 and V_0 do not differ much from the first few terms in the expansion of these functions in a Taylor series around U_0 and V_0. For this reason, their solutions can serve as a quite good approximation to the exact solutions for systems with power-law nonlinearity in these regions. Therefore the TVAI, TNAI, and TRDC systems can serve as possible variants of basic models (in the terminology of Ref. 3) for investigating autowaves in excitable media and they are examples for which it is convenient to study some general features of the behavior of autowaves, irrespective of whether or not an exact justification of these models can be found for some reaction–diffusion system. For example, it is easy to verify that the TVAI and TNAI systems can have one or two stationary states (the TNAI system can have four stationary states), depending on the parameters, or they may not have any stationary states at all. Therefore such systems make it possible to study different variants of the asymptotic behavior of autowaves in the presence or absence of stationary states and different types of stability of these states.

By analogy to Ref. 9 we seek the solution of the system (2)–(3) in the form

$$u = \ln \Psi(z,\overline{z},t), \quad v = \ln \Phi(z,\overline{z},t),$$

$$\Psi = |g(z)|^2 \{a_1(t)|\psi_1|^2 + b_1(t)|\psi_2|^2 + c_1(t)\psi_1(z)\psi_2^*(\overline{z}) + c_1^*(t)\psi_2(z)\psi_1^*(\overline{z})\}, \quad (7)$$

$$\Phi = |g(z)|^2 \{a_2(t)|\psi_1|^2 + b_2(t)|\psi_2|^2 + c_2(t)\psi_1(z)\psi_2^*(\overline{z}) + c_2^*(t)\psi_2(z)\psi_1^*(\overline{z})\},$$

where $z = x + iy$, $\overline{z} = x - iy$, $\Delta = 4(\partial/\partial z \partial \overline{z})$, the symbol * denotes complex conjugation, the functions $a_1(t)$, $b_1(t)$, $a_2(t)$, and $b_2(t)$ are real and functions $c_1(t)$ and $c_2(t)$ complex functions of t, and $\psi_1(z)$, $\psi_2(z)$, and $g(z)$ are analytic functions of the complex variable z. Substituting expressions (7) into Eq. (2) we obtain the following identities:

$$\frac{\partial u}{\partial t}-D_1\Delta u=-D_1\frac{|g(z)|^4(a_1b_1-|c_1|^2)|W_{12}(z)|^2}{\Psi^2}$$
$$+\frac{|g(z)|^2(\{\dot a_1|\psi_1(z)|^2+\dot b_1|\psi_2(z)|^2+\dot c_1\psi_1(z)\psi_2^*(\overline{z})+\dot c_1^*\psi_2(z)\psi_1^*(\overline{z})\}}{\Psi};\tag{8}$$

$$\frac{\partial v}{\partial t}-D_2\Delta v=-D_2\frac{|g(z)|^4(a_2b_2-|c_2|^2)|W_{12}(z)|^2}{\Phi^2}$$
$$+\frac{|g(z)|^2(\{\dot a_2|\psi_1(z)|^2+\dot a_2|\psi_2(z)|^2+\dot c_2\psi_1(z)\psi_2^*(\overline{z})+\dot c_2^*\psi_2(z)\psi_1^*(\overline{z})\}}{\Phi},\tag{9}$$

here

$$W_{12}(z)=\psi_1\frac{d}{dz}\psi_2-\psi_2\frac{d}{dz}\psi_1$$

is the Wronskian of the two functions $\psi_1(z)$ and $\psi_2(z)$. The Wronskian is different from zero when the functions $\psi_1(z)$ and $\psi_2(z)$ are linearly independent. Therefore we assume that these functions are linearly independent. In order that the expressions on the right-hand sides of the identities (8) be identical to expression (3), the following conditions must hold:

$$a_2(t)=\dot a_1-\mu_1a_1,\quad b_2(t)=\dot b_1-\mu_1b_1,\quad c_2(t)=\dot c_1-\mu_1c_1,\tag{10}$$

$$(a_1b_1-|c_1|^2)D_1=\lambda_1=\text{const},\quad (a_2b_2-|c_2|^2)D_2=\lambda_2=\text{const},\tag{11}$$

$$|W_{12}|^2|g|^4=1,\quad \mu_1=\text{const},\quad \mu_2=\text{const};\tag{12}$$

$$\frac{d}{dt}(\dot a_1-\mu_1a_1)=-\nu_1\nu_2a_1+\mu_2(\dot a_1-\mu_1a_1),$$
$$\frac{d}{dt}(\dot b_1-\mu_1b_1)=-\nu_1\nu_2b_1+\mu_2(\dot b_1-\mu_1b_1),\tag{13}$$
$$\frac{d}{dt}(\dot c_1-\mu_1c_1)=-\nu_1\nu_2c_1+\mu_2(\dot c_1-\mu_1c_1).$$

The three equations (13) have the same general form as the equation of damped oscillations

$$\ddot F-(\mu_1+\mu_2)\dot F+(\mu_1\mu_2+\nu_1\nu_2)F=0\tag{14}$$

with damping decrement $\gamma=(\mu_1+\mu_2)/2$ and characteristic oscillation frequency $\Omega=\sqrt{\mu_1\mu_2+\nu_1\nu_2}$. Equation (14) has solutions of three basic types:

$$F(t)=\begin{cases} e^{-\gamma t}(F_1\cos(\omega t)+F_2\sin(\omega t)), & \omega^2>0; \\ e^{-\gamma t}(F_1\cosh(\omega t)+F_2\sinh(\omega t)), & \omega^2<0; \\ e^{-\gamma t}(F_1 t+F_2), & \omega^2=0, \end{cases} \tag{15}$$

where F_1 and F_2 are integration constants and $\omega^2-\Omega^2-\gamma^2$. In the case $\omega^2>0$ we can set

$$a_1(t)=e^{-\gamma t}(A_1\cos(\omega t)+A_2\sin(\omega t)),$$

$$b_1(t)=e^{-\gamma t}(B_1\cos(\omega t)+B_2\sin(\omega t)),$$

$$c_1(t)=e^{-\gamma t}(C_1\cos(\omega t)+C_2\sin(\omega t)),$$

where A_1, A_2, B_1, and B_2 are arbitrary real constants and C_1 and C_2 are arbitrary complex constants. Then

$$a_1b_1-|c_1|^2=e^{-2\gamma t}((A_1B_2+A_2B_1-C_1C_2^*-C_2C_1^*)\cos(\omega t)\sin(\omega t)$$
$$+(A_1B_1-|C_1|^2)\cos^2(\omega t)+(A_2B_2-|C_2|^2)\sin^2(\omega t)).$$

A similar expression also holds for a_2, b_2, and c_2. In order for the parameters λ_1 and λ_2 to be constants, the following relations must be satisfied:

$$\gamma=(\mu_1+\mu_2)/2=0, \quad A_1B_2+A_2B_1-C_1C_2^*-C_2C_1^*=0,$$
$$(A_1B_1-|C_1|^2)=(A_2B_2-|C_2|^2). \tag{16}$$

Then

$$\omega=\Omega, \quad \lambda_1=D_1(A_1B_1-|C_1|^2), \quad \lambda_2=D_2(A_1B_1-|C_1|^2)(\Omega^2+\mu^2),$$

where $\mu=\mu_1=-\mu_2$ and $\Omega^2=\nu_1\nu_2-\mu^2$.

The corresponding class of exact solutions of the TVAI model can be represented in the form

$$u(z,\overline{z},t)=\ln P^+(z,\overline{z})+\ln\cos(\Omega t-\Theta_1(z,\overline{z})),$$
$$v(z,\overline{z},t)=\ln Q^+(z,\overline{z})+\ln\cos(\Omega t+\Theta_2(z,\overline{z})), \tag{17}$$
$$P^+(z,\overline{z})=\sqrt{H_1^2+H_2^2}, \quad Q^+(z,\overline{z})=\frac{1}{\nu_1}\sqrt{(\Omega H_2-\mu H_1)^2+(\mu H_2+\Omega H_1)^2},$$
$$\tan\Theta_1(z,\overline{z})=\frac{H_1(z,\overline{z})}{H_2(z,\overline{z})}, \quad \tan\Theta_2(z,\overline{z})=\frac{\mu H_2+\Omega H_1}{\Omega H_2-\mu H_1},$$

where

$$H_1(z,\overline{z})=\frac{A_1|\psi_1|^2+B_1|\psi_2|^2+C_1\psi_1\psi_2^*+C_1^*\psi_2\psi_1^*}{|W_{12}|}, \tag{18}$$
$$H_2(z,\overline{z})=\frac{A_2|\psi_1|^2+B_2|\psi_2|^2+C_2\psi_1\psi_2^*+C_2^*\psi_2\psi_1^*}{|W_{12}|}$$

and the constants A_1, A_2, B_1, B_2, C_1, and C_2 satisfy the relations (16). The functions Ψ and Φ are related by the simple relation

$$\Phi = \frac{1}{\nu_1}(\dot{\Psi} - \mu\Psi). \tag{19}$$

The functions $\psi_1(z)$ and $\psi_2(z)$ are arbitrary analytic functions.

The solutions obtained for the TVAI system are a more general solution of the Cauchy problem for the system (2)–(3) with an initial distribution of the functions $u = u(z, \overline{z}, 0)$ and $v = v(z, \overline{z}, 0)$ as quadratic forms that depend on the two arbitrary analytic functions $\psi_1(z)$ and $\psi_2(z)$. This makes it possible to satisfy a wide class of initial conditions of the problem with some general properties of the solutions at infinity, for example, $u \to$ const and $v \to$ const as $r = \sqrt{x^2+y^2} \to \infty$ — the medium is in equilibrium at infinity.

The solutions of the TNAI system (2)–(4) are obtained from the solutions of the system (17) by means of the very simple transformation

$$\tilde{u} = u - v = \ln\left\{\frac{\Psi}{\Phi}\right\}, \quad \tilde{v} = u + v = \ln\{\Psi\Phi\}, \tag{20}$$

where $\tilde{u}$ and $\tilde{v}$ are solutions of the TNAI system and u and v are solutions of the TVAI system (17).

Of all types of solutions, the time-periodic solutions of the spiral-wave type are of special interest. These solutions can be obtained in an explicit form, if the functions $\psi_1(z)$ and $\psi_2(z)$ are chosen in a special manner, for example,

$$\psi_1(z) = p_1 z^m, \quad \psi_2(z) = p_2 z^n,$$

where p_1, p_2, and $m \neq n$ are arbitrary complex constants. Time-periodic solutions exist if $\Omega^2 > 0$. As one can easily see, however, after a finite time interval such solutions are no longer bounded anywhere (the functions Ψ and Φ change sign). Nonsingular solutions exist for $\Omega^2 < 0$:

$$u(z,\overline{z},t) = \ln P^-(z,\overline{z}) + \ln\{\cosh(\Omega t + \Theta_1(z,\overline{z}))\},$$
$$v(z,\overline{z},t) = \ln Q^-(z,\overline{z}) + \ln\{\cosh(\Omega t + \Theta_2(z,\overline{z}))\}, \tag{21}$$
$$P^-(z,\overline{z}) = \sqrt{H_1^2 - H_2^2}, \quad Q^-(z,\overline{z}) = \frac{1}{\nu_1}\sqrt{(\Omega H_2 - \mu H_1)^2 - (\mu H_2 - \Omega H_1)^2},$$
$$\tanh\Theta_1(z,\overline{z}) = \frac{H_2(z,\overline{z})}{H_1(z,\overline{z})}, \quad \tanh\Theta_2(z,\overline{z}) = \frac{\Omega H_1 - \mu H_2}{\Omega H_2 - \mu H_1},$$

where the functions H_1 and H_2 are determined by relations (18), and the functions Ψ and Φ are related by the relation (19). The solutions (21) are nonsingular if the functions H_1, H_2, P^-, and Q^- are nonsingular. They comprise a single solitary wave of a complicated form. These results, obtained for TVAI, also hold *in toto* for TNAI. Therefore, to search for systems possessing nonsingular time-periodic solutions, it is of interest to investigate the more general models of the type (6).

Nonsingular periodic solutions exist in the multicomponent models (6). This result can be obtained on the basis of the following general considerations. Let us consider the sequence of functions $U_i = \ln \Psi_i$, where

$$\Psi_i(\zeta, \overline{z}, t) = |g(z)|^2 \{a_i(t)|\psi_1|^2 + b_i(t)|\psi_2|^2 + c_i(t)\psi_1\psi_2^* + c_i^*(t)\psi_2\psi_1^*\}, \quad i = 1, \ldots, n. \tag{22}$$

These functions satisfy the identities

$$\frac{\partial U_i}{\partial t} - D_i \Delta U_i = -D_i \frac{|g(z)|^4 (a_i b_i - |c_i|^2)|W_{12}(z)|^2}{\Psi_i^2} + \frac{|g(z)|^2 (\{\dot{a}_i|\psi_1(z)|^2 + \dot{b}_i|\psi_2(z)|^2 + \dot{c}_i\psi_1(z)\psi_2^*(\overline{z}) + \dot{c}_i^*\psi_2(z)\psi_1^*(\overline{z})\}}{\Psi_i},$$

$$i = 1, \ldots, n. \tag{23}$$

We require that the following conditions be satisfied:

$$\dot{a}_i = \sum_{j=1}^{n} \mu_{ij} a_j, \quad \dot{b}_i = \sum_{j=1}^{n} \mu_{ij} b_j, \quad \dot{c}_i = \sum_{j=1}^{n} \mu_{ij} c_j, \quad i = 1, \ldots, n;$$

$$(a_i b_i - |c_i|^2) f_i^2 D_i = \lambda_i = \text{const}, \quad |W_{12}|^2 |g|^4 = 1.$$

Then the system of identities (23) assumes the form of the TRDC system of equations with a nonlinearity of the form (6). The equations for the functions a_i, b_i, and c_i comprise a system of ordinary first-order differential equations. In the simplest case, when the μ_{ij} are all constant, the coefficients in these equations are also constant. For nonsingular periodic solutions to exist these equations must have solutions of the form

$$F_i(t) = A_i + B_i \cos(\Omega t + \phi_0),$$

where $|A_i| > |B_i|$ for all i. These conditions must hold for a_i, b_i, and c_i. Such requirements hold even in the case of a three-component system. The corresponding solutions can be easily found. However, because of space limitations, they are not presented here.

In closing, I thank S. V. Chervon and V. K. Shchigolev for their unflagging interest in this work.

[a)]e-mail: zhuravl@themp.univ.simbirsk.su

[1] H. Haken, *Synergetics: An Introduction,* Springer-Verlag, New York, 1978 [Russian translation, Mir, Moscow, 1980].
[2] I. Prigogine, *From Being to Becoming: Time and Complexity in the Physical Sciences*, W. H. Freeman, San Francisco, 1980 [Russian translation, Nauka, Moscow, 1991].
[3] V. A. Vasil'ev, Yu. M. Romanovskiĭ, and V. G. Yakhno, *Autowave Processes* [in Russian], Nauka, Moscow, 1987.
[4] V. A. Davydov and V. G. Morozov, Usp. Fiz. Nauk **166**, 327 (1996).
[5] B. S. Kerner and V. V. Osipov, *Autosolitons: Localized Strongly Nonequilibrium Regions in Homogeneous Dissipative Systems* [in Russian], Nauka, Moscow, 1991.

[6] V. A. Davydov, V. S. Zykov, and A. S. Mikhaĭlov, Usp. Fiz. Nauk **161**, 45 (1991) [Sov. Phys. Usp. **34**, 665 (1991)].
[7] P. K. Brazhnik, V. A. Davydov, and A. S. Mikhaĭlov, Teor. Mat. Fiz. **74**, 440 (1988).
[8] A. N. Leznov and M. V. Savel'ev, *Group Methods for Integration of Nonlinear Dynamical Systems* [in Russian], Nauka, Moscow, 1985.
[9] V. M. Zhuravlev, Prikl. Mat. Mekh. **58**, 61 (1994).
[10] A. M. Zhabotinskiĭ, *Concentration Oscillations*[in Russian], Nauka, Moscow, 1974.
[11] G. Nicolis and I. Prigogine, *Self-Organization in Non-Equilibrium Systems*, Wiley, New York, 1977.

Translated by M. E. Alferieff

Channels in rotating liquids for conducting discharges, transporting currents and particle and radiation fluxes, and lowering breakdown thresholds

G. A. Askar'yan and A. V. Yurkin
Institute of General Physics, Russian Academy of Sciences, 117942 Moscow, Russia

(Submitted 21 November 1996; resubmitted 8 January 1997)
Pis'ma Zh. Éksp. Teor. Fiz. **65**, No. 3, 291–294 (10 February 1997)

The formation of gas channels in rotating liquids is investigated and the application of such channels as capillaries for high-power discharges in x-ray lasers, for transporting particle and radiation fluxes, and lowering breakdown thresholds (including with the use of metal fillings), for structural systems for microwave generation and particle acceleration, and for photochemical and shock action on a liquid, and so on, is discussed. It is noted that tubular active elements and samples can be fabricated by solidification and crystallization during rotation. © *1997 American Institute of Physics.* [S0021-3640(97)01303-0]

PACS numbers: 47.32.−y, 52.80.Wq, 47.60.+i, 77.22.Jp, 52.90.+z

The production of gas channels in liquids is of great interest for a number of applications: for experimental and applied physics at high-energy densities, since the channels make it possible to obtain reusable high-power capillary discharges (for example, x-ray and other lasers) with self-recovering capillaries, without the ordinarily observed degradations of the properties and damage to the surfaces of the walls, especially in the case of surface breakdowns; for transporting particle beams and currents; for lowering breakdown thresholds in liquids; for electrohydraulic or ultraviolet action on liquids (pumping of lasers, treatment of water and oils, photochemistry); and so on.

We have performed simple experiments on the production of gas channels in rotating liquids and in liquids flowing around different bodies.

A gas bubble with the required composition was introduced into (in the case of low saturated vapor pressure or low content of dissolved gas) or remained in the liquid (water, vacuum oils, alcohol), and the liquid was made to rotate or rotated as it flowed through special structures.

1. FORMATION OF A GAS CHANNEL IN A LIQUID IN A ROTATING TUBE

A cylindrical glass tube, filled with a liquid into which a bubble was introduced or remained, was secured on the axis or connected with the axis of an electric motor and rotated with frequency $f=50$ or 100 Hz. Within fractions of a second the gas bubble became detached, approached the axis, and spread out into a thin channel along the entire axis. The diameter of the channel depended on the amount of liquid or gas. In the case of a closed vessel, the volume of the liquid remained practically unchanged (since the rotational centrifugal pressure hardly changed the volume of the liquid because of the low

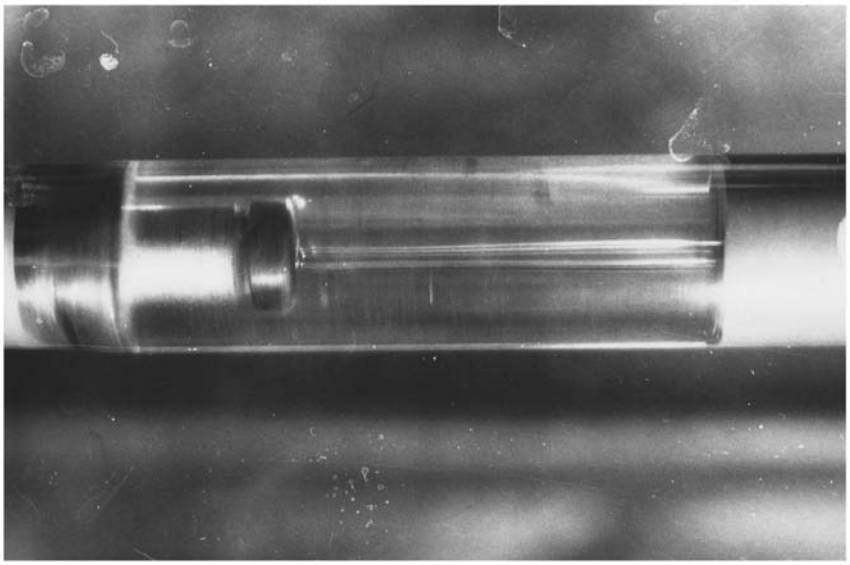

FIG. 1. Photograph of a gas channel on the axis of a rotating liquid. The channel diameter equals 1 mm. The rotation frequency equals 100 Hz. Liquid — vacuum oil. Gas — air.

compressibility of the liquid) and the channel volume was determined by the volume of the gas introduced or the incomplete filling with liquid. The diameter of the channel could be easily increased up to 1 mm. The channel length reached 20 cm. It could also be changed by adjusting the opening on the axis. Under normal rotation (no beats and no decentering) the channel was stable and even. A photograph of this arrangement with vacuum oil in rotation and a 1 mm in diameter and 4 cm long channel is displayed in Fig. 1. As a result of the high centrifugal accelerations,

$$a_{\perp} \cong (2\pi f)^2 r > 10^5 r > 10^4 \text{cm/s}^2 \gg g_0 \cong 10^3 \text{cm/s}^2 \quad \text{for} \quad r > 1 \quad \text{mm},$$

the channel formation was virtually independent of the orientation of the rotation axis relative to the direction of gravity. Identical results were obtained with both water and alcohol. The motion of the introduced bubble and extraction of unneeded gas by evacuation from the rotating liquid were much more rapid than in the case when a bubble floated upward under the action of gravity. We call attention to the possible small channel radii and the smoothness of the channel walls, properties necessary for a uniform discharge, which is so desirable in x-ray lasers.

The maximum admissable channel diameters can be estimated by equating the constricting surface-tension pressure $P_{\text{surf}} \cong \sigma/r$ to the centrifugal pressure $P_{\text{cf}} \cong \rho\omega^2\Delta$, where σ is the surface tension, ρ is the density of the liquid, and Δ is the thickness of the liquid layer. Therefore $r_{\min} \sim \sigma/\rho\omega^2\Delta$, or $r_{\min} \simeq \omega^{-1}\sqrt{\sigma/10\rho} \simeq 10^{-2}$ cm for $\Delta \simeq 10r$ and our rotation frequencies.

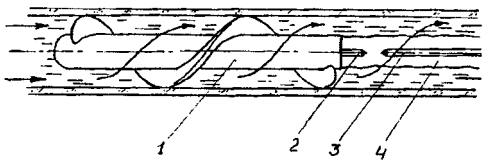

FIG. 2. Diagram of the rotation of a moving liquid with a gas channel on the rotation axis: *1* — axial rod on which a helix is wound, *2* — electrode secured on the end of the rod, *3* — second discharge electrode, *4* — gas channel. The arrow indicates the direction of flow of the liquid.

2. CHANNEL FORMATION DURING MOTION OF THE LIQUID

The formation of a gas channel during the rotation and motion of a liquid through helical elements was investigated. Tap water was passed through an 18 mm in diameter tube into which an axial cylinder with a helical finned surface, which caused the water to rotate as it flowed over the cylinder (see Fig. 2), was inserted. For 3-mm deep fins the pitch of the screw was equal to 0.5 turns/cm of cylinder length.

A gas channel formed on the axis at a water flow velocity of only 3–30 cm/s (tube diameter of 18 mm and water flow rate of $10^{-2}-10^{-1}$ liters/s). The radius of the channel depended on the flow velocity and ranged from one to several millimeters. Apparently, this channel became filled with air dissolved in the water and was stable, its length varying from 0.5 to 5 cm depending on the velocity of the water flow.

The finned rod was also used to hold electrodes for investigating breakdowns in the channel. It was observed that an unfinned axial body inserted into the flow also gives gas channels where electrodes can be inserted and breakdown can be conducted, but the length of this channel is small for our flow velocities, though the length can be controlled by placing on the rod ends attachments that change the regime of the flow over the rod and the detachment of the flow.

3. ELECTRICAL BREADDOWN ALONG THE LIQUID SURFACE AND IN THE GAS CHANNEL

Electric breakdown was investigated between two electrodes with a radius of 1 mm placed on the rotation axis (see Fig. 3). When a gas channel formed during rotation, breakdown was observed at the breakdown voltage for air. Breakdown was not observed without rotation, since the breakdown threshold in water is higher.

The channel withstands high short gas-kinetic and ablation pressure pulses as a result of the inertia of the liquid, and it is rapidly restored as a result of the large centrifugal force.

Breakdowns in water have been observed previously in the presence of metal suspensions and filings, which substantially lower the breakdown threshold. These experiments suggested the possibility of producing closing suspensions, each suspension having an average density less than that of the liquid — for example, composite metal–dielectric filings (a thin layer of metal on a light dielectric). This was implemented experimentally. Such particles were distributed on the surface of the channel.

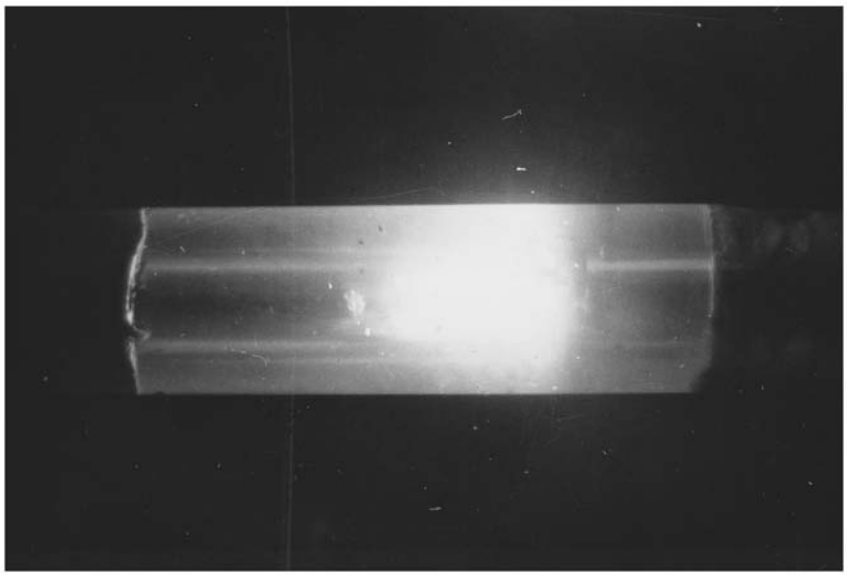

FIG. 3. Pulsed electric discharge in a gas channel in a rotating tube containing a liquid. The rotation frequency equals 50 Hz. Liquid — water, gas — air. The electrodes are 1 mm in diameter and separated by 1.5 mm. Voltage — 3 kV, discharge capacitance — 0.6 μF.

Panels — metal fillings impregnated with epoxy resin and slightly polished — as well as electrodes with alternating polarity were also tried. They likewise lowered the breakdown threshold. In these experiments, breakdown voltages from 1 to 3 kV with capacitances of 0.1–10 μF were used. Sometimes, in order to peak breakdown and make the energy release explosive, voltage was applied through a spark gap or a fast high-resistance switch. Ultraviolet light, enveloping neighboring electrodes with the breakdown, propagated well in the gas channel; this also enabled the use of a sequence of electrodes with alternating polarity, making it possible to break down large gaps by means of a voltage which was not very high.

Suspensions, which lower the breakdown threshold and make it possible to increase the length of the breakdown gap, can be produced with the use of filings, which will be distributed over the surface of the channel if their average microdensity is less than the density of the liquid. Multielectrode panels can be inserted into stationary and rotating liquids. Suspensions not only lower the breakdown threshold, but they will also make it possible to increase the number of working media for realizing x-ray lasers (vapors of the metals of the suspensions). Moreover, under the conditions of a multiple (almost continuous) and not a streamer discharge on a cylindrical surface, the implosion will be more perfect and the temperatures and pressures will be higher on the cumulation axis.

We note that powerful particle or radiation beams passing through gas channels and liquids can themselves maintain or smooth the channel sections or expand them from small starting sizes.

The production of ripples on the surface of the liquid of the channel walls (for

example, by exciting surface capillary waves with the aid of ultrasound) will make it possible to produce restorable, incombustible structures for generating microwaves by passing powerful beams or bunches of charged particles almost on/or near the riffled surfaces.

Such vacuum and gas channels can be used to accelerate charged particles by the Coulomb field of an electron cloud formed under the action of an ultrapowerful ultrashort light pulse, which pulls out electrons when the light field touches the channel walls.[1] This requires frequent renewal of the channel surface because of the destructive action of intense light.

This effect can be used in both melts and solutions, which when rotated will also give a channel that will set on solidification, cooling, and crystallization. We demonstrated this in an experiment with paraffin and rosin melt in a tube, which gave a channel and set together with it on cooling. Such tubular blocks of active elements can be used for efficient pumping and for particle acceleration by a converging light wave on the axis of a laser.[2]

What we have said suggests that gas channels have tremendous prospects for applications in new areas of physics — from x-ray capillary lasers to generation of radio waves and particle acceleration — and in chemical physics — for photochemical and shock action on a liquid, for treatment, purification, and decontamination of water, oils, and other liquids.

[1] G. A. Askar'yan, JETP Lett. **52**, 323 (1990).
[2] K. Shimoda, Appl. Opt. **1**, 33 (1962); *Lasers* [Russian translation, Inostr. Lit. Press, Moscow, 1963, p. 458].

Translated by M. E. Alferieff